Technische Universität München

Fakultät für Maschinenwesen

Lehrstuhl für Angewandte Mechanik

Gear contact modeling for system simulations and experimental investigation of gear contacts

Franciscus Leendert Johannes van der Linden

Vollständiger Abdruck der von der Fakultät für Maschinenwesen der Technischen Universität München zur Erlangung des akademischen Grades eines

Doktor- Ingenieurs

genehmigten Dissertation.

Vorsitzender:	Prof. Dr.-Ing. habil Boris Lohmann
Prüfer der Dissertation:	
	1. Prof. dr.ir. Daniel J Rixen
	2. Prof. Dr.-Ing. Bernd-Robert Höhn
	3. Prof. Dr.-Ing. Martin Otter

Die Dissertation wurde am 04.02.2016 bei der Technischen Universität München eingereicht und durch die Fakultät für Maschinenwesen am 22.09.2016 angenommen.

Acknowledgments

In 2007, I started my work at DLR German Aerospace Center with a focus on health monitoring algorithms for electromechanical actuators. For these monitoring methods, I needed dynamic models of (damaged) gears for the development of the monitoring algorithms. During this work, I discovered that the modeling of gears is a very interesting research topic from the point of view of a system engineer and decided to write my PhD thesis about this topic.

I thank Dr.-Ing. Bals and dr.ir. Looye for their continued support of my work and possibility to build the test rig to do the experimental validation of the theory. A special thank goes to the members of my doctoral committee: Prof. dr.ir. Daniel Rixen for his personal and very inspiring supervision, Prof. Dr. Höhn as an expert on gear theory, Prof. Dr.-Ing. Otter as an expert on modeling and Modelica and Prof. Dr.-Ing. Lohmann for being the head of my doctoral committee.

This work would never have been completed without my colleagues and friends (especial, but not limited to: Dr. Andreas Klöckner, Dr. Dirk Zimmer, Reiko Müller and Dr. Tobias Petzold). Their technical and also moral support, has been crucial in many phases of my PhD. For the input on the german parts of my work I would like to thank Rainer Wilke.

I am further grateful for the support and contributions of my sister and brother (Sophia Wolff and Lennert van der Linden), especially for their help with the cover. Furthermore, a very special thanks goes to my parents Catharina and Franciscus van der Linden who supported me over the last years in countless discussions on the phone. Lastly I would like to thank Diana Wilke who has always supported me, especially in the last parts of my work.

Oberpfaffenhofen, 27th December 2016
Frans van der Linden

Abstract

Gear transmissions are believed to be used for already 4600 years by mankind. Although gears have been studied for a very long time, gear modeling is still a very active field of research. The use of gear transmissions is widely distributed through all fields of engineering. Systems like wind turbines, vehicle transmissions, aircraft turbines and electromechanical positioning actuators all rely on gear transmissions. The electrification of many systems in favor of hydraulic systems further increases the need for gear transmissions as such applications typically need a high-torque, low velocity output. A good example here is the abandoning of hydraulic actuators in aircraft to reduce maintenance costs and lower system weight.

Gear design is a complex and specialized task demanding highly specialized knowledge. Therefore the design of gear transmissions and the complete systems is usually done by different companies or different departments. For a good performance, the gears must be designed to withstand the expected loads. Furthermore, vibration and noise should be minimized by gear flank modifications. Gear designers therefore use specialized programs which are optimized for gear design. System designers on the other hand, integrate the gear transmission in the overall system. They use simplified gear models to keep the computational performance of their models low.

However, as the demands on the systems rise, transmissions often play an important role in the overall system dynamics. The design of the gear transmission and the overall system now must be integrated to reach the needed performance. Especially for positioning applications, the tooth elasticity and friction play a crucial role in the system performance. Also the simulation of damaged components for the development of health monitoring algorithms need the interaction between the teeth contacts and the system.

To create complete system models with high accuracy gear models, the computational performance of the models is crucial. Often the performance of such systems is tuned using optimization routines where the simulation can be carried out thousands of times.

In this thesis a gear transmission model is presented that bridges the gap between models used by gear designers and models used by system designers. It is fast enough to be used in system simulations and accurate enough to represent the effect of the meshing teeth and the effect of a damaged gear tooth.

The transmission error of the gears is represented in these models. Furthermore, gear elasticity and friction are both described depending on the load and position of the gear contact. Also gear stiction which can occur at standstill or the change of the rotational direction in the combination with preload is included in the modeling. This allows the model to be used in positioning applications as well.

For the validation of the models, measurements have been carried out on a single stage spur gear transmission. Two gear sets have been analyzed; a healthy gear transmission and a damaged gear transmission with an artificially removed tooth. The transmission error has been measured. Moreover the deformation, stiffness and friction of the gears have been obtained dependent on the position and loading condition of the gears.

A study on a Torque-Vectoring Drive (TVD) for an electric vehicle has been carried out to show the possibilities of the integration of detailed gear models in system simulations. It demonstrates that the interaction between system and transmission can lead to stick-slip problems when the drive axles of the vehicle are not stiff enough.

Zusammenfassung

Zahnradübertragungen werden seit ungefähr 4600 Jahren von den Menschen für die unterschiedlichsten technischen Aufgaben genutzt. Zahnräder sind daher schon seit langem ein Gegenstand der Forschung. Nichtsdestotrotz ist die Zahnradmodellierung auch heute noch ein sehr aktives Forschungsgebiet. Zahnräder als Teil von Getrieben kommen als Baugruppen in technischen Systemen in nahezu allen Bereichen des Maschinenbaus zum Einsatz. So sind Systeme wie z.B. Windturbinen, Kraftfahrzeuggetriebe, Flugzeugturbinen und elektromechanische Positionierungsaktuatoren auf Zahnradübertragungen angewiesen. Insbesondere die Elektrifizierung von vielen vorher hydraulisch betätigten Systemen führt zu einer weiteren Zunahme der Verwendung von Getrieben, da solche Systeme üblicherweise hohe Momente bei niedrigen Drehzahlen voraussetzen. Ein gutes Beispiel für diese Entwicklung sind die hydraulischen Flugzeugaktuatoren, die zur Reduzierung der Flugzeugmasse und zur Minimierung der Wartungskosten zunehmend durch elektrisch angetriebene Systeme ersetzt werden.

Die Getriebeentwicklung ist ein äußerst komplexes Fachgebiet, welches hochspezialisiertes Fachwissen voraussetzt. In der Praxis werden daher Getriebe und Systeme von unterschiedlichen Personenkreisen entwickelt. Grundlegend für die Systementwicklung sind Getriebe, welche die zu erwartenden Lasten aushalten und zugleich Vibrationen und Lärm minimieren. Um diese Anforderungen zu erfüllen, kann der Getriebeentwickler im Rahmen der Getriebeentwicklung auf diverse Spezialsoftware zurückgreifen. Demgegenüber müssen Systementwickler die Getriebe im Gesamtsystem integrieren. Sie verwenden dazu vereinfachte Getriebemodelle, um die Rechenlast niedrig zu halten.

Wenn sich die Anforderungen an das System erhöhen, steigt in der Regel auch der Einfluss des Getriebes auf die Systemdynamik. Um eine bestimmte Systemleistung überhaupt zu erreichen, kann es erforderlich sein, die Getriebeauslegung in die Erarbeitung des Systementwurfs zu integrieren. Ein solches Erfordernis besteht häufig bei Positionierungsaufgaben, bei denen die Elastizität und die Reibung der Zahnräder entscheidend für die Systemleistung sind. Eine Bewertung der Wechselwirkungen von Getriebe und System ist ferner z.B. für Simulationen von beschädigten Komponenten und die Auslegung von Health-Monitoring-Algorithmen notwendig.

Für die Entwicklung von kompletten Systemmodellen auf Basis präziser Getriebemodelle stellt die Rechenleistung einen limitierenden Faktor dar. Oft wird die Leistung von solchen Systemen mittels spezieller Optimierungsalgorithmen verbessert, wobei meist viele tausend Simulationen ausgeführt werden müssen.

In der vorliegenden Arbeit wird ein Getriebemodell vorgestellt, welches die Lücke schließt zwischen den Modellen, die in der Getriebeauslegung und denen, die in der Systementwicklung verwendet werden. Dieses Modell ist hinreichend schnell für Systemsimulationen und zugleich hinreichend genau um die Effekte von Zahneingriffen und Zahnfehlern darzustellen.

Das Modell berücksichtigt den übersetzungsfehler des Getriebes. Desweiteren werden die Getriebeelastizität und die Reibung in Abhängigkeit von der Last und Position des Getriebekontakts als relevante Parameter einbezogen. Die Haftreibung, die im Stillstand sowie bei einem

Laufrichtungswechsel in Kombination mit einer Vorspannkraft auftritt, ist ebenfalls inbegriffen. Diese Eigenschaften ermöglichen auch die Verwendung des Modells in Positionierungsaufgaben.

Zur Validierung des Modells erfolgten Labormessungen an einem einstufigen Getriebe. Es wurden zwei Zahnradpaare zur Simulation eines gesunden Getriebes und eines schadhaften Getriebes untersucht. Bei letzterem war an einem Zahnrad ein Einzelzahn entnommen worden. Es wurden der übersetzungsfehler sowie die Verformung, Steifigkeit und Reibung des Getriebes abhängig von der Position und Belastung des Getriebes gemessen. Desweiteren wurden mittels einer Studie an einem Torque-Vectoring Getriebe eines Elektrofahrzeugs Möglichkeiten des Zusammenfügens von detaillierten Getriebemodellen in Systemsimulationen geprüft. Ein Ergebnis der Studie ist, dass das Zusammenspiel zwischen System und Getriebe zu Haft-Gleit-Effekten führen kann, wenn die Antriebsachsen des Fahrzeuges nicht ausreichend steif sind.

Contents

1 Introduction

The modeling of gears is an ongoing topic of research. The current research addresses many different fields and the model complexity varies greatly. The models used in industry span from gear models which represent an ideal rotational transformer for transmission ratio studies up to FEM models with contact descriptions for detailed study of the forces in the gear contact for optimal gear tooth design. In Figure 1.1 the different gear analysis and computational methods are shown which are used nowadays. On the left, the low complexity models are shown which are usually used by engineers who develop complete systems of which the transmission is only a small part of their systems (system designers). On the right the high complexity models that are used by engineers who focus on the optimization of tooth profiles for the best performance of transmissions. Both groups of engineers seem to have created their own set of analysis methods to help them perform their tasks as can be seen by the lack of overlapping methods for both system and gear designers.

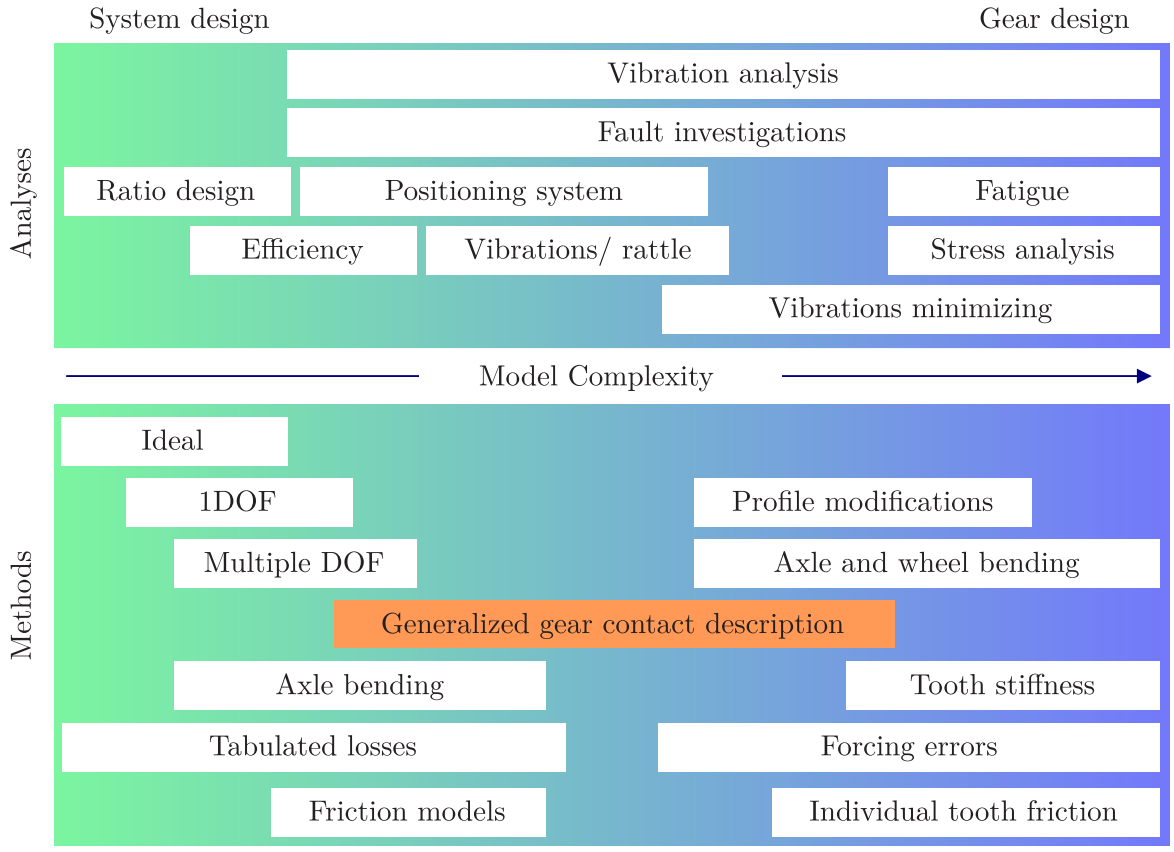

Figure 1.1: Overview of the in literature known analysis and methods of gear design. With the increasing model complexity, in most cases also the computational costs increase. The orange highlighted *Generalized gear contact description* is the topic of this thesis.

Figure 1.2: Antikythera mechanism fragment (fragment A) by User: Marsyas (2005). The mechanism consists of a complex system of 30 wheels and plates with inscriptions relating to signs of the zodiac, months, eclipses and Panhellenic games.

1.1 Gear history

Gear connections exist since around the 2th century BC, although legends date the first gearing mechanisms much earlier. A "south pointing chariot" is believed to be used already 4600 years ago (Yan & Chen, 2006). These chariots used differential gears to keep a pointer at the same direction, independent of the movement and turning of the chariot itself. Also Archimedes (287–212 BC) is believed to have used gears in odometers, but also in this case, no evidence is left.

The first evidence of gears are found in the Antikythera mechanism as shown in Figure 1.2 and is dated to approximately 150–100 BC (Freeth et al., 2006). The mechanism is believed to be one of the first analog computers. It consisted of at least 30 bronze gears and is believed to be a multifunctional device, which functions were amongst others the prediction of eclipses and the cycle of the Panhellenic games. Due to the high level of perfection of the gears, it is believed that gears have been used before this mechanism.

All these early devices have in common that the gears were not designed to carry loads, but only to generate a fixed transmission ratio. This transmission ratio was used for calculations: the prediction of events, the measurement of a distance or pointing to a certain direction. Since the Antikythera mechanism, many other applications have been found for gears of all forms: around 1180, the first windmills have been built which used cage gears followed by the first clocks which are based on gearing between 1280–1320. In 1894, Panhard et Levassor introduced the first modern gear transmission for passenger cars. They used discrete gear changes as done nowadays instead of a sliding transmission which was common for that time.

Although it is often thought that gears are a human invention, also in nature gear mechanisms occur as can be seen in Figure 1.3. The in Europe commonly found juvenile form of the insect *Issus coleoptratus*, a planthopper, uses a gearing mechanism to synchronize its hind-legs (Burrows

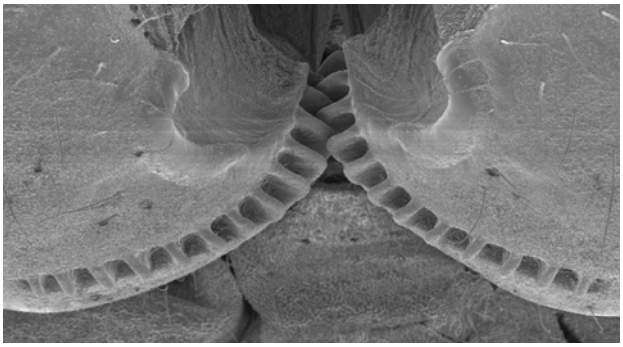

Figure 1.3: Scanning electron micrograph of the hind legs synchronizing mechanism of the Issus coleoptratus nymphs by *Burrows & Sutton*.

& Sutton, 2013). During a jump, the hind-legs of the *Issus* reach speeds up to 200 000 °/s. Without synchronization of the hind-legs, the juvenile insect would have problems to jump without getting into a spinning motion. These biological gears are therefore probably the oldest form of gears on earth.

1.2 State of the art gear modeling

Nowadays gear transmissions are widely used in many applications. Examples range from very large slow turning wind turbines, passenger car transmissions, aircraft turbine transmissions, geared electromechanical actuators for aircraft, positioning systems to very small geared systems etched in silicon (e.g. Dao et al., 2008). Due to the electrification of many systems where usually a high torque is needed, gear transmissions are often used to optimally load the electrical motor. A good example of electrification is the move from hydraulic aircraft actuators to electromechanical actuators. Weight benefits from removing the hydraulic system in an aircraft, leading to lower fuel consumption are envisioned. Also maintenance and production benefits are expected since electrical cables can be easier routed and cannot leak in contrast to hydraulic pipes.

Although gear transmissions have been investigated for many years, the upscaling of the gear transmission with high ratios as used in wind turbines often leads to problems. A study by Fischer, Besnard, and Bertling (2012) shows that gear transmissions account for approximately 9–13 % of all downtime accounts for transmission faults (including bearings). Especially emergency brake scenarios lead to very high loading of the gears as indicated in the report by Oyague (2009). The high vibrational loads with torque reversal during such an emergency brake operation can lead to very high internal gearbox loads.

Moreover commercial programs exist which can simulate geared transmissions in great detail. Examples of such specialized programs are *FVA-Workbench (FVA GmbH)* (2015), *CONCEPT (Romax Technology)* (2015) and *KISSsoft (KISSsoft AG)* (2015). These programs are developed for the design and analysis of gear trains. Gear- and bearing loads can be assessed for different load cases to optimize the gear design.

1.3 Literature overview

High quality research of gear transmissions is not limited to the last few decades. Buckingham (1949) has written a very interesting and extensive work in 1949. Partly due to the lack of powerful computers, he addresses all his calculations of gear connections with analytical methods. Also Niemann and Winter (1989) as well as Anderson and Loewenthal (1984) use analytical methods with multiple gear contacts and different friction models. For the calculation of the efficiency of a gear, an integral over a complete mesh cycle is used to average the losses. Since these methods are not made with time simulations in mind, the effect of the different frictions at different mesh positions cannot be used. However, the idea of averaging the gear friction over a complete mesh cycle can be redesigned for time simulations using computers. Due to the analytical nature of these methods, the computational costs are low.

Vibrations, noise and gear rattle can be caused by elasticity changes between the meshing teeth. These effects are well researched and are still an active field of research (e.g. Heider, 2012; Kahraman & Singh, 1990, 1991; Kohn et al., 2014; Russo, Brancati, & Rocca, 2009; Tangasawi et al., 2008). Due to the changing elasticity the system is excited internally when the system is loaded. Also forcing/ transmission errors can lead to vibrations, noise and rattle as they also excite the system internally (e.g Åkerblom, 2001; Henriksson, 2009; Ottewill, Neild, & Wilson, 2009). These transmission errors are often called forcing errors, as the geometric errors of the gear forces the gear wheels to move in a non ideal movement. It must be noted that in many studies, the analysis of gear rattle is done without analysis of the connecting drivetrain, as its main mode is the oscillation of free running of gear that impacts with the driving gears. This does not directly have an influence on the complete system. However, these impacts can potentially trigger eigenmodes of the coupled system, causing the system to resonate, which can lead to higher noise levels. Most of these studies on gear noise, vibrations and rattle are based on estimates of the varying stiffness and transmission error. However, the transmission error has also been experimentally investigated (e.g. Harris, 1958; Houser & Blankenship, 1989; Kohler & Regan, 1985; Sweeney & Randall, 1996). There is a consensus that the transmission error is often a combination of many different effects: manufacturing imperfections like misalignments, eccentricities, pitch errors and involute errors exist in all measured gears and play an important role in the internal excitation of the gear train. Since the transmission error is often partially caused by manufacturing errors, it can therefore change for each produced part in the same product series. First approaches to include the uncertainty of these manufacturing errors in the design process are now developed (e.g. Klocke, Brumm, & Hellmann, 2014). By including these manufacturing uncertainties in the design stage, it is possible to design tooth corrections which will be optimal for the complete set of produced gears. Such a design lowers the chances that an unlucky match of multiple manufacturing errors causes a malfunctioning system.

The damping of the gear mesh is hardly investigated. In most research works, either a model damping is added or a damping coefficient is assumed (e.g. Fakhfakh, Chaari, & Haddar, 2004; Harris, 1958; Yang, Shang, & Luo, 2013). This is probably due to the fact that measuring the damping of the gear is very difficult, since it is dependent on the lubricant and rotation speed.

To tackle problems where gear elasticity as well as friction play a role in the gear dynamics, Velex and Cahouet (2000) have developed a method in which they combine the sliding friction, tooth shape deviations and non-linear mesh stiffness in one model. To solve this model, several iteration loops are needed: First the contact points are iteratively found for the rigid bodies, thereafter in another iterative loop, the mesh stiffness is calculated and used to find the local deformations. Also He, Gunda, and Singh (2007b) have investigated gears with friction and elasticity. In contrast to

many other researchers, they use a full 3D friction and elasticity model to model the gear wheels in 3D. However, they do not use finite element code, improving simulation speed. The friction forces and moments are calculated based on pre-defined integrals and contact zones that describe which tooth pairs are in contact and if these contacts are before or after the pitch line.

Modeling of broken gears is also an active topic of research. The most active fields of research is the prediction of the behavior of damaged gears, which is used to identify the fault based on speed, current or other measurements. The modeling of the gears on this topic differs from position dependent varying stiffness to full FEM models. Some examples are Mohammed, Rantatalo, and Aidanpää (2015) who simulate a root crack followed by different detection algorithms like RMS, Kurtosis, and Crest[1] analysis, Kar and Mohanty (2008) who model and detect removed teeth using multi-resolution Fourier transformations and Wavelets and Jia and Howard (2006) who investigate a gear spall[2] and crack using FE analysis. They use a narrow band enveloping[3] method with amplitude and phase modulation to identify the fault from the simulation speed of the pinion as well as bearing vibration data. Hepermann (2013) studied the effects of various failures on the gear using experimental testing and numerical calculations.

A small amount of research is going to the analysis of gears used in positioning devices. In these devices, the gears seldom move at a constant velocity. This means that no steady state is obtained which complicates simulations and measurements. Since positioning applications are often preloaded by spring action or by gravity, stiction plays an important role in these systems. It seems that the major research groups who investigate the gear contact in great detail are not very much interested in such applications. Therefore, the sparse publications available are usually written by system engineers who need gear models for their control purposes. The models which are used in the studies are mostly descriptive models which deal with the mesh forces using a generalized friction which usually includes stiction, backlash and elasticity. Ahmed, Laghrouche, and El Bagdouri (2012) investigate the modeling of a geared air path actuator mainly for control applications. Their measurements clearly show the stiction of the system. They highlight that stiction, deadband (no output with changing input) and hysteresis have a big influence on the performance of the system. In a closed loop system, stiction often leads to hunting. They conclude that a good control system must compensate the nonlinearities of the system and therefore a good system description is needed. Garcia, de Santos, and de Wit (2002) point out that also in robotic legs driven by worm gears, stiction is a problem in low speed applications leading to stick-slip, making smooth movements of the robot legs very hard. Furthermore, they also observe a position dependent friction torque which leads to vibrations of the robot leg.

Most of the research discussed in this section is either done on an academic level, where very specialized implementations often limit commercial use, or is implemented in specialized commercial programs, which limit the use for system simulations since these programs cannot be coupled to complete system simulations. There are a few exemptions, where gearing models are implemented in a system simulation environment. The Modelica PowerTrain Library is nowadays often used in the automobile industry for simulations of the engine, clutch, gear and vehicle. These simulations are used for shift quality and handling studies as well as fuel economy optimizations on specified driving cycles. For these optimizations of drive cycles, a high simulation speed is crucial as these driving cycles are long: A complete European driving cycle (EXE-15)[4] consists of 1180 s, the

[1] Indication of the peakedness of a signal

[2] Cracking and flaking of particles out of a surface (ASM, 1999)

[3] Bandpass filtering followed by demodulation or rectification of the signal (Howieson, 2003)

[4] United States Code of Federal Regulations, Title 40: Protection of Environment, Part 86: Control of emissions from new and in-use highway vehicles and engines, 40 C.F.R.

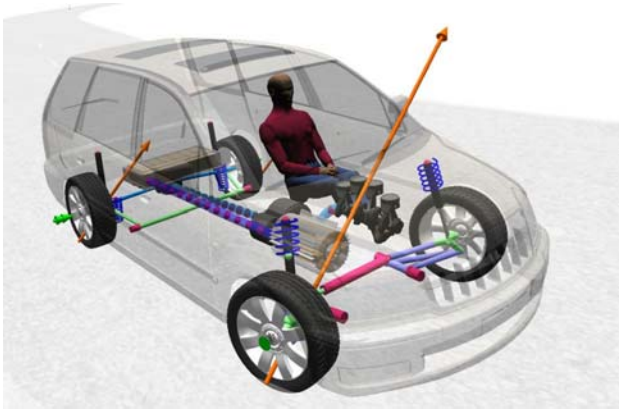

Figure 1.4: Modelica PowerTrain Library. This library is used for the simulation of powertrain and vehicle

US driving cycle (FTP-75)[5] of 2639 s. For an optimization of the gear train, thousands of such drive-cycles must be simulated to find the optimal solution. Pelchen, Schweiger, and Otter (2002) introduced a modeling of the gear contact in the PowerTrain Library that describes the gear contact as a friction using a state machine which allows a different set of equations for the *stuck* phase and the movement of the gear. The losses are based on tabulated values which allows to readily include measured values. Due to the fact that no contact searching algorithms are used, the models have a very high simulation speed. Also the multi-body package SIMPACK (Drivetrain) (Ebrahimi & Eberhard, 2006) has specialized gear elements to model a gear connection in a complete system. These contact elements can also be used on flexible gear wheels which can be implemented using reduced FE models. Specialized contact finding algorithms are used to identify all gear contacts of the flexible teeth. This implementation method greatly speeds up the calculations. With respect to full FE models, a decrease of the simulation time is reported from 22 h to 2.0 s for the simulation of 0.001 s. A further method without tooth flexibility mentioned in the same paper has a simulation time of 0.2 s for 0.001 s simulation time. Although these simulations are carried out on computers from 2006, the performance of the models on recent computers will probably not reach real time simulation capability. These SIMPACK models are currently used in the wind turbine industry for detailed simulations of the gear, including elastic housing and carrier. The housing elasticity must be included in such cases, as the eigenfrequencies of such gear housings in the range of 100–300 Hz (Marrant, 2012), which is in the range of the gear meshing frequency in many cases.

1.4 Relevance of research

When developing Health Monitoring (HM) algorithms for Electro Mechanical Actuators (EMA's) of aircraft, the only sensors which are often available are the on-board sensors of the actuator. Adding extra sensors increases costs, and decreases at the same time the reliability, which is not desirable. When a gear train of such an actuator must be monitored, the dynamics of the complete system is important. High frequent excitations by the broken gear can lead to changes in the sensor signals from the available sensors due to vibrations and position dependent effects like friction and stiffness of the drive train.

[5] United Nations Economic Commission for Europe, E/ECE/324/Rev.2/Add.100/Rev.3- E/ECE/-TRANS/505/Rev.2/Add.100/Rev.3

Figure 1.5: Electromechanical Actuator, ©Liebherr GmbH

It is usually not possible to do much testing, since such actuators are only available in a late stage of the design cycle and the costs as well as time investments involved with testing are very high. Thus, there is often no possibility to experimentally investigate the effects of faulty EMA parts. Gear transmission HM algorithms can usually not be designed separately from the complete EMA due to the stiff coupling and interacting system dynamics with the rest of the system. Therefore specialized gear programs cannot be used as they lack the possibility to represent the behavior of the complete system including power electronics, sensors, motor, aircraft structures and loading. Also generating a lookup table from these specialized programs and the integration in a system model is not possible as this approach cannot include the dynamics of the gear train.

In contrast, very detailed methods like FEM methods are prohibitively expensive since many and often long simulations must be run under many different conditions. Even multi-body methods like SIMPACK that use contact-finding algorithms on rigid wheels are prohibitively expensive when long time simulations are needed to check for false-positive results of the developed HM algorithm. As often the faults in the system cannot be predicted with high accuracy, an extremely high accuracy of the system simulations is not needed. Therefore, for these kind of developments, medium accurate models are needed which can represent the behavior of a system fault with low computational costs.

Depending on the task of an engineer developing an EMA, different models are needed to describe the different problems. The model requirements of a system engineer who is designing a geared electromechanical actuator for aircraft are completely different from the model requirements of a gear designer who focuses on the gear transmission of the EMA and who is optimizing the tooth forces on the gear flanks. To highlight the differences between the current design steps of both designers, they will be discussed in the next two sections.

Gear design - the point of view of a gear designer

The design of a high performance gear train often follows a design pattern (e.g. Kohn et al., 2014). This design pattern usually consists of multiple steps where the design of the gear is refined in each step:

- **Gear structure design**: The gear ratio is defined, taking into account parameters like the drive characteristics, volume constraints and energy efficiency. Furthermore the topology of the gearbox is determined. The amount of stages to reach the specified gear ratio is set and the gearing configuration must be fixed. Often, a trade-off between configurations like multiple spur gears or epicyclic gearing configurations must be made.
- **Main geometry design**: The rough design of the gear geometry from the load capacity is made. In this design stage, the gear flank width and size of the gear wheels are defined.
- **Elasticity and lifetime analysis**: The shaft and bearings are designed. Detailed shaft and bearing deformations are taken into account as well as eventual housing flexibility. The bearing lifetime is calculated from anticipated loading scenarios.
- **Flank geometry design**: The flank loading is analyzed in detail taking into account the bending of the axis and the bearing deformations. Based on this analysis an iterative process is started to optimize the flank for optimal load capacity and low excitation of the system. The goal of this step is to design the flank modifications.

The gear designer uses advanced design tools like *FVA-Workbench* or *CONCEPT* by Romax Technologies to develop an optimal gear train. However, these tools can nowadays not be coupled to complete system simulations, which makes it almost impossible to design an optimal system as no overall system performance can be assessed. At the moment, the gearbox is usually designed to given specifications. Therefore, to be able to make an optimal gear design, the gear designer must rely on accurately and detailed specified design parameters to assure an optimal gear design from an overall point of view.

Gear design - the point of view of a system designer

A system engineer/ system integrator who is building e.g. a geared electromechanical actuator for an aircraft, faces many and often contradicting problems: The actuator should be lightweight and have a good performance, should be highly reliable and should operate at temperature constraints often ranging from $-55\,°C$ to $70\,°C$. Nowadays, Health Monitoring algorithms are often also required (e.g. Todeschi & Baxerres, 2014) to avoid jamming of aircraft actuators and save cost applying condition-based maintenance. Furthermore the cost of the actuator should be kept low. To systematically develop such an actuator, the design goes through multiple stages. The typical development stages specified by Airbus for aircraft design are divided into 4 major phases: concept phase, system specification phase, system development phase and system verification phase (Giese et al., 2010).

- **Concept phase**: In this stage the performance and functional requirements are fixed and the overall configuration of the system is designed. The design questions of the transmission focuses on the amount of gear stages and the interaction with the electrical motor. A trade-off study between the torque of the motor and the amount of gear stages is carried out. In this stage, the gear is usually modeled without elasticity and incorporate simple friction estimations (e.g. 3% friction loss per stage).
- **System specification phase**: Based on the design from the concept phase, the design is further optimized. Nonlinear motor models including saturation will be used. To describe the gear transmission, models which include friction and temperature dependency to cover

the operational range of the actuator are needed. Furthermore, first control algorithms will be developed to prove the working of the system. The needed sensors must be specified. Optionally, the approach to monitor the actuator for faults is ready.

- **System development phase**: Component tests are carried out to ensure the designed components meet the specifications. These test results are used to improve the model validity. For the motor, position dependent effects like cogging will be included and the model parameters updated with the measured results. The gear models have to include detailed friction effects including stiction and elasticity. The controller architecture is fixed and a first controller design is ready. Furthermore, position dependent effects like transmission errors and stiffness variations should be included to ensure the operation of the final actuator and describe the system in a faulty situation. Models which represent the fault behavior of the components to be monitored are ready and tested with the health monitoring algorithms. This usually involves many *what-if* scenarios: What does happen if sensors with better accuracy are chosen? How does the noise of the sensors influence the system performance? What is the influence of varying friction of the gear on my system performance? What happens if a analog filter is added to the sensor signals? In most cases, the system designer is looking for qualitative results which help him to understand the system. The accuracy of the sensors and converters is specified to meet the control and monitoring specifications.

- **Verification phase**: The actuator has reached maturity and (prototypes) are produced. Control design as well as optional health monitoring functions are implemented. In this phase, system tests are carried out to validate the models. These models can be used for virtual testing. Monte Carlo simulations (e.g. Metropolis & Ulam, 1949) can be carried out to prove that even with uncertain model parameters, the system works correctly. This virtual testing can play a crucial role in acceptance testing, as usually not all fault scenarios and parameter variations can be tested. Therefore, the models must be able to describe the system under all circumstances, including the system in a worn state. Furthermore they should be able to accurately describe the faults in the system.

The model accuracy increases when more information becomes available and there is need for a more accurate description of the actuator. These development stages therefore clearly depict the need for different models during the design. The goal of such design methodologies is to prevent design faults. These design faults can quickly become costly and can lead to large delays. What also must be noted, is that a typical system designer is usually not using specialized gear development tools. This is caused by the fact that the gear design is usually done by a specialist, either in-house by a different department or outsourced to specialized companies. The transmission is, from the point of view of the system designer, a part which has to be specified and is not developed by him. The gear transmission is therefore handled just like an electrical motor or a ballscrew.

A system designer often cannot properly specify his needs to the gear designer. On the other hand, the gear designer, lacking proper specifications, cannot design the optimal gearing solution. To create the optimal system, a model and design gap must be bridged to allow the engineers to simulate the influence of these gearing effects in system models. The overall assessment of the system can lead to a better design of the system with is the optimum between weight, cost and performance.

1.5 Problem description

The research in this thesis is driven by the need for gear models for the development of Health Monitoring (HM) algorithms and controllers for Electromechanical Actuators (EMA's) for aircraft. Such actuators are historically hydraulic actuators with a low jamming risk. However, the move to EMA's also increases the jamming probability of these actuators. Since a jamming actuator can in some cases lead to the loss of the airplane, the jamming probability must be very low. Due to the many parts in such an actuator combined with weight and construction envelope constraints, the jamming risk can often not be reached using mechanical means. The severity of this problem can be understood when one realizes that even explosive releases are considered for passenger aircraft (Stridsberg, 2005). To mitigate the jamming risks, there are big research efforts in multiple (international) research programs such as *LuFo V-EMA*[6], *ACTUATION 2015*[7], *Vivace*[8] and *OMAHA*[9]. The main research effort to reduce this jamming probability is the use of Health Monitoring algorithms.

On first sight, the modeling of aircraft actuators seems to be an easy task. However, this needs a multi-disciplinary approach as such actuators are highly dynamic and a great interaction between the parts is given. Furthermore, the environmental conditions of these actuators are challenging: An aircraft must reliably operate after the start from a desert where the aircraft has been parked in the sun for multiple hours heating up the actuator to 70 °C But also while flying at 10 km height where the temperature of the actuator can reach −55 °C, such an actuator must operate as specified. Such temperature changes have a great influence on the lubrication, leading to very different friction at these extreme temperatures. Also aerodynamic forces lead to preloading of the actuator which leads to high breakout forces of the gears. Moreover, temperature constraints as well as aircraft approval certifications limit the available sensors and processors leading to high noise and often low discretization of the analog signals. Due to the weight constraints, the electrical motors are usually operated in the saturation regime, leading to high nonlinear behavior. In most cases, the control of the actuator must include the high bus delays from the aircraft flight computer. Altogether, a complete EMA is a surprisingly complex system to model.

To develop health monitoring algorithms, accurate models which can represent the behavior of an EMA are needed. However, in most cases not much data is available of these EMA's. Especially in the system specification phase, as the algorithms should be developed in parallel with the actuator, hardly any friction data is available. On the other hand, detailed information is needed for the design: To be able to find faults in the final actuator, the correct accuracy of sensors and analog to digital converters must be determined in the system specification phase or early into the system development phase.

1.6 Contributions of this thesis

As outlined in the previous sections, there is a need for suitable gear models for the development of HM algorithms. Therefore a library with gear models has been developed. This library includes nonlinear mesh stiffness and friction descriptions. Gears in nominal state and the behavior of gears with defects can be represented. For the development of this library, further applications have been considered: gear trains for electrical cars, especially using Torque Vectoring Drives (TVD) (e.g.

[6] See e.g. `http://www.bmwi.de/DE/Themen/Technologie/schluesseltechnologien,did=232982.html`
[7] See e.g. `http://www.actuation2015.eu`
[8] See e.g. `http://www.transport-research.info/web/projects/project_details.cfm?id=11092`
[9] See e.g. `http://www.dfki.de/web/research/projects?pid=909`

Gwinner, Otto, & Stahl, 2014; Shibahata, 1995) as well as wind turbines gearboxes. These models have been developed from the point of view of the system designer. However, gear designers who need more detailed system information can also use these models.

The main contribution of the thesis are the models that bridge the gap between fast, but inaccurate models currently used for system design and highly detailed models for gear design. The proposed model includes:

- Static forcing errors/ transmission errors,
- Nonlinear tooth stiffness,
- Position dependent tooth stiffness,
- Position dependent friction models including stiction.

The developed models are implemented in a new Modelica library. This library is developed in a way that avoids the direct implementation of the stiffness and friction variation caused by the meshing gear tooth. To include the effect of these variations, only the effect thereof is implemented. This makes it possible to reduce the system complexity and speeds up the simulation. To achieve such a fast and accurate gear model, the gear contact is analyzed in detail. Thereafter the model complexity is reduced with an averaging method that avoids costly contact searching methods. Using this approach, it is possible to simulate complete systems with multiple gear connections. Examples of such complete system simulations are aircraft simulations with high fidelity EMA models and an electric vehicle with an advanced gearing concept (see Chapter 5).

Another major contribution are the position- and load dependent measurements of the stiffness and friction of a healthy and damaged gearset. They allow the validation of the models which are developed in this thesis. Furthermore, these measurements of a broken gear set give insight into the behavior of gears in a not-optimal state. Such results are of great value for the development of health monitoring algorithms, as they show the behavior of broken, but still running gear.

Other contributions of the thesis are concepts that allow these models to be used on a day by day basis by system engineers in the design process of a system with gear transmission:

- **Models to support system designers during the design cycle**: The need for different models during the design steps from system design to system acceptance is covered. The transition between the complexity levels of the models is smooth and without redesigning the system model.
- **Models supporting epicyclic gearing**: To model all possible gear configurations, the developed models are planar models. Using a planar environment, the complexity of the system is kept low, while still representing the full movement of the gear wheels.
- **Gear models of a gear with a damaged tooth**: Models of defective gears have been developed to aid the development of health monitoring algorithms. This enables simulation of broken components to give insight to the behavior of the system in a defective state. Since hardware tests can usually be only executed very late in the design process, this helps the system design in an early phase. Furthermore, due to the amount of failure possibilities, it is often impossible to test all cases on a test rig.
- **Parametrization of the gear for system engineers**: The parametrization of the gears is possible by system engineers with only minor gear knowledge. More advanced parametrization bridges the gap between the system engineer and gear designer.

- **Validation of the developed models using hardware**: Measurements have been done for healthy as well as broken gears to validate the generated models for special cases.

1.7 Thesis outline

The outline of the main body of the thesis is following:

- Chapter 2 presents the main theoretical contribution of this thesis. The forces on a gear contact are systematically analyzed. By averaging these forces over the whole contact, a gear contact model is developed that includes gear friction without tracking the gear contacts.
- A gear test rig is developed to measure the stiffness and friction of gear contacts in Chapter 3. The specifications and setup of the rig are highlighted in this section.
- In Chapter 4, the models presented in Chapter 2 are extended to represent the effect of forcing errors as well as position dependent stiffness and friction variations. In this chapter, also the measurements of the gear test rig are presented and compared with the models.
- To showcase an implementation example of a complete system with integrated gear transmission model, an electric car with Torque-Vectoring Drive is used. The example shows, based on a realistic example, that it is important to do complete system simulations while some effects only occur when the complete system is simulated.

  The appendices contain further repeated measurements (A) and the development of the first implementation of a planar elastic gear (Appendix B) in Modelica in combination with an eigenfrequency analysis using these models. Furthermore, in Appendix C, a method to systematically introduce faults in the Modelica language is developed. This work is used throughout the thesis to enable the faults in the simulations.

2 Modeling and validation of gear contacts with elasticity and friction

As motivated in the introduction, models that can be used to bridge the gap between system design models and gear design models are needed. Therefore, a gear model is developed which includes friction and elasticity of the gear contact in a single model. This also enables the possibility to study stiction effects. Multiple well established friction and elasticity models will be included. The presented models are based on a 2D (planar) approach and the stiffness and friction description are validated using a test rig which will be presented in Chapter 3. This approach inherits elements of existing 1D models, but overcomes their limitations. It extends the models from a previous publication, which only included elastic effects (see Appendix B, F. L. Van der Linden (2012)).

Multiple modeling approaches have been investigated in the frame of this thesis before the modeling approach to include friction and stiffness as presented in this chapter was developed. These early investigations were limited to rotational systems plus two bearing stiffnesses (F. L. J. Van der Linden & Vazques de Souza Silva, 2009) as shown in Figure 2.1. The friction used in this early approach was heavily based on the 1D gears from Pelchen et al. (2002) and shared the same way of implementation as introduced in Otter, Elmqvist, and Mattsson (1999). In the work of Pelchen et al., the gears are rigid and represent the friction by a tabulated efficiency. This efficiency is dependent on the direction of the energy transfer through the gear. The state machine depicted in Figure 2.2 is used to handle the transition between the operational modes (forward, backward, stuck). Depending on the operational mode, the appropriate equations to describe the friction are selected. To switch between these modes, two further auxiliary modes are used to enable reliable switching from the stuck mode to the forward or backward mode (StartForward and StartBackward).

In the stuck mode[1], the velocity of the gears is forced to zero, and the differential equations are reordered so that instead of calculating the friction force from the load and speed of the gear, the friction force needed to prevent the gear from moving is calculated. To be able to reuse the approach from Pelchen et al. (2002) in a model that combines friction and elasticity, the stuck mode must be handled similarly. By fixing the speed at which the gears move through point P to zero (see Figure 2.1) instead of fixing the velocity of the gear wheel to zero, a similar approach as Pelchen et al. could be achieved. This approach assumed that all forces needed to keep the mesh speed to zero could be transferred to the support of the gear. During further research, it became clear that this approach has two drawbacks when epicyclic gear connections are used: At first, such epicyclic gear connections cannot transfer the force to the support, as there is no support available in such gearing configurations. Secondly, the decoupling of the systems which is caused by the fixing of the mesh speed does not happen in reality as forces can still be transmitted from one gear wheel to the other.

By including elasticity in the gear contact, the motion of the gear wheels cannot be represented

[1] The stuck mode is the mode of a gear where the gear preload prevents gear motion

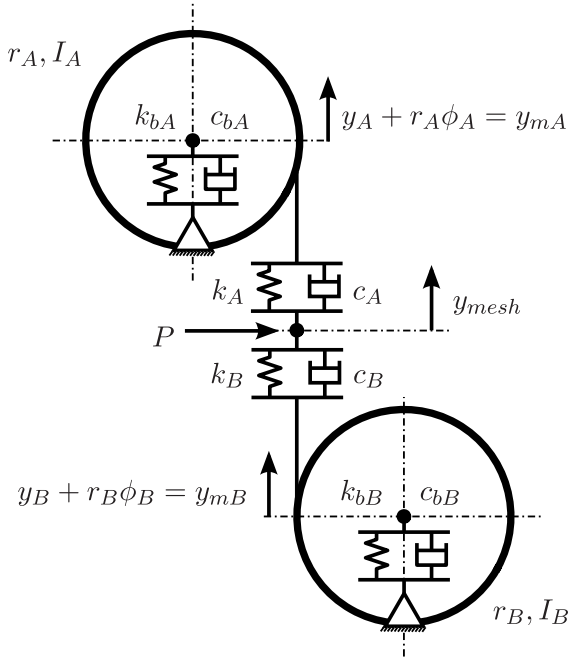

Figure 2.1: 3-DOF elastic gear model as presented in (F. L. J. Van der Linden & Vazques de Souza Silva, 2009)

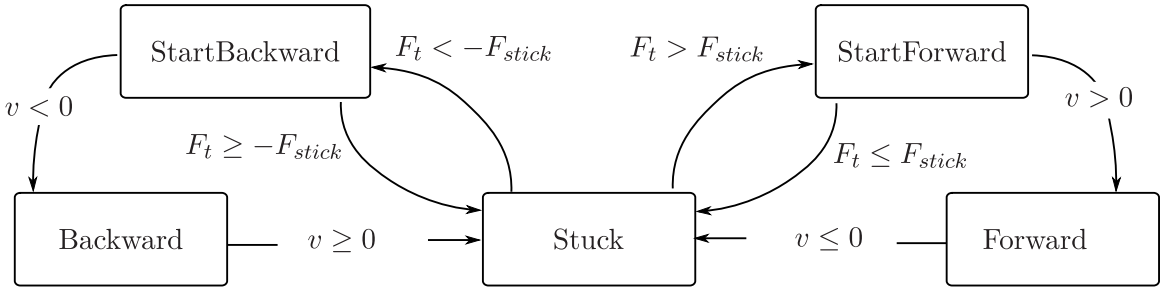

Figure 2.2: State machine as used by Otter et al. (1999) and Pelchen et al. (2002)

anymore by geometric relationships. This limits the use of 1D contact descriptions to rigid gear connections (e.g. Modelica Powertrain Library[2]).

Therefore the approach using a 1D model to describe the gear contact has been abandoned and a new way is investigated to include friction and elasticity into the gear models. In this Chapter, a two-dimensional analysis of the forces and torques is introduced which is needed to represent a generalized gear contact. This theory will be used throughout this thesis as the main friction and elasticity theory for all gear models. The presented implementation method to model gear friction and stiffness in the same model will be further extended in Chapter 4. Multiple position dependent effects will be added: forcing error, stiffness and friction.

The remainder of this chapter is based on work published by the author in *Proceedings of the Institution of Mechanical Engineers, Part C: Journal of Mechanical Engineering Science* (F. L. J. Van der Linden, 2015).

[2]The gear train models of the Modelica Powertrain Library are built around the work of (Pelchen et al., 2002)

2.1 Problem description

To be able to describe the gear contact with sufficient detail for the development of (positioning) control- and health monitoring algorithms, the following requirements must be met:

- Integration of the gear model into complete system models for control and health monitoring design,
- Modularity to enable different friction laws as well as different stiffness models,
- Fast simulation performance to support optimization runs using a complete system model,
- Operation in all quadrants since the power flow is often reversed in positioning applications,
- Sticking of the gear: The breakout force/ torque at zero speed must be able to accommodate non steady friction coefficients to deal with static/ dynamic friction coefficients.

Since the model performance must be high enough for complete system simulations and optimization runs, contact searching algorithms (e.g. Ebrahimi & Eberhard, 2006) are prohibitively expensive. By avoiding these contact searching algorithms, the deformations of bearings, axis and teeth cannot be taken into account for the calculation of the gear forces. Instead of finding the contacts positions, the gear forces must be estimated using average friction forces. To be able to model position dependent effects caused by the tooth contact, pre-calculated values can be used.

In this work, a new modeling level is presented. It is aiming at enabling the system engineer to model gear components with just enough details to allow accurate system level analysis and design. In this paper, the approach to reach this modeling level is outlined.

The specificities of the approach is outlined next.

2.2 Gear forces

The forces acting on the rotational axis of a spur gear set are shown in Figure 2.3. These forces and torques are needed for a full planar description of the two gear wheels and will finally be used for the interface to the planar multi-body Modelica environment. For the calculation of these forces, the individual tooth forces are analyzed and averaged over the contact length. This enables fast calculations by pre-calculating the contact parameters of the teeth. By using a position dependent averaging, it is possible to include the effects of multiple teeth contacts.

2.2.1 Gear contact description

The gear contact is considered to be an involute gear contact since this is the most used gear connection in engineering applications. In Figure 2.4, a schematic overview of two gear wheels in contact is shown as is commonly used in literature (e.g. Buckingham, 1949; DIN 3990 Teil 4, 1987; Niemann & Winter, 1989). In this Figure, the contact point C moves along the green line of action. [3] The position of the contact point on this line is given by d_A (and consequently d_B). The gear ratio is defined by $\frac{r_A}{r_B} = \frac{l_A}{l_B} = i$. This ratio is constant for each gear contact point. d_A, d_B, r_A and r_B are defined in Figure 2.4. The contact angle $\phi_{contact}$ defines the orientation of the line of action.

[3] In this work, the commonly used notation C for the contact point and P for the pitch point has been used. This is different to the notation used in the DIN, ISA and AGMA standards where P is the contact point and C the pitch point.

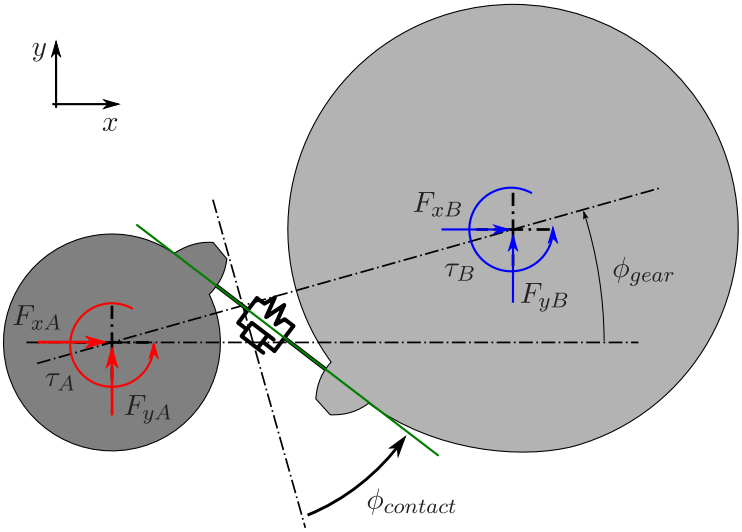

Figure 2.3: Basic gear forces on the contact of a single tooth.

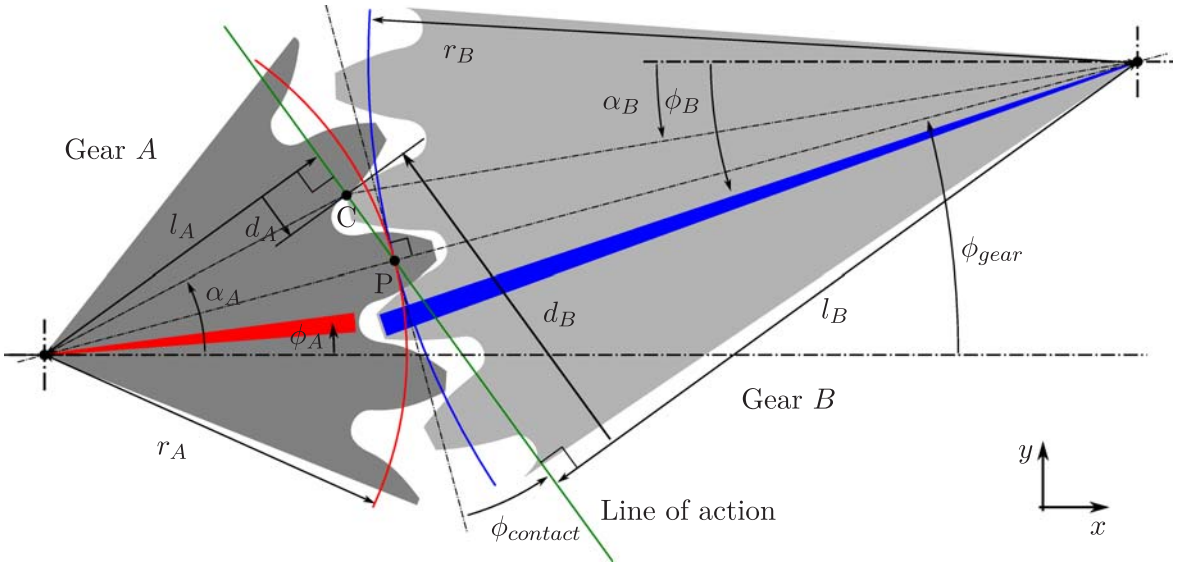

Figure 2.4: Schematic overview of two involute gears in contact. The blue and red triangles are fixed markers on the gear wheels. In the figure $\omega_A < 0$ and Gear A drives gear B.

This contact angle is dependent on the loading direction; in the case where gear A drives gear B the $\phi_{contact}$ is as displayed in the Figures 2.4 and 2.5, in the opposite case where B drives A, the other side of the gear teeth are in contact and therefore $\phi_{contact}$ will be negative.

Figure 2.5 shows a free body diagram of the two gears in contact. The forces of only one contact point are displayed. Using Figure 2.5, it is possible to create the torque and force balances of each gear wheel. These forces and torques are resolved in the fixed coordinate system shown in this Figure. Instead of using a gear-fixed coordinate system, a fixed coordinate system and variable gear angle ϕ_{gear} is used, which defines the rotation of the gear system with respect to the reference frame. This makes it possible to use the contact model also in more complex gear systems with multiple gear contacts (e.g. all kinds of Epicyclic gearing configurations). The resulting forces for this gear contact are:

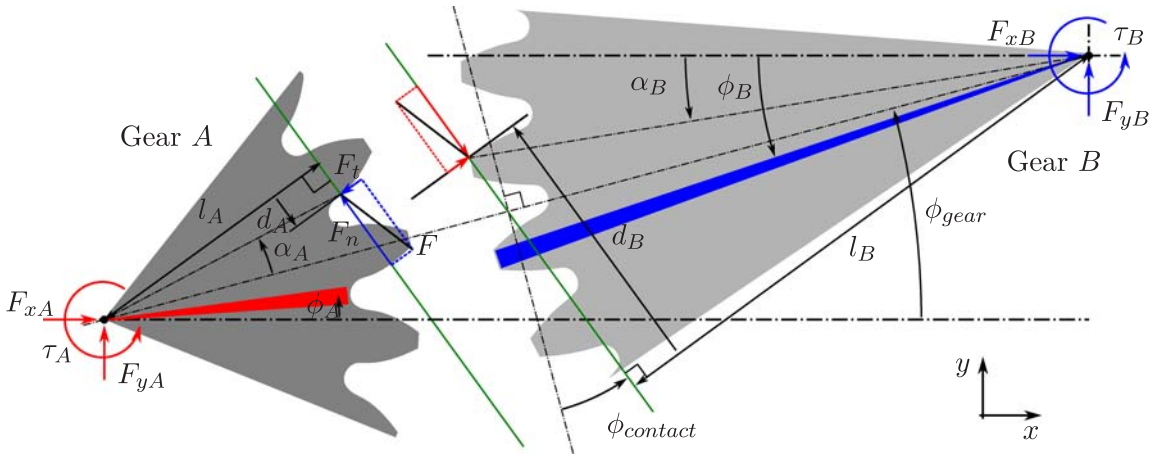

Figure 2.5: Free body diagram of two involute gears. In the figure $\omega_A < 0$ and Gear A drives gear B.

$$\tau_A = F_n l_A - F_t d_A \ , \tag{2.1}$$
$$\tau_B = F_n l_B - F_t d_B \ , \tag{2.2}$$
$$F_{xA} = -F_n \sin(\phi_{gear} - \phi_{contact}) - F_t \cos(\phi_{gear} - \phi_{contact}) \ , \tag{2.3}$$
$$F_{yA} = F_n \cos(\phi_{gear} - \phi_{contact}) - F_t \sin(\phi_{gear} - \phi_{contact}) \ , \tag{2.4}$$
$$F_{xB} = -F_{xA} \ , \tag{2.5}$$
$$F_{yB} = -F_{yA} \ . \tag{2.6}$$

Note that the lengths d_A and d_B are changing depending on the position of the contact on the line of action.

2.2.2 Introduction of mesh distance, mesh velocity and mesh deformation

For the calculation of the (position dependent) gear forces and friction, the mesh position x_{mesh}, the mesh deformation Δ_{AB} and the mesh velocity v_{mesh} will be needed in following Sections. In this Section, these terms will be introduced.

To keep track of how the gear wheels move with respect to each other, the mesh distance x_{mesh} is introduced. The distance x_{mesh} can be calculated for both gear wheels and is defined as the distance the gear wheels have traveled through the meshing point P (see Figure 2.4 for reference on the definition of the variables). The total meshed distance can be calculated for both gearwheels:

$$x_{mesh,A} = \phi_A r_A - \phi_{gear} r_A \ , \tag{2.7}$$
$$x_{mesh,B} = -\phi_B r_B + \phi_{gear} r_B \ . \tag{2.8}$$

In these equations, r_A and r_B are the pitch radii from gear A and B. From Equations (2.7) and (2.8) it becomes clear that the mesh distance ($x_{mesh,A}$ or $x_{mesh,B}$) can be constant although the gear wheels are rotating. This is the case if $\phi_A = \phi_{gear}$ or $\phi_B = \phi_{gear}$. This is not only a theoretical implication; in a Ravigneaux gearset used as differential for example this is often the case. Note that the gear axis have to be constraint on a distance $r_A + r_B$ as a relative motion will alter $x_{mesh,A}$ and $x_{mesh,B}$.

The mesh deformation represents the difference between the mesh positions. It is defined by the deformation of the gear contact including tooth bending:

$$\Delta_{AB} = x_{mesh,A} - x_{mesh,B} \ . \tag{2.9}$$

For position dependent stiffness and friction effects, the average mesh position is needed. It is assumed that the deformation of the gear wheels is equal: Gears with higher number of teeth have a relatively high tooth bending, which is compensated by the stiff tooth contact (due to the low curvature). For gears with a lower number of teeth, the effect is the other way around: The low tooth bending is compensated by a lower contact stiffness caused by the higher curvature. The mesh position is defined as:

$$x_{mesh} = \frac{x_{mesh,A} + x_{mesh,B}}{2} \ . \tag{2.10}$$

The average mesh velocity is given by differentiation of the average mesh position (2.10) with respect to time. This velocity represents the feed velocity of the gears through the meshing point P.

$$v_{mesh} = \frac{\dot{x}_{mesh,A} + \dot{x}_{mesh,B}}{2} \ . \tag{2.11}$$

2.2.3 Friction Force

The friction force F_t is dependent on the normal force F_n and the sliding speed v_s between the gears. To calculate the sliding speed, the gear contact is examined: In Figure 2.6 and 2.7, the gear contact in two different loading conditions is shown. In these Figures, T_1 and T_2 are the contact points of the line of action and the base circle of gear A respectively B. The mesh contact is from point A to B. Point A is the first contact point of the mesh and is defined by the intersection between the line of action and the addendum circle of gear B. Point B is the last point of contact and is defined by the intersection from the line of action with the addendum circle of gear A. The meshing point P is the intersection of the line $O_A O_B$ and the line of action. It is also the position where the pitch circles of gear A and B are touching.

The tangential velocities of the gears A and B ($v_{t,A}$ & $v_{t,B}$) are defined as the velocity of each gear at the contact point C perpendicular to the line of action. These velocities in the tangential direction are obtained by a multiplication of the rotational speed (ω_A, ω_B) by the arm perpendicular on the tangential velocity (d_A, d_B).

$$v_{t,A} = \omega_A d_A \ , \tag{2.12}$$

$$v_{t,B} = \omega_B d_B \ , \tag{2.13}$$

where is used: $\omega_A = \dot{\phi}_A$ and $\omega_B = \dot{\phi}_B$.

In Figure 2.6, the tangential velocity for each possible gear position is highlighted for the indicated case. The red triangle is the tangential velocity of Gear A, the blue triangle the tangential velocity of Gear B. The magnitude of the tangential velocity is shown by the size of the triangle. The relative tangential velocity v_s between gear A and B is the sliding velocity which occurs in the contact point. A more detailed description can be found in gear design books (e.g. Buckingham, 1949; Niemann & Winter, 1989).

$$\begin{aligned} v_s &= v_{t,A} - v_{t,B} \ , \\ &= \omega_A d_A - \omega_B d_B \ . \end{aligned} \tag{2.14}$$

Note that at pitch point P, the relative tangential velocity is zero as expected (pure rolling at the pitch circle).

The friction force F_t is defined using the speed dependent friction coefficient $\mu(v_s)$, which can also be written as $\mu(v_{mesh}, d_A)$ since the sliding velocity is dependent on the total mesh speed v_{mesh} and the distance d_A (see Figure 2.4 and 2.6). This yields:

$$F_t = \begin{cases} s_v(v_{mesh}, d_A)\mu(v_{mesh}, d_A)|F_n| & \textbf{if } v_{mesh} \neq 0 \\ & \textbf{or } |F_t| \geq |\mu(v_{mesh}, d_A)F_n| \\ \text{so that } v_{mesh} = 0 & \textbf{if } v_{mesh} = 0 \\ & \textbf{and } |F_t| < |\mu(v_{mesh} = 0, d_A)F_n| \end{cases} \tag{2.15}$$

In Equation (2.15), s_v is the sign of the sliding velocity v_s. The normal force F_n must be absolute since it does not matter which gear face is pressed on the other. The second part of the equation deals with the results in the case of $v_{mesh} = 0$. In this case, the friction force F_t is calculated as the force to keep the mesh velocity v_{mesh} zero. This is the case as long as $|F_t| < |\mu(v_{mesh} = 0, d_A)F_n|$, as this is the upper bound of the friction at zero mesh velocity.

In Figure 2.7, a different loading condition is shown. In this loading condition, the line of action is flipped and therefore the contact points are different. Using the same analysis, it is possible to define $s_v(v_{mesh}, d_A)$ also for the load-case shown in Figure 2.7. To deal with the other two gear loading possibilities, the gear velocities must be inverted. This inversion leads then directly to the inversion of $s_v(v_{mesh}, d_A)$. Using this property, it is possible to create an overview of all possible conditions. This overview is given in Table 2.1. In this table, $s_{v,AP}$ is the sign of the sliding velocity $s_v(v_{mesh}, d_A)$ between point A and point P, $s_{v,PB}$ between P and B.

Table 2.1: Sliding velocity of contact point of each loading condition. The quadrant is the operational mode of the gear.

v_{mesh}	Power flow	F_n	$\phi_{contact}$	Quadrant	$s_{v,AP}$	$s_{v,PB}$
> 0	$A \to B$	> 0	< 0	1	1	-1
	$B \to A$	< 0	> 0	2	-1	1
< 0	$B \to A$	> 0	< 0	3	-1	1
	$A \to B$	< 0	> 0	4	1	-1
$= 0$	-	-	-	0		

2.3 Individual Gear Tooth Forces reduction to overall Gear Forces

In the previous section, all gear forces are defined for a single tooth contact of a spur gear. Using a contact finding algorithm, this could be directly implemented. However, for an efficient simulation of large systems, such contact searching algorithms must be avoided. To avoid these contact searching algorithms, two approaches are possible:

1. Generation of a lookup table which expresses the gear forces τ_A, τ_B and F_t as function of F_n, v_{mesh}, $\phi_{gear} - \phi_{contact}$ and the exact gear geometry.

2. Construction of an analytical function which approximates the gear forces based on averaging.

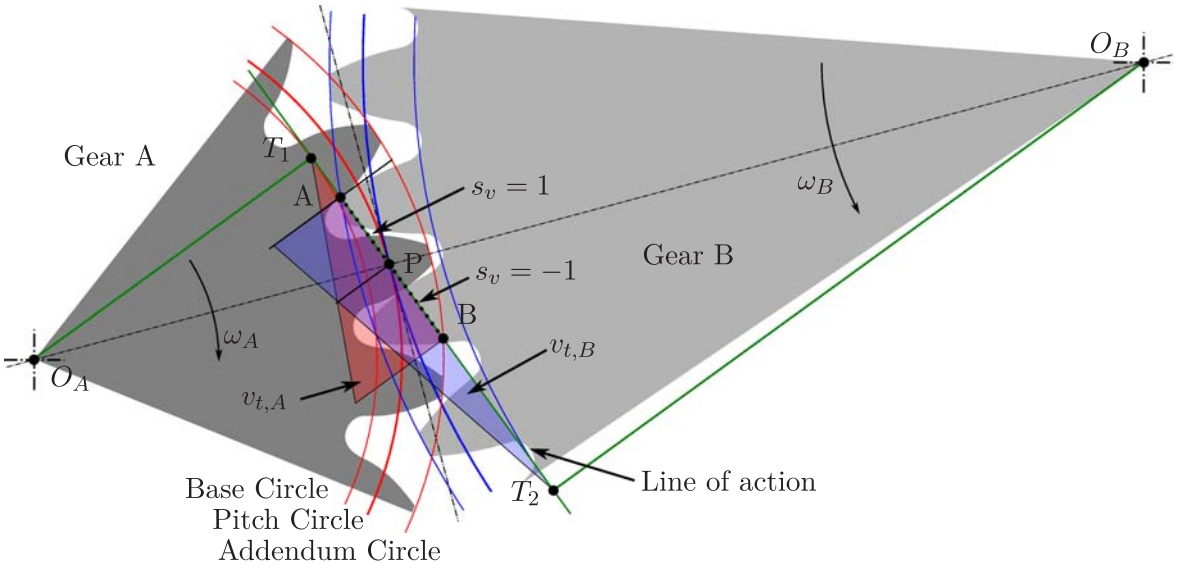

Figure 2.6: Schematic overview of two involute gears in contact operating in quadrant 4: Gear A drives gear B, the rotational speed is indicated by the direction of the arrows next to ω_A and ω_B ($\omega_A < 0 \vee \dot{\phi}_{gear} = 0 \Rightarrow v_{mesh} < 0$). The contact angle $\phi_{contact}$ is positive.

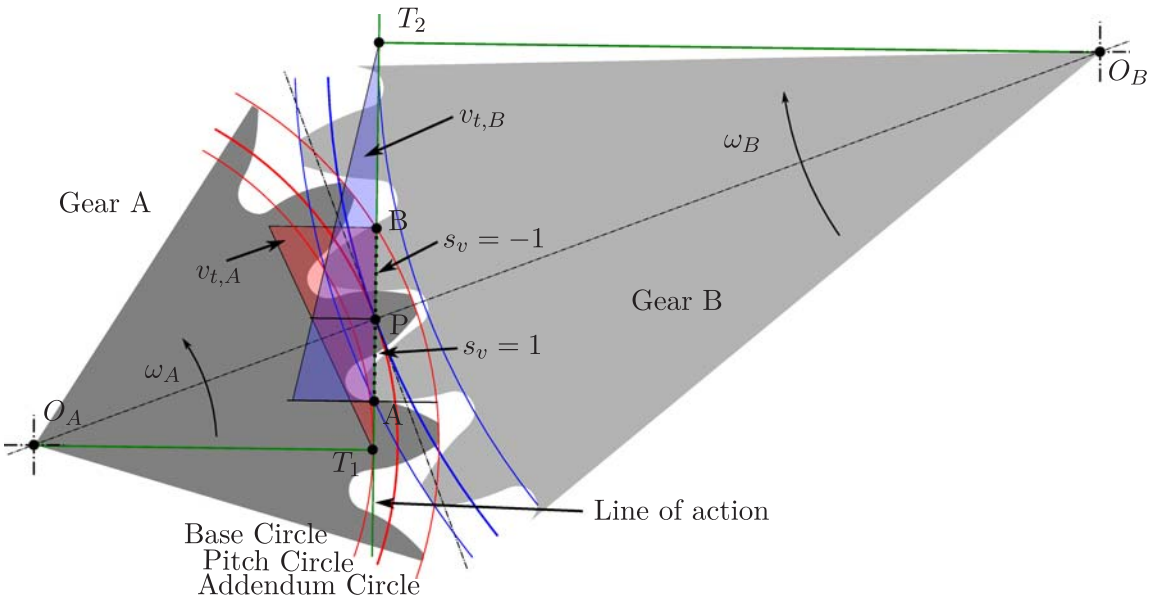

Figure 2.7: Schematic overview of two involute gears in contact operating in quadrant 1. Gear A drives gear B, the rotational speed is indicated by the direction of the arrows next to ω_A and ω_B ($\omega_A > 0 \vee \dot{\phi}_{gear} = 0 \Rightarrow v_{mesh} > 0$). The contact angle $\phi_{contact}$ is negative.

To generate an accurate lookup table, the gear geometry and properties must be precisely known to cover all of its effects. Including the influence of deforming teeth on the gear properties, the gear contacts must be assessed for all operating conditions using specialized programs (e.g. Kissling & Raabe, 2006). For the study of broken parts, pre-design or the generation of detailed gear specifications, this approach cannot be used as the design of the gear is in most cases not known. In this case, an approximation must be made based on available knowledge. This approximation should be able to include the effects of gear meshing, without modeling the individual contact.

On the other hand, it is possible by averaging the friction forces to obtain an analytical function expressing the friction forces on the gear. This approach makes it possible to obtain a sufficiently detailed model without an accurate knowledge of the system geometry, which makes it suitable for pre-design stages and cases where the exact geometry is not known. To obtain the analytical function, several assumptions have to be made.

Anderson and Loewenthal (Anderson & Loewenthal, 1980) calculate the average power loss over a tooth contact to calculate gearbox efficiencies. To do so, the integral of the power losses over the contact length is divided by the contact length. To calculate the mean friction forces, a similar approach is used in this paper. The average friction force is obtained by integrating the friction forces over the contact length and dividing by the integral of the contact position (total contact length)

$$\overline{F}_t = \frac{\int_A^B F_t(d_A)\,\mathrm{d}d_A}{\int_A^B \mathrm{d}d_A} \tag{2.16}$$

To calculate the average friction force, the integral must be split in multiple parts to take the discontinuity of the normal force over the contact length into account, which is caused by different contact ratios [4]. The varying normal force and tooth contacts are shown in Figure 2.8. For a tooth ratio between 1 and two, the gear contact points vary between one and two. When a constant torque is given to the gear wheels, the tooth load for a single contact is double the load as for a double contact, since the load is shared between both contact points. Assuming a contact ratio between one and two, the integral must be split into three parts to take the discontinuities of the normal force into account:

$$\overline{F}_t = \frac{\int_A^{X1} F_t(d_A)\,\mathrm{d}d_A}{\int_A^{X1} \mathrm{d}d_A} + \frac{\int_{X1}^{X2} F_t(d_A)\,\mathrm{d}d_A}{\int_{X1}^{X2} \mathrm{d}d_A} + \frac{\int_{X2}^{B} F_t(d_A)\,\mathrm{d}d_A}{\int_{X2}^{B} \mathrm{d}d_A}\,. \tag{2.17}$$

It is possible to solve Equation (2.17) now for the different parts of the contact on the line of action to obtain the average friction force. This can be done using a pre-processing method that has access to a detailed contact description. It pre-calculates the integral before a simulation

[4] The contact ratio is a measure of the average number of teeth in contact. A contact ratio of 1.5 would mean that for 50% of the line of action there is a single tooth contact and for 50% of the line of action there are two teeth in contact.

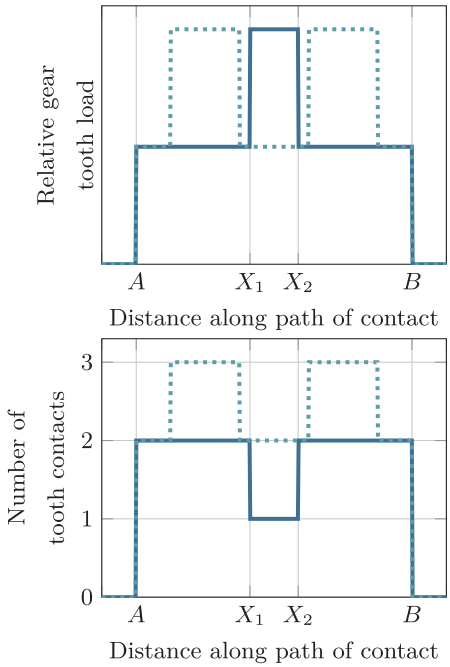

Figure 2.8: Relative tooth load for contact ratios between 1 and 2 (——) and for a ratio between 2 and 3 (·····). For a contact ratio between 1 and 2, there are two contacts between A and X_1 as well as between X_2 and B. Between $X1$ and $X2$ there is only a single tooth contact. The varying number of teeth in contact lead to variable gear tooth loading.

and stores the results in a lookup table as suggested before. However, in order to be concise, two assumptions will be made:

Assumption 2.1 *The normal force F_n is constant over the line of action.*

This assumption makes it possible to reduce Equation 2.17 again to 2.16. It avoids the calculations that are needed to deal with the discontinuities caused by the different numbers of engaging teeth in the contact. Moreover, this assumption causes F_n to be independent of d_A, further simplifying the calculations. If Assumption 2.1 holds true, it means that the individual teeth forces are now treated as a generalized gear force. Hereby the individual teeth forces and therefore the effects of single meshing teeth are no longer relevant. Note that this assumption does not limit the global variation of the normal force F_n, enabling time varying loads.

This assumption is not only a theoretical assumption, it can be reached by using helical gears with sufficient helix angle and width. Such configurations are designed to avoid discontinuities in the normal forces by distributing the contact over a large area of the line of action. Assumption 2.1 is true when the complete line of action from A to B is in contact, while at the same time for each point on this line, a constant fraction of the width of the gear wheel is in contact.

Using Assumption 2.1, it is possible to derive an average of the contact forces over all possible contact positions. In most cases, only a global coefficient of friction is known, which can be dependent on the mesh velocity. This can be used to further simplify the calculations if the friction coefficient is assumed to be independent of the local sliding velocity on the contact line.

Assumption 2.2 *The friction coefficient is constant over the line of action.*

When the friction coefficient is assumed to be constant over the line of action, $\mu(v_{mesh}, d_A)$ becomes independent of d_A. Hence it is possible to use $\mu(v_{mesh})$ as the friction coefficient. This causes the gear friction to be only dependent on the sign of the sliding speed s_v, the normal force F_n and the overall gear mesh velocity. Note that this assumes a friction coefficient that is independent on the locally varying sliding velocity on the line of action. An average friction coefficient is therefore used over the complete line of action which is only dependent on the mesh velocity v_{mesh} as sometimes used for gear design (e.g. DIN 3990 Teil 4, 1987)

Using Assumption 2.2 it is therefore possible to use a global varying friction coefficient which is constant over the gear contact. Using Table 2.1, it is possible to calculate for each loading condition and speed the mean gear forces and torques. In the sections below, the calculations are made for a single loading condition.

To obtain the moments τ_A and τ_B, only the tangential parts of the resultant forces (2.1) - (2.2), $\tau_{t,A} = -F_t d_A$ and $\tau_{t,B} = -F_t d_B$ have to be analyzed since only F_t is changing over the contact position. $\tau_{n,A} = F_n l_A$ and $\tau_{n,B} = F_n l_B$ are not dependent on F_t or d_A and thus do not need averaging.

2.3.1 Average tangential force

The average friction force is presented in Equation (2.16). Using Assumption 2.1, it follows that the integral does not need to be split up into multiple parts as done in Equation (2.17) as the normal force F_n is continuous over the contact line. In this Section, the case $F_n > 0$ and $v_{mesh} < 0$ is worked out. Taking Equation (2.16) and combining it with Equation (2.15) gives:

$$\overline{F}_t = \frac{\int_A^B F_t(d_A)\,\mathrm{d}d_A}{\int_A^B \mathrm{d}d_A} = \frac{\int_A^B s_v(v_{mesh}, d_A)\mu(v_{mesh}, d_A)|F_n(d_A)|\,\mathrm{d}d_A}{\int_A^B \mathrm{d}d_A} \,. \tag{2.18}$$

Using Assumption 2.2, it is possible to obtain an integral which is only dependent on the gear geometry. The integral has to be split up into 2 parts, because s_v is not continuous in d_A. This yields:

$$\overline{F}_t = \mu(v_{mesh})|F_n| \frac{\int_A^P s_{v,AP}\,\mathrm{d}d_A + \int_P^B s_{v,PB}\,\mathrm{d}d_A}{\int_A^B \mathrm{d}d_A} \,. \tag{2.19}$$

From Table 2.1, we see that $s_{v,AP} = -s_{v,PB}$. Substituting this and working out the integral yields:

$$\overline{F}_t = \mu(v_{mesh})|F_n| s_{v,AP} \frac{d_A\big|_A^P - d_A\big|_P^B}{d_A\big|_A^B} \,, \tag{2.20}$$

$$\overline{F}_t = \mu(v_{mesh})|F_n| s_{v,AP} \frac{2\overline{T_1P} - \overline{T_1A} - \overline{T_1B}}{\left(\overline{T_1B} - \overline{T_1A}\right)} \,. \tag{2.21}$$

The notation for the distance between points X and Y is defined as $\overline{XY}$. In Equation (2.21), the distances $\overline{T_1A}$, $\overline{T_1B}$ and $\overline{T_1P}$ are constant. To simplify the notation, the new constant $\overline{d_F} = \frac{2\overline{T_1P}-\overline{T_1A}-\overline{T_1B}}{(\overline{T_1B}-\overline{T_1A})}$ is introduced:

$$\overline{F_t} = \overline{d_F}\ s_{v,AP}\ \mu(v_{mesh})|F_n|\ . \tag{2.22}$$

Analyzing $\overline{d_F}$ shows that in the case of two uniform gears in contact, $\overline{d_F}$ (and therefore $\overline{F_t}$) is zero since $2\overline{T_1P} = \overline{T_1A} + \overline{T_1B}$. This interesting result is caused by the fact that the friction force on both sides from pitch point P (see Figure 2.6) is equal, but inversed since s_v changes at the pitch point.

2.3.2 Derivation of the mean moment

The mean moments $\overline{\tau_{t,A}}$ and $\overline{\tau_{t,B}}$ can be calculated in the same way as the average friction force $\overline{F_t}$. The case $F_n > 0$ will be used for the calculations in this section leading to $\tau_{t,A} = -F_t d_A$. For the case of $F_n < 0$, the contact line flips as already shown. This leads to a different gear torque: $\tau_{t,A} = F_t d_A$.

Calculation of $\overline{\tau_{t,A}}$:

$$\overline{\tau_{t,A}} = \frac{\int_A^B -F_t d_A \,\mathrm{d}d_A}{\int_A^B \mathrm{d}d_A} = \frac{\int_A^B -\mu(v_{mesh}) s_v(v_{mesh}, d_A)|F_n| d_A \,\mathrm{d}d_A}{\int_A^B \mathrm{d}d_A}\ . \tag{2.23}$$

Since $s_v(v_{mesh})$ is discontinuous, the integral is split up in two continuous parts, similar to the approach in Equation (2.19).

$$\overline{\tau_{t,A}} = \frac{\int_A^P -\mu(v_{mesh}) s_{v,AP}|F_n| d_A \,\mathrm{d}d_A}{d_A\Big|_A^B} + \frac{\int_P^B -\mu(v_{mesh}) s_{v,PB}|F_n| d_A \,\mathrm{d}d_A}{d_A\Big|_A^B}\ . \tag{2.24}$$

Utilizing $s_{v,AP} = -s_{v,PB}$ again, it is possible to simplify $\overline{\tau_{t,A}}$ to:

$$\overline{\tau_{t,A}} = -\mu(v_{mesh})|F_n| s_{v,AP} \frac{\int_A^P d_A \,\mathrm{d}d_A - \int_P^B d_A \,\mathrm{d}d_A}{d_A\Big|_A^B}\ . \tag{2.25}$$

Working out the integrals yields:

$$\overline{\tau_{t,A}} = -\mu(v_{mesh})|F_n| s_{v,AP} \frac{d_A^2\Big|_A^P - d_A^2\Big|_P^B}{2d_A\Big|_A^B}\ , \tag{2.26}$$

$$\overline{\tau_{t,A}} = -\mu(v_{mesh})|F_n| s_{v,AP} \frac{2\overline{T_1P}^2 - \overline{T_1A}^2 - \overline{T_1B}^2}{2\left(\overline{T_1B} - \overline{T_1A}\right)}\ . \tag{2.27}$$

Again, in this equation the notation $\overline{T_1A}$ means the distance between point T_1 and point A. Since $\overline{T_1A}$, $\overline{T_1B}$ and $\overline{T_1P}$ are constant, a new constant $\overline{d_{\tau,A}} = \frac{2\overline{T_1P}^{\,2}-(\overline{T_1A}^{\,2}+\overline{T_1B}^{\,2})}{2(\overline{T_1B}-\overline{T_1A})}$ is introduced:

$$\overline{\tau_{t,A}} = -\mu(v_{mesh})|F_n|s_{v,AP}\,\overline{d_{\tau,A}}\ . \tag{2.28}$$

The constant $\overline{d_{\tau,A}}$ can be interpreted as an average lever arm on which the tangential force F_t acts.

Calculation of $\overline{\tau_{t,B}}$:

The average $\overline{\tau_{t,B}}$ is calculated analog to the calculation of $\overline{\tau_{t,A}}$:

$$\begin{aligned}\overline{\tau_{t,B}} &= \frac{\int_A^B -F_t d_B \,\mathrm{d}d_B}{\int_A^B \mathrm{d}d_B} \\ &= \frac{\int_A^B -\mu(v_{mesh})s_v(v_{mesh},d_A)|F_n|d_B\,\mathrm{d}d_B}{\int_A^B \mathrm{d}d_B}\ .\end{aligned} \tag{2.29}$$

Working out these integrals leads to:

$$\overline{\tau_{t,B}} = -\mu(v_{mesh})|F_n|s_{v,AP}\frac{2\overline{T_2P}^2-\overline{T_2A}^2-\overline{T_2B}^2}{2\left(\overline{T_2B}-\overline{T_2A}\right)}\ . \tag{2.30}$$

Since $\overline{T_2A}$, $\overline{T_2B}$ and $\overline{T_2P}$ are constant, a new constant $\overline{d_{\tau,B}} = \frac{2\overline{T_2P}^{\,2}-(\overline{T_2A}^{\,2}+\overline{T_2B}^{\,2})}{2(\overline{T_2B}-\overline{T_2A})}$ is introduced:

$$\overline{\tau_{t,B}} = -\mu(v_{mesh})|F_n|s_{v,AP}\,\overline{d_{\tau,B}}\ . \tag{2.31}$$

$\overline{d_{\tau,A}}$ and $\overline{d_{\tau,B}}$ contain the geometric information of the gear needed for the friction calculations. These values are purely defined by the gear geometry and are constant.

2.4 Determination of the friction forces and moments in the case of $v_{mesh} = 0$

The static friction coefficient for $v_{mesh} = 0$ is defined as μ_0. Dependent on the position of the gear, the friction at zero speed can be zero (at rest with a single contact at the pitch point P, leading to $v_s = 0$) or $\mu_0|F_n|$. Since no contact finding algorithms are used, the exact position of the gears is not known. It is therefore assumed that the contact is not at the pitch point and therefore not zero. Using Assumption 2.1 and 2.2, Equation (2.15) can therefore be written as:

$$F_t = \begin{cases} s_v\mu(v_{mesh})|F_n| & \textbf{if } v_{mesh} \neq 0 \textbf{ or } |F_t| \geq |\mu(v_{mesh})F_n| \\ \text{so that } v_{mesh} = 0 & \textbf{if } v_{mesh} = 0 \ \textbf{ and } |F_t| < |\mu_0 F_n| \end{cases}\ . \tag{2.32}$$

Note that μ_0 (with $v_{mesh} = 0$) is not necessarily the same as $\mu_{v_{mesh}}$ with $v_{mesh} \to 0$. This makes it possible to include static friction into the gear contact model using a state machine leading to a numerical efficient model. Using Equation (2.32), the maximal friction force and moments for $v_{mesh} = 0$ is given by:

$$\left.\begin{array}{ll} \overline{F_t} & = \mu_0 |F_n| \overline{d_F} \\ \overline{\tau_{t,A}} & = \mu_0 |F_n| \overline{d_{\tau,A}} \\ \overline{\tau_{t,B}} & = \mu_0 |F_n| \overline{d_{\tau,B}} \end{array}\right\} \textbf{for} \quad v_{mesh} = 0 \ . \tag{2.33}$$

2.5 Determination of the friction forces and moments

In Table 2.2 the friction forces and moments are shown for each operational mode. This is done by substituting $s_{v,AP}$ in Equation (2.22). For Equation (2.28) and (2.31), the contact angle $\phi_{contact}$ has to be considered next to $s_{v,AP}$ (see Figure 2.6 and 2.7). For $\phi_{contact} < 0$ this leads to an extra multiplication with -1 to incorporate the correct direction of the average moments.

By analyzing Table 2.2 it becomes clear that the tangential part of the moment $\overline{\tau_t}$ and the

Table 2.2: Operational modes of the Gearbox. Q is the operational quadrant.

Q	v_{mesh}	Power flow	F_n	$\phi_{contact}$	$\overline{F_t}$	$\overline{\tau_{t,A}}$	$\overline{\tau_{t,B}}$
0	0	-	-	-	$\mu_0 \lvert F_n \rvert \overline{d_F}$	$\mu_0 \lvert F_n \rvert \overline{d_{\tau,A}}$	$\mu_0 \lvert F_n \rvert \overline{d_{\tau,B}}$
1	> 0	$A \to B$	> 0	<0	$\mu(v_{mesh}) \lvert F_n \rvert \overline{d_F}$	$\mu(v_{mesh}) \lvert F_n \rvert \overline{d_{\tau,A}}$	$\mu(v_{mesh}) \lvert F_n \rvert \overline{d_{\tau,B}}$
2	> 0	$B \to A$	< 0	>0	$-\mu(v_{mesh}) \lvert F_n \rvert \overline{d_F}$	$\mu(v_{mesh}) \lvert F_n \rvert \overline{d_{\tau,A}}$	$\mu(v_{mesh}) \lvert F_n \rvert \overline{d_{\tau,B}}$
3	< 0	$B \to A$	> 0	<0	$-\mu(v_{mesh}) \lvert F_n \rvert \overline{d_F}$	$-\mu(v_{mesh}) \lvert F_n \rvert \overline{d_{\tau,A}}$	$-\mu(v_{mesh}) \lvert F_n \rvert \overline{d_{\tau,B}}$
4	< 0	$A \to B$	< 0	>0	$\mu(v_{mesh}) \lvert F_n \rvert \overline{d_F}$	$-\mu(v_{mesh}) \lvert F_n \rvert \overline{d_{\tau,A}}$	$-\mu(v_{mesh}) \lvert F_n \rvert \overline{d_{\tau,B}}$

friction force $\overline{F_t}$ are based on geometric gear constants, the mesh velocity, the friction coefficient and the normal force. To determine the mesh parameters from an unknown gear geometry, a good approximation can be made based on experience.

2.5.1 Friction models

To obtain the friction using the calculations from last sections, the friction coefficient $\mu(v_{mesh})$ must be known. The friction coefficient can be calculated with different friction models and can be integrated in the gear model. In Assumption 2.2, the friction force is assumed to be constant over the line of action, and only dependent on the mesh velocity v_{mesh}. A modular approach is used for the implementation of the friction models which makes it possible to easily select the needed friction model. Following friction models are presented in the sections below:

1. Coulomb friction,
2. Friction model according to DIN3990-4,
3. Calculation of the friction coefficient from tabulated efficiency.

Depending on the purpose for which the model is used, a suitable friction model can be selected. The tabulated efficiency is not a real friction model, but allows the user to prescribe a speed dependent efficiency.

Coulomb friction:

The Coulomb friction model is a simple friction model which is often used, when insufficient data is available. The Coulomb friction applies:

$$\mu(v_{mesh}) = \begin{cases} \mu & \textbf{if} \quad |v_{mesh}| > 0 \\ \mu_0 & \textbf{if} \quad v_{mesh} = 0 \end{cases} . \tag{2.34}$$

In this model, a different friction coefficient for the stuck phase ($v_{mesh} = 0$) can be selected. This can be used to model a higher breakout force. To model a physical system, the static friction coefficient μ_0 should be chosen such that: $\mu_0 \geq \mu$. This also avoids numerical chattering around $v_{mesh} = 0$.

Friction estimation from DIN3990-4:

Norm DIN3990-4 (DIN 3990 Teil 4, 1987) proposes a friction model which depends on the mesh speed. This model is based on the dynamic oil viscosity η_{oil}, as well as on the loading of the gear. Its nonlinear friction characteristics can be used to estimate the gear friction for gear design based on design parameters.

$$\mu(v_{mesh}) = \begin{cases} 0.12(\dfrac{w_{Bt}}{\eta_{oil} v_{\sum C}})^{0.25}(\dfrac{R_a}{\sigma_{redC}})^{0.25} & \textbf{if } |v_{mesh}| > 0 \\ \min\left(\mu_0, 0.12(\dfrac{w_{Bt}}{\eta_{oil} v_{\sum C}})^{0.25}(\dfrac{R_a}{\sigma_{redC}})^{0.25}\right) & \textbf{if } v_{mesh} = 0 \end{cases} \tag{2.35}$$

In Equation (2.35), w_{Bt} is the force per toothwidth, R_a the mean roughness of the gear faces. Furthermore, the sum of the tangential velocities ($v_{\sum C}$) at the pitch point P is given by:

$$v_{\sum C} = 2|v_{mesh}| \sin(\alpha_{wt}) . \tag{2.36}$$

Here is α_{wt} the pressure angle of the gear. σ_{redC} is the effective radius of curvature and is given by:

$$\sigma_{redC} = 1e3 \frac{i}{(1+i)^2} \frac{a \sin(\alpha_{wt})}{\cos(\beta_b)} , \tag{2.37}$$

where β_b is the helix angle, i the gear ratio and a the shaft center distance.

Tabulated efficiency:

In the design process of aircraft actuators, usually experimental measurement results or estimates based on experiments are used. The design of controllers for such actuators is critical at low velocities and low temperatures where friction is high. For this condition however, hardly any

theoretical results to predict the friction coefficient are valid. Therefore usually a tabulated gear efficiency is used that is defined as.

$$\eta(v_{mesh}) = \begin{cases} -\frac{\tau_A \omega_A}{\tau_B \omega_B} & \textbf{for quadrant 1 and 4} \\ -\frac{\tau_B \omega_B}{\tau_A \omega_A} & \textbf{for quadrant 2 and 3} \end{cases} . \tag{2.38}$$

Substituting $\tau_A = cos(\phi_{contact}) F_n r_a + \overline{\tau_{t,A}}$ and $\tau_B = cos(\phi_{contact}) F_n r_b + \overline{\tau_{t,B}}$ leads to:

$$\eta(v_{mesh}) = \begin{cases} -\frac{cos(\phi_{contact}) F_n r_a + \overline{\tau_{\tau,A}} \omega_A}{cos(\phi_{contact}) F_n r_b + \overline{\tau_{\tau,B}} \omega_B} & \textbf{for quadrant 1 and 4} \\ -\frac{cos(\phi_{contact}) F_n r_b + \overline{\tau_{\tau,B}} \omega_B}{cos(\phi_{contact}) F_n r_a + \overline{\tau_{\tau,A}} \omega_A} & \textbf{for quadrant 2 and 3} \end{cases} . \tag{2.39}$$

To be able to integrate this efficiency into the gear model, the efficiency must be expressed in the form of a friction coefficient which yields the set efficiency. Therefore $\overline{\tau_{\tau,A}}$ and $\overline{\tau_{\tau,B}}$ are substituted with the equations from Table 2.2. Now using symbolic manipulations with a standard symbolic computation tool, it is possible to express the friction coefficient $\mu(v_{mesh})$ as a function of the total mesh velocity.

$$\mu(v_{mesh}) = \begin{cases} \left| \frac{r_a r_b \cos(\phi_{contact})(\eta(v_{mesh}) - 1)}{\overline{d_{\tau,B}} r_a - \overline{d_{\tau,A}} \eta(v_{mesh}) r_b} \right| & \textbf{for quadrant 1 and 4} \\ \left| \frac{r_a r_b \cos(\phi_{contact})(\eta(v_{mesh}) - 1)}{\overline{d_{\tau,A}} r_b - \overline{d_{\tau,B}} \eta(v_{mesh}) r_a} \right| & \textbf{for quadrant 2 and 3} \end{cases} . \tag{2.40}$$

In this equation, $\eta(v_{mesh})$ is the tabulated efficiency. The static friction coefficient at $v_{mesh} = 0$ is given by the maximum of the friction coefficients:

$$\mu_0 = c_{\mu_0} \max \left(\left| \frac{r_a r_b \cos(\phi_{contact})(\eta(v_{mesh}) - 1)}{\overline{d_{\tau,B}} r_a - \overline{d_{\tau,A}} \eta(v_{mesh}) r_b} \right|, \quad \left| \frac{r_a r_b \cos(\phi_{contact})(\eta_0 - 1)}{\overline{d_{\tau,A}} r_b - \overline{d_{\tau,B}} \eta_0 r_a} \right| \right) . \tag{2.41}$$

$c_{\mu_0} \geq 1$ is a constant which scales the efficiency in the stuck phase. It can be used to simulate a breakout friction with a friction coefficient higher than the friction at $v_{mesh} \to 0$. When $c_{\mu_0} = 1$, the friction coefficient at $v_{mesh} = 0$ is the same as $v_{mesh} \to 0$.

2.5.2 Gear stiffness and damping

To model the gear stiffness and damping, several elasticity models are available. These spring models can be used for different simulations. These models range from a constant stiffness model for early design and simple modeling up to nonlinear stiffness with backlash, which can be used e.g. for rattling analysis of automotive gearboxes.

The proposed elasticity characteristics are implemented using an object oriented approach similar to the friction models from last section. This makes it possible to adjust the model to the simulation requirements. Furthermore, literature sources are not consistent on how the tooth stiffness varies with the load (e.g. ISO 6336-1 (ISO 6336-1, 2007) and Niemann & Winter (Niemann & Winter, 1989) define the nonlinear spring characteristics differently). The modular approach

chosen for the modeling of the gear contact can easily accommodate these different methods by supplying different spring characteristics. All models define F_n as a function of Δ_{AB}, the mesh deformation (Equation 2.9). In all models, a viscous damping is used. In Figure 2.9, an overview of the different elasticity characteristics is presented where the stiffness is defined as $\frac{\delta F_n}{\delta \Delta_{AB}}$. This is the elasticity when the model is linearized in a certain operation point. To be concise, only a selection of the stiffness models from Figure 2.9 is presented in the next Sections. The other models can be obtained similarly.

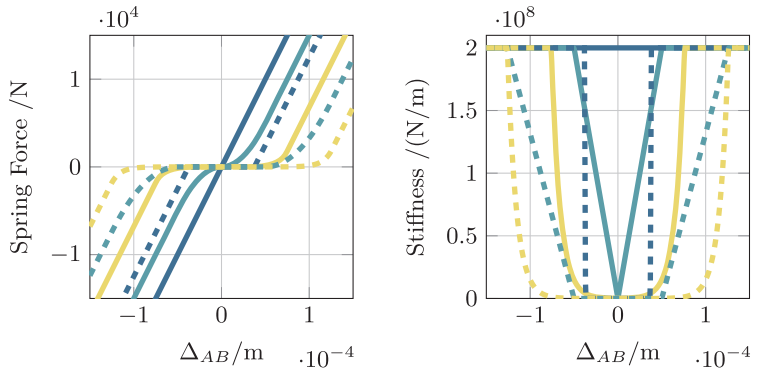

(a) Deformation of the contact **(b)** Elasticity of the mesh

Figure 2.9: Characteristics of the different elasticity models: ▬ is a linear elasticity model, ▬ a model with backlash, ▬ a progressive elasticity model to according to ISO 6336-1 (▬ ISO 6336-1 model with backlash), ▬ a progressive elasticity model from Niemann and Winter (▬ Niemann and Winter model with backlash).

Linear spring and damper:

A simple stiffness model is provided for standard analysis with linear spring and damper characteristics. The normal force F_n is defined by:

$$F_n = c\Delta_{AB} + d\dot{\Delta}_{AB} \ . \tag{2.42}$$

Nonlinear spring according to ISO 6336-1:

Surface roughness R_q (Shi & Polycarpou, 2005) and tooth form deviations (Niemann & Winter, 1989) lead to a progressive tooth stiffness. The ISO 6336-1 norm (ISO 6336-1, 2007) proposes a progressive stiffness increasing linearly with the displacement. The maximal stiffness is reached at $\Delta_{AB} = R_q$ where R_q represents the surface roughness of the gears in contact. The normal force is given by:

$$F_n = \begin{cases} \dfrac{c}{2R_q}{\Delta_{AB}}^2 \operatorname{sgn}(\Delta_{AB}) + d\dot{\Delta}_{AB} & \textbf{if } \ |\Delta_{AB}| < R_q \\ c\left(-\dfrac{R_q}{2} + |\Delta_{AB}|\right)\operatorname{sgn}(\Delta_{AB}) + d\dot{\Delta}_{AB} & \textbf{if } \ |\Delta_{AB}| \geq R_q \end{cases} . \tag{2.43}$$

In this equations, c is the nominal stiffness coefficient and d the damping coefficient.

Backlash:

To simulate backlash of the gears, a dead zone b is defined, in which the gears cannot transmit force. When the dead zone is passed, a linear stiffness model is used. In Equation (2.44) the normal force for the backlash model is developed:

$$F_n = \begin{cases} c\left(\Delta_{AB} + \frac{b}{2}\right) + d\dot{\Delta}_{AB} & \textbf{if } \Delta_{AB} < -\frac{b}{2} \\ c\left(\Delta_{AB} - \frac{b}{2}\right) + d\dot{\Delta}_{AB} & \textbf{if } \Delta_{AB} > \frac{b}{2} \\ 0 & \textbf{else} \end{cases} . \tag{2.44}$$

Backlash with nonlinear spring:

The model of the Nonlinear spring according to ISO 6336-1 and the Backlash model can be combined in a single model with backlash and stiffness. The normal force F_n is defined for this case by:

$$F_n = \begin{cases} c\left(-\frac{R_q}{2} + \left|\Delta_{AB} + \frac{b}{2}\right|\right)\operatorname{sgn}(\Delta_{AB}) + d\dot{\Delta}_{AB} & \textbf{if } \Delta_{AB} \leq -\frac{b}{2} - R_q \\ \frac{c}{2R_q}\left(\Delta_{AB} + \frac{b}{2}\right)^2 \operatorname{sgn}(\Delta_{AB}) + d\dot{\Delta}_{AB} & \textbf{if } -\frac{b}{2} - R_q < \Delta_{AB} < -\frac{b}{2} \\ 0 & \textbf{if } -\frac{b}{2} \leq \Delta_{AB} \leq \frac{b}{2} \\ \frac{c}{2R_q}\left(\Delta_{AB} - \frac{b}{2}\right)^2 \operatorname{sgn}(\Delta_{AB}) + d\dot{\Delta}_{AB} & \textbf{if } \frac{b}{2} < \Delta_{AB} < \frac{b}{2} + R_q \\ c\left(-\frac{R_q}{2} + \left|\Delta_{AB} - \frac{b}{2}\right|\right)\operatorname{sgn}(\Delta_{AB}) + d\dot{\Delta}_{AB} & \textbf{if } \Delta_{AB} \geq \frac{b}{2} + R_q \end{cases} . \tag{2.45}$$

2.6 Example: Modeling a spring loaded actuator

In this Section, a simple spring loaded actuator is modeled. The behavior of the gear contact under preload has been investigated. It highlights the need for a gear model which can represent the behavior in a sticking phase.

2.6.1 Model implementation

An existing Modelica model of a gear contact without friction as presented in Appendix B has been used and is extended with an object-oriented implementation of friction and stiffness. A hybrid modeling approach, presented by Otter et al. (Otter et al., 1999), is used to implement the friction including stiction as described in Table 2.2. This hybrid method calculates in quadrant 1 to 4 the friction force F_t from the normal Force F_n and friction coefficient $\mu(v_{mesh})$. In quadrant 0, a "stuck" mode is entered in which a different set of equations is used; Here the friction force is calculated from the force to keep the model from moving. For more detailed information see Otter et al. (Otter et al., 1999).

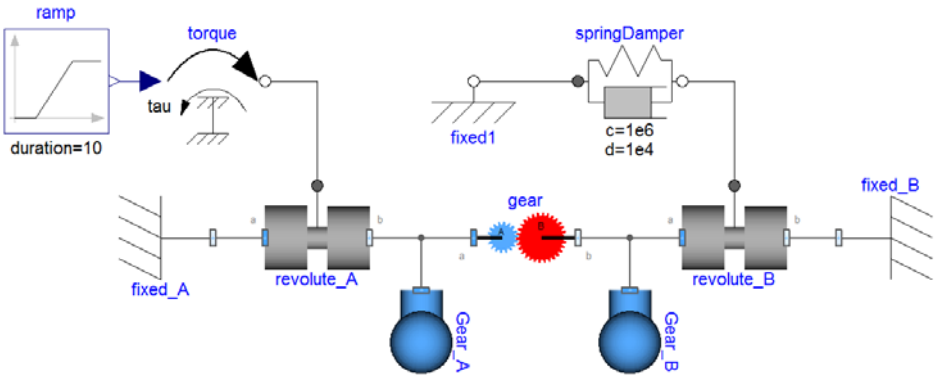

Figure 2.10: Gear model setup for sticking analysis

Due to the correct friction handling at zero velocity as presented before, the model makes it possible to accurately model transmissions during normal continuous operation as well as low speed positioning- and position holding applications.

The PlanarMechanics Library (see Zimmer (Zimmer, 2012)) is used to model the gear constraints and supply the model interfaces.

2.6.2 Preloaded actuator sticking

To show the functionality of the proposed model, gear sticking under preload is used to showcase the sticking behavior of the gear model. Ahmed (Ahmed et al., 2012) and Garcia (Garcia et al., 2002) have shown the influence of stiction in geared actuators. In these actuators, the gears are often pre-loaded. This pre-load can originate from an aerodynamic load in the case of aircraft actuators or a pre-loading spring as used for example in geared air path actuators (Ahmed et al., 2012). In the following example, a simplified model of such a spring loaded geared actuator is presented. The pre-load is realized in this example with a nonzero loading of gear A. This mimics a pre-stressed spring of a spring loaded actuator. In Figure 2.10 an overview of the combined model is shown. It consists of two elements to define the position of the bearings (`fixed_A` and `fixed_B`). Two actuated revolute joints are shown as well: `revolute_A` is driven by a constant torque ramp to mimic an electrical motor with a current ramp, and `revolute_B` is connected to a spring damper system to mimic the pre-loaded spring. Also two bodies, `Gear_A` and `Gear_B` are used to model the gear mass and inertia. The `gear` element is the gear contact element proposed in this paper, using the DIN3990-4 friction model combined with the linear spring model. The tabulated and measured parameters of the gearbox are presented in Table 2.3, the fitted parameters in Table 2.4. The parameters of a real gear contact are used, which will be used for the validation of the gear model.

In the gear simulation, the gear is preloaded with 5 N m and a ramp with 1 N m/s is applied. The results are shown in Figure 2.11. As can be seen from this Figure, the model enters a stick-slip state, where the model sticks most of the time. When the breakout force is high enough, the model leaves the stuck phase, starts moving, to be stuck again shortly thereafter. The modeling approach described in Table 2.2, guarantees that the mesh velocity stays zero in the stuck phase and no creepage due to imperfect handling of the friction at zero velocity is possible.

Note that the gear wheels A and B can still move at $v_{mesh} = 0$. This movement is the elastic deformation of the gears. The overshoot in the position of gear A is caused by the dynamic effect

Table 2.3: Measured or tabulated Gearbox properties for the gearing examples

Gearbox parameter	value	description
r_A	10 mm	Radius of gear A (pitch radius).
r_B	30 mm	Radius of gear B (pitch radius).
$\phi_{contact}$	20°	Contact angle.
m	1 mm	Gear modulus.
r_{aA}	11 mm	Radius of the addendum circle of gear A.
r_{aB}	31 mm	Radius of the addendum circle of gear B.
$\overline{d_F}$	0.84	Average friction force scaling factor (Calculated from the gear geometry).
$\overline{d_{\tau,A}}$	−9.2 mm	Average lever arm of τ_A (Calculated from the gear geometry).
$\overline{d_{\tau,B}}$	15.0 mm	Average lever arm of τ_B (Calculated from the gear geometry).
c	2E8 N/m	Gear stiffness.
I_A	5E−4 kg/m^2	Inertia of gear A.
I_B	1E−3 kg/m^2	Inertia of gear B.
η_{oil}	275 Pa s	Dynamic oil viscosity

Table 2.4: Estimates and tuned valued for the gearing examples

Gearbox parameter	value	description
$K_{H\beta}$	28 %	Load distribution factor.
b	15 µm	Gear Backlash.
d	2E5 N s/m	Gear damping.
R_a	0.8 µm	Gear roughness.
μ_0	0.2	Static friction coefficient.

of the inertia of gear A and the contact stiffness of the gear and `springDamper` element. When the gear contact comes in `Forward` mode, Gear A increases its speed and a small overshoot is seen before the gear enters the `Stuck` mode again.

The computational costs of the simulation of the proposed system for 10 s (Figure 2.11) is 0.19 s computation time (Intel Xeon E5-1620, 16GB ram, DASSL solver, Dymola 2015). Using the proposed methods it is therefore possible to simulate a simple system approximately 50 times faster than real-time. This makes it possible to do optimization runs and long time simulations using the proposed gear contact model.

2.7 Validation of the stiffness and friction models

In this section, the presented gear contact model is validated against test rig results. This validation will be for selected friction- and stiffness models.

In Chapter 3, the gear test rig used for the validation will be presented in detail. Using this test rig for spur gears (see Figure 2.13), the elasticity and losses of the gear can be investigated. To do

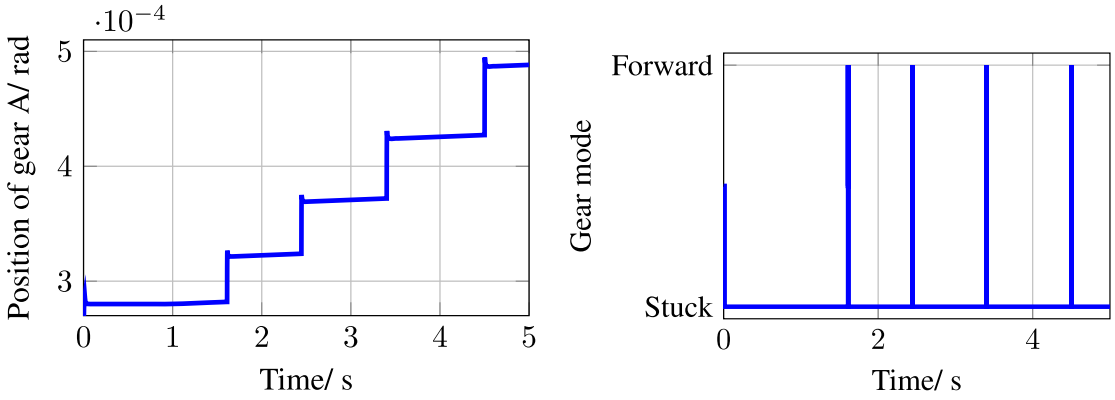

(a) Position of the gear **(b)** Gear mode

Figure 2.11: Gear sticking during the loading of a spring loaded gear. The shown stick slip phenomenon must be accurately handled for positioning actuators, since they can greatly influence the performance of the system.

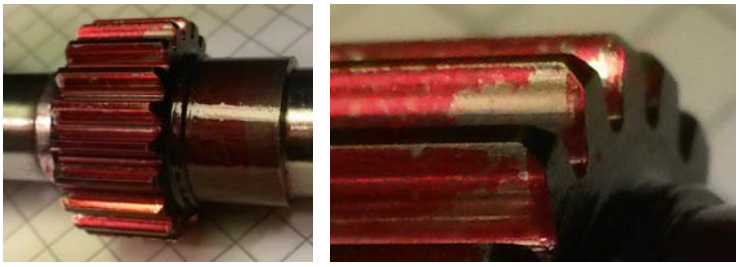

(a) Tooth contact pattern **(b)** Closeup of tooth contact pattern

Figure 2.12: Contact analysis of the gear.

so, the same test rig has been modeled using the proposed gear models, combined with standard blocks from the Modelica Standard Library. The Modelica model of the testrig is presented in Figure 2.14.

The losses are modeled according to DIN3990-4 friction model. As contact model, the backlash and spring damper to Niemann & Winter (Section 2.9b) has been selected.

2.7.1 Gear contact analysis

A gear contact of a gear transmission often has no perfect contact between the teeth. This non-perfect contact can be caused by misalignment of the gears and production imperfections of the gear wheels and shafts. In the gearbox from the test rig analyzed in this paper, the tooth contact pattern of the gears has been visualized using layout fluid. Running the gear at 80 N per one millimeter tooth width, the abrasion of the contact fluid shows the contact of the gears as depicted in Figure 2.12. From the contact pattern it can be seen that not the complete gear face is in contact. Accordingly the tooth width has been decreased to match the simulation. Setting the load distribution factor $K_{H\beta}$ to 28% (which decreases the contact width of the gear to 28%) leads to matching stiffness results. This result also matches the abrasion pattern from Figure 2.12.

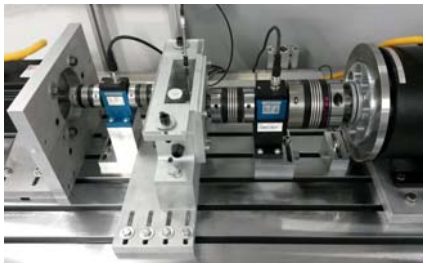

Figure 2.13: Gear testrig.

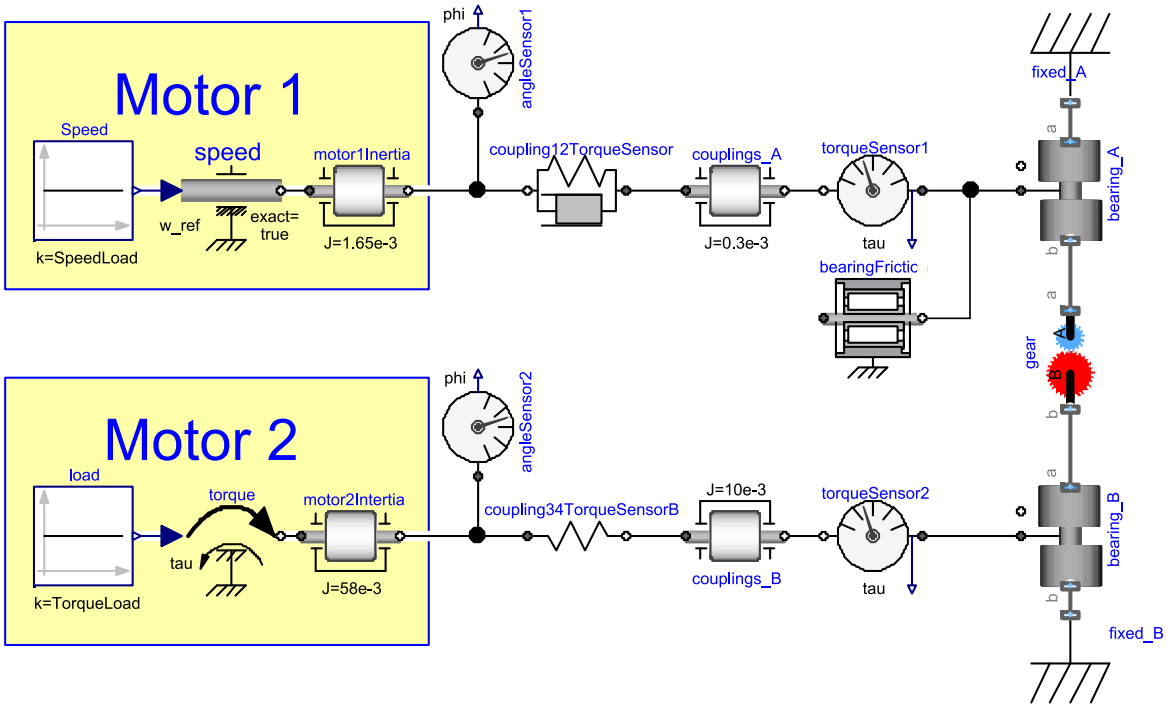

Figure 2.14: Testrig modeled in Dymola. Using this model the test results have been compared with the simulation results. In the model, the sensors, stiffness of the components and inertia of the masses have been taken into account.

2.7.2 Mesh deformation and stiffness

The mesh deformation and the stiffness of the proposed model are compared with the experimental testrig results in this section. To do so, the deformation Δ_{AB} (see Equation 2.9) is obtained as a function of the tooth loading F_n. This is done by stepwise increasing the load on the gear, while maintaining a constant low velocity of $\omega_A = 10\,\mathrm{rad/s}$ (see Chapter 3 or (F. L. J. Van der Linden, 2014a) for a detailed description). Note that ϕ_A and ϕ_B cannot be directly measured, since the position sensors are not directly at gear A and B. To obtain the mesh deformation Δ_{AB}, the stiffness of the gear train is taken into account:

$$\Delta_{AB} = \Delta_{12} - F_n c_{train} \ . \tag{2.46}$$

In this equation, Δ_{12} is the deformation between the sensor positions and c_{train} the apparent stiffness of the train at the contact position including the stiffness of the couplings, sensors and axis.

The stiffness is obtained using data-sheets of couplings and sensors as well as stiffness calculations based on the cross section of the axis. The stiffness of the gear contact is obtained by differentiation of the deformation of the gear with respect to the load. To avoid the influence of the rotational position of the gears like eccentricities and tooth effects, the average of the deformation and stiffness of all gear positions has been used.

To compare the presented models with the test rig, the test rig has been modeled including the train stiffness. The contact stiffness of the gear has been estimated to be 20 N/µm per 1 mm tooth width as suggested by Niemann and Winter (Niemann & Winter, 1989, Chapter 21.5). The effective tooth width is identified to match the stiffness measured on the testrig. The effective tooth width has been optimized to fit the measurement data and is identified to be 28% of the original tooth width ($K_{H\beta} = 28\%$). This result can be matched with the tooth contact pattern as seen in Figure 2.12a. The gear backlash is set to 15 µm to match the measurement results. The lumped static friction of the seals and bearings of the gear has been measured to be 0.05 N/m. This is included in the Modelica model with a standard bearing model (`bearingFriction` in Figure 2.14) which acts as a constant, speed independent friction. An overview of the measured and tabulated parameters is given in Table 2.3, the fitted parameters in Table 2.4.

Mesh deformation and stiffness measurements:

In Figure 2.15, a comparison of the average relative displacement of the gear as well as the stiffness of the gear as a function of the contact load is shown. The solid lines show the measurement data, the dashed lines simulation data. In this figure, the gear has been run at positive and negative angular velocities to be able to show all 4 quadrants.

Stiffness validation:

Comparing the measurement results with the simulation results, the gear contact deformation of the simulations shows a good fit with the measurement data (see Figure 2.15a). The maximal deviation between the simulation and measurement is 10 µm with an average error of 3.4 µm. The comparison of the stiffness between model and simulation shows a larger deviation (Figure 2.15b). Looking at the measurement data, the stiffness increases linearly with the load, but is not symmetric: At positive loads a higher stiffness is observed than with negative loads. This can be caused by manufacturing imperfections like gear roughness and misalignment of the gears and axis. The stiffness of the simulation model also increases linear with the load. However, it cannot exactly predict the stiffness of the gear contact with a high accuracy. This is mainly due to the fact that the gear parameters with respect to manufacturing errors are not available. The gear stiffness could be made dependent on the loading side of the gear, and a contact stiffness fitted to match the gear contact if required. However, this poses the question on how such data can be obtained, and if this data is consistent between different gear contacts.

2.7.3 Gear contact losses

The gear contact losses are modeled using the approach from the DIN3990-4 Norm. The parameters for the gear friction model are the same as in the testrig: The oil viscosity is 320 mm^2/s. Again, the tooth width is set to 28% of the original tooth width, as identified before. The gear roughness is set to 0.8 µm. The mean losses of the gearbox can be estimated by:

$$\tau_{friction} = \tau_A + \tau_B \frac{r_A}{r_B} \ . \tag{2.47}$$

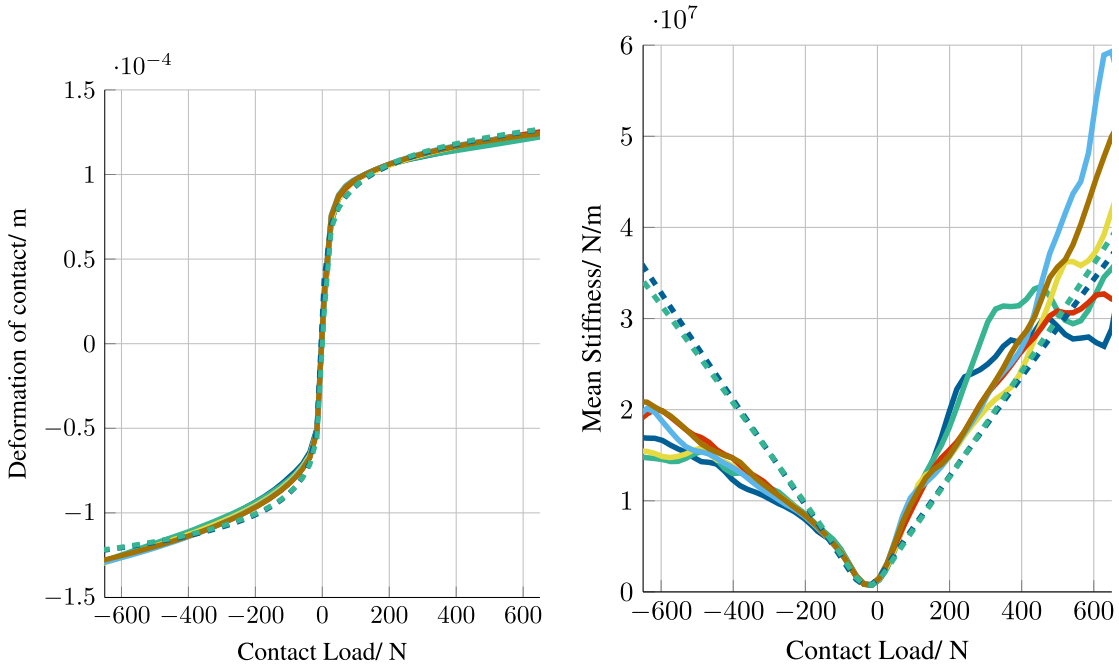

(a) Deformation of the gear contact

(b) Elasticity of the gear contact

Figure 2.15: The average deformation of the mesh and mesh stiffness of the gear as a function of the contact load. The results show two simulation results with opposite rotational velocity (dashed lines) as well as 6 measurements results (solid lines).

Note that the friction losses in Equation 2.47 are the combined friction losses of the gear plus bearings and seals since the test rig does not allow direct friction measurements without the bearings and seals. The friction estimated in Equation (2.47) is shown as a function of the contact load in Figure 2.16. The friction increases with the gear load and simulation results predict the gear losses accurately. However, also here can be seen that just like the gear stiffness, the friction of the gears is not symmetric. As discussed before, this asymmetry can be explained by manufacturing imperfections. The maximal deviation is 0.09 N m and the mean deviation of the friction is for all load cases 0.023 N m. The measured no-load friction is confirmed to be 0.5 N m. Using the presented models it is possible to accurately represent the behavior of real life gear contacts if the gear parameters are well known.

2.8 Summary

With the presented gear model, it is possible to model a gear contact with involute teeth. Elastic effects as well as the contact friction are considered. The model ensures a good trade-off between simulation accuracy and good computational performance. This makes the model suitable for design and optimization of gear transmission integrated in complete systems like aircraft actuators. The treatment of the friction at zero velocity enables analysis with stiction and stick-slip cases. This enables the modeling of positioning systems as well as low speed applications like low temperature and therefore high friction environments such as electromechanical aircraft actuators. Due to the modular implementation, it is possible to use the presented gear contact without modification of the

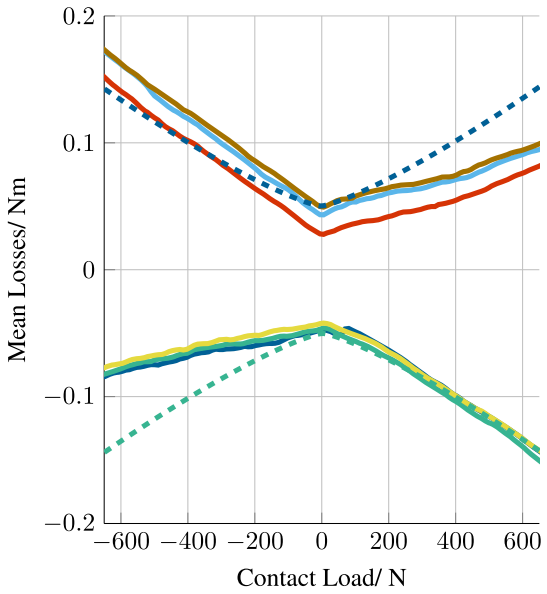

Figure 2.16: The average friction characteristics of the gear are shown as a function of the contact load. The dashed lines are simulation results with opposite rotational velocity, the solid lines are measurement results.

contact itself in different gearing configurations. Different friction models have been implemented, as well as different stiffness models to cater for different gearing scenarios. The load dependent friction and stiffness of the simulations have been validated using a dedicated gear testrig.

3 Test rig presentation

The gear test rig presented in this chapter has been developed as a multi-functional health-monitoring testrig. The rig allows two setups: the first configuration is a configuration for bearing testing. In this configuration, a motor drives a shaft with two load-carrying bearings and a single test-bearing as shown in Figure 3.1. The second configuration, is a configuration for gear testing. The gear testing configuration will be described in detail in this chapter.

To ensure the same vibration and coupling paths of the installed acceleration- and acoustic emission sensor, a housing has been developed which can accommodate bearing testing as well as gear testing by the help of an add-on setup. This add-on is the top part stacked on the gear housing as can be seen in Figure 3.1. The gear housing is used for both the bearing-testing setup as well as the gear testing setup.

The bearing-test configuration allows a pre-defined loading of the test bearing using a disc springs stack which is tensioned using a spindle. To test the failure modes of ball bearings, the test bearing was calculated to have a short life without overloading the bearings. However, using the presented setup, no satisfactory results were achieved. The test bearing remained intact and no data of failed bearings could be obtained. Even with large bearing overloading, the bearing survived elongated testing. Eventually, testing with pre-damaged bearings have been performed. However, since the relation of the test with reality using artificially damaged bearings could not be proved, this research path was not continued and the focus of the testing has switched to the validation of gear models.

The final testrig which is described in this chapter, is the result of a process to find a gear measurement setup that can measure the deformation and friction of the gear contact. Since the testrig is also designed to be used for health monitoring applications, its first design goal was to be as close as possible to the configuration of a geared aircraft actuator. However, the measurements

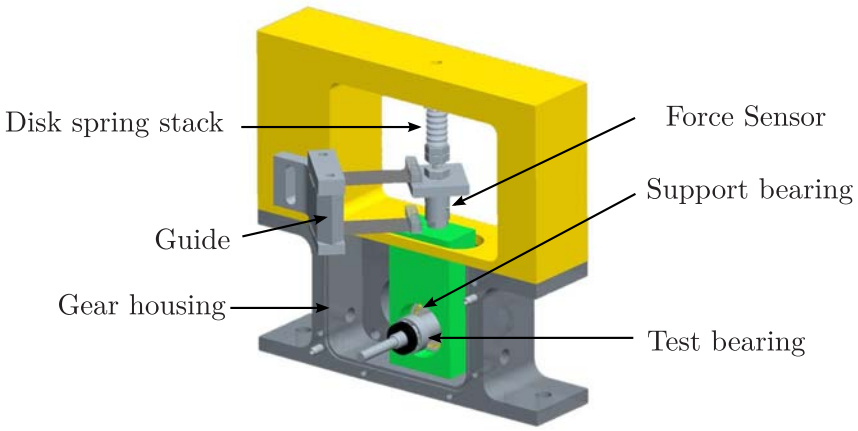

Figure 3.1: Bearing test apparatus for testing bearing health.

needed for the validation of the gear models were not possible using this configuration of the testrig. Therefore a set of gradual upgrades have been carried out:

- **High resolution position sensors added**: The position sensing is now accurate enough to measure the deformation of the gear. Still, the load, which is estimated using the motor current is found to be not accurate enough.
- **Added moment sensor to the load-side**: Testrig loading can be well controlled and measured after this upgrade. However, the friction can not be measured accurately enough as the drive-side load is still estimated using the motor current.
- **Added drive-side moment sensor**: By adding an extra load sensor, gear losses can now be well represented. However, it is found that the gear stiffness cannot be measured well due to torsion of the ground plate which is used to attach all components.
- **Added stiff groundplate**: This is the current state of the rig. Adding this groundplate removed torsional deformations which influenced the measurements.

After these incremental upgrades, it is possible to measure the friction and stiffness of a gear train using the presented testrig. In this chapter, the testrig will be specified in great detail to be able to fully understand the measurements which will be presented in Chapter 4 to validate the developed gear models.

This chapter is based on the paper *Gear test rig for health monitoring and quasi static- and dynamic testing; design, construction and first results*, presented in 2014 at the *International Gear Conference* in Lyon (F. L. J. Van der Linden, 2014a).

3.1 Test rig description

The test rig presented in this chapter is shown in the schematic overview in Figure 3.2 and as designed and constructed in Figure 3.3. The rig uses two permanent magnet synchronous motors which are controlled by inverters. This configuration enables to prescribe the position and the load of the gearbox simultaneously. Each motor is connected to a moment sensor and finally to the gear box using torsional stiff couplings. To monitor the gear connection, an acceleration sensor as well as an acoustic emission (AE) sensor is used. Furthermore the housing, environment and oil temperature are measured.

3.2 Test rig setup

The test rig is based on an aluminium frame supporting the base of the rig; a 6 cm thick steel plate with DIN 650 size 16 T-slots to eliminate any twisting of the support. To connect all parts to this plate, adapters are constructed to fix the components to the T-slots. The adapters are aligned to the nuts using tenons (DIN 6322 / DIN 6323). In this way, it is possible to align the parts on the plate with high accuracy and very high versatility. Before the T-slots and tenons were added to the test rig, it has been proven very difficult to achieve a good alignment of the parts. Furthermore the assembly and disassembly was more complicated. The base plate has shown to be of great influence on the measurements, as the twist of individually connected aluminium profiles proved to lead to measurement errors.

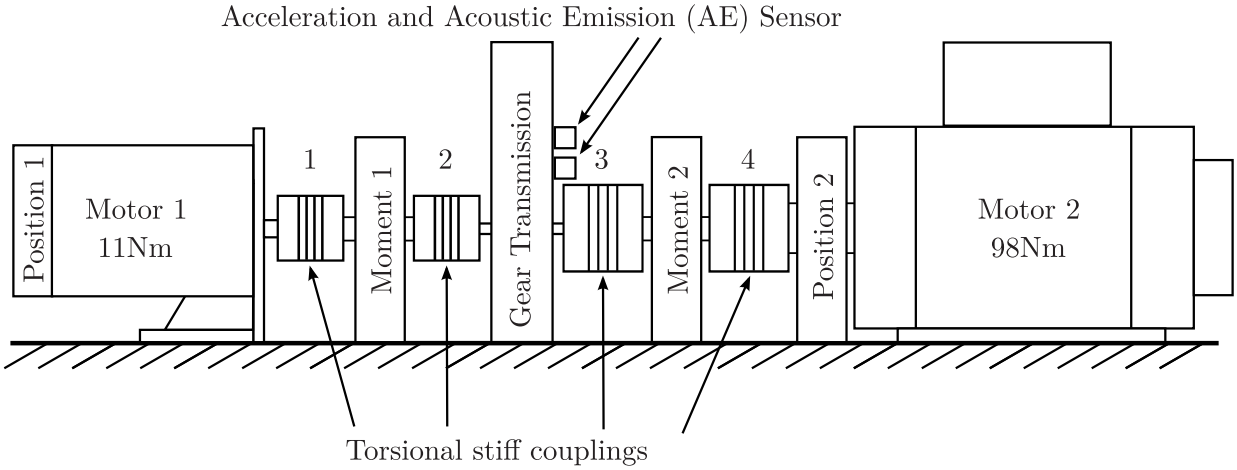

Figure 3.2: Basic gear contact with transmission error.

3.3 Sensor setup

The rig can be used for many applications like elasticity measurements, friction measurement and health monitoring algorithm testing. These different applications call for different sensors. In Table 3.1 an overview of all sensors and their accuracy is shown.

The sensors are selected based on their accuracy and bandwidth. The high bandwidth of the sensors enables the measurement of high frequency effects like tooth meshing effects.

3.4 Moment sensor stiffness properties

The moment sensors used in the test rig are based on strain gauge technology. Therefore the sensors have a non-negligible stiffness. The stiffness of the sensors is shown in Table 3.2.

3.5 Motor properties

The electric motors used in the test rig are permanent magnet synchronous motors controlled by inverters. Both motors can be operated in current, speed or position control mode. Furthermore it is possible to directly control an input using an internal PID controller. This makes it possible to have a torque control mode too by using feedback from the moment sensors. The motor properties are listed in Table 3.3. Motor 2 is selected such to enable test gears up to a gear ratio of 1:8. For gears with a gear ratio smaller than approximately 1:3, motor 2 limits the maximal speed to 1200 RPM.

3.6 Inverter properties

The inverters to control the motors use field control with position feedback. Since in the presented configuration always one motor is used in generator mode, the generated power is returned to the drive motor over the DC link. Using this setup, the power consumption of the test rig is limited, even under high load conditions.

Table 3.1: Sensors of the test rig

Sensor description	Accuracy	Bandwidth	Range	Brand/Type number
Positions sensor 1	± 7″ differential nonlinearity, ± 45″ system	>12000 RPM	-	Stegman / SinCos SRS 50
Positions sensor 2	± 5″ differential nonlinearity, ± 12″ system	>3000 RPM	-	Heidenhain / ERM220
Moment sensor 1	< ± 0.2 % nonlinearity	3 kHz @3dB	20 N m	Kistler / 4502A20RAU
Moment sensor 2	< ± 0.2 % nonlinearity	3 kHz @3dB	20 N m	Kistler / 4502A100RA
Acceleration sensor	< 2 % sensitivity	0.3–10 000 Hz	±10 g	Crossbow / CLX10HF3
Acoustic Emission (AE) sensor		100–900 kHz	75 dB re 1 V/µbar	Vallen/ ASCO-PH5 & VS900-M
Temperature sensor (oil)	< 0.1 % nonlinearity	-	0–150 °C	PT100
Temperature sensor (housing)	< 0.1 % nonlinearity	-	0–150 °C	PT100
Temperature sensor (environment)	< 0.1 % nonlinearity	-	0–150 °C	PT100

Table 3.2: Stiffness properties of the moment sensors

Sensor	Torsional Stiffnedd	Measurement Range
1	4.58 kN m/rad	20 N m
2	28.6 kN m/rad	100 N m

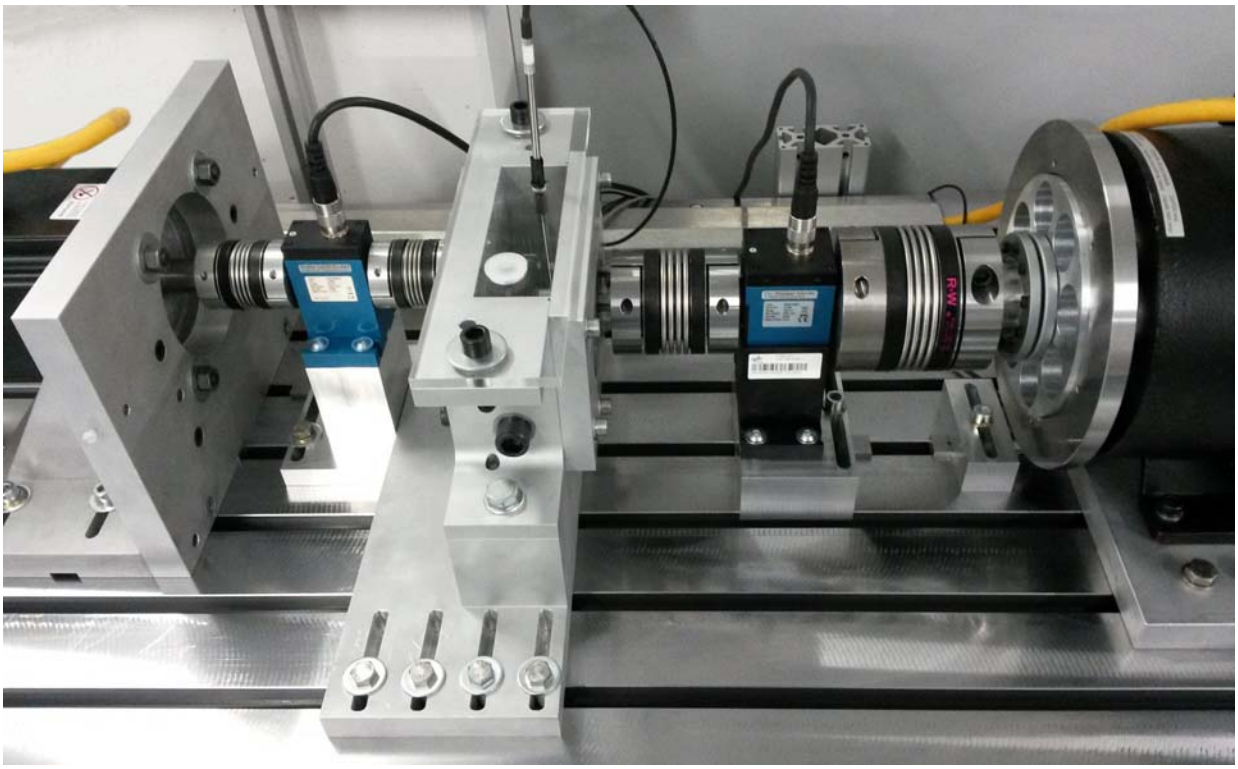

Figure 3.3: Gear test rig and contact pattern

Table 3.3: Properties of the motors

Motor description	Nominal power	Nominal torque	Nominal current	Max speed	Inertia	Brand/ type number
Motor 1	5.2 kW	11.0 N m	10 A	4500 RPM	1.65e−3 kg m^2	Baumueller / DSD071L64U45-5
Motor 2	12.4 kW	98 N m	22.5 A	1200 RPM	58e−3 kg m^2	Baumueller / DS132M54U12-5

Table 3.4: Properties of the inverters

Inverter description	Nominal power	Switching frequency	Brand/type number
Inverter 1	11 A	4 kHz	Baumueller /BM4423-STO-01200-03
Inverter 2	30 A	4 kHz	Baumueller /BM4433-STO-01200-03

Table 3.5: Properties of the couplings

Coupling	Torsional stiffness	Inertia	Brand/Type number
1,2	39×10^3 N m/rad	0.14×10^{-3} kgm^2	R+W /BKH / 30 /69
3	175×10^3 N m/rad	1.9×10^{-3} kgm^2	R+W /BKH / 150 /95
4	450×10^3 N m/rad	7.6×10^{-3} kgm^2	R+W /BKH / 300 /111

Table 3.6: Properties of the gears

Gear	Number of teeth	Face width	Module	Tooth quality	Material	Surface treatment
A	20	10 mm	1.0	7e25	Steel (16MnCr5)	Case-hardened, grinded, HRC 58±2
A	60	10 mm	1.0	7e25	Steel (16MnCr5)	Case-hardened, grinded, HRC 58±2

3.7 Coupling properties

Bellow couplings are used in the test rig because they are rotational symmetric and therefore the stiffness and torque loss are independent from the motor position.

3.8 Transmission properties

The gear wheels used in the test rig are standard, straight cut gears of module 1. A transmission ratio i=3 is selected to make sure that always the same teeth are meshing. Although whole number transmissions ratios are usually avoided to assure even meshing conditions, they simplify the analysis of the gear transmission. To avoid play of the gears on the axle, a press fit is used to connect the gears to the axle.

Both gear axles are supported by ball bearings. The gears and bearings are lubricated with Meguin CLP320 gear oil for the low speed elasticity measurements. This is a thick gear oil to assure a good lubrication at low speeds.

3.9 Drive shaft properties

The shafts of both gear wheels are made from steel. Their properties can be found in Table 3.7. The multiple length and dimensions found in this table are caused by a stepped shaft. For the stiffness calculation, the length up to the gear wheel is measured, as only this part is torsional loaded. For the calculations, a shear modulus of 79.3 GPa is selected for normal steels.

Table 3.7: Properties of the axis

Axle	Material	Length between coupling and gear	Diameter	Stiffness
A	Steel	32 mm	10 mm	16 kN/rad
		12 mm	12 mm	
B	Steel	24 mm	18 mm	65 kN/rad
		12 mm	15 mm	
		19 mm	14 mm	

3.10 Train stiffness

To calculate the stiffness of the gear contact, the stiffness of the complete gear train without the gear contact must be known. This train stiffness is obtained by lumping the stiffness of all parts to the side of motor 1 using the gear ratio i:

$$\frac{1}{c_{lump}} = \frac{1}{c_{coupl1}} + \frac{1}{c_{coupl2}} + \frac{1}{i^2 c_{coupl3}} + \frac{1}{i^2 c_{coupl4}} + \frac{1}{c_{sens1}} + \frac{1}{i^2 c_{sens2}} + \frac{1}{c_{axle1}} + \frac{1}{i^2 c_{axle2}} \tag{3.1}$$

Using the properties from Table 3.2, Table 3.5 and Table 3.7 the total lumped gear train stiffness at the side of motor 1 is 3.0 kN/rad.

3.11 Signal acquisition and data logging

The test rig is controlled and the measurement data is logged using a real-time Target/Host system using Labview. A standard PC (Xeon W3530, Quadcore, 2.8 GHz) with 3GB RAM is used as target PC. Two multifunction measurement cards measure the signals: a NI PCIe-6343 for the position sensors and signals used for control feedback, and one NI-PC-6031E card for all signals without feedback (temperature, acceleration, Acoustic Emission (AE)). All sensors (except the position sensors), are analogue sensors which are connected to the Target-PC using standard breakout boxes (NI BNC-2090 & NI BNC-2090A). All analogue sensor signals are low pass filtered at 1.8 kHz with a first order analogue filter to avoid aliasing effects. These filters have been realized inside the breakout boxes before sampling of the signal using an RC filter with 2.69 kΩ resistors and 33 nF capacitors. The position sensor signals (quadrature encoder signals) are connected to the digital interfaces and decoded by the measurement cards. All data are recorded in the streaming data logging format TDMS at 8 kHz.

3.12 Gear stiffness and loss measurements

To measure position- and load dependent stiffness, as well as the position and load dependent friction, the test rig controllers and measurements need to be reconfigured. It is chosen to command a constant velocity on motor 1, while controlling the load of motor 2 using feedback from the moment sensor 2 (see Figure 3.3). To obtain a load dependent elasticity, the load is increased stepwise on motor 2 every 3 revolutions. In Figure 3.4, an overview of a load scenario is depicted with a moment increase of 5 N m in each step. For a higher resolution with respect to load, the

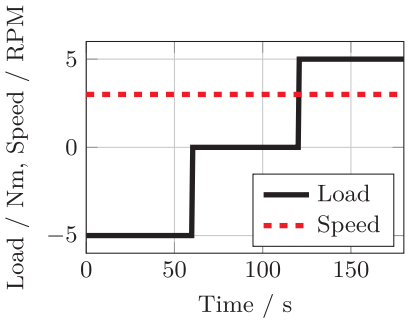

Figure 3.4: Commanded speed and load of the gear during a stiffness measurement

load steps can be chosen smaller. For a typical measurement 0.1–0.3 N m steps are used. Increasing the resolution of the moment steps will increase the measurement and calculation time.

To avoid dynamic effects from the measurements, a small rotation velocity is selected. This eliminates high accelerations and enables to treat the measurements as quasi static measurements.

3.13 Summary and discussion

A test rig to measure the position dependent elasticity, losses and position error is presented. All properties of the test rig with its components are thoroughly documented. The test rig is currently used to accurately measure stiffness and losses of gearboxes under varying circumstances. These measurements include damaged components and different lubrications. The presented measurements are done using quasi-static measurements. In the future, also tests at normal operational speeds are planned. During the development of the test rig, the accuracy of the position sensors proved to be crucial for the measurements as the stiffness variations are small. Approximations of the motor moments using the motor current proved to be unusable due to the varying motor constant with load and position and have been replaced with moment sensors. Furthermore a rigid base plate was found to be needed to avoid the influence of test rig twisting on the gear measurements.

4 Simulation and measurement of position dependent forcing error, stiffness and friction.

4.1 Introduction

The transmission error as well as the varying stiffness and friction of a gear during rotation greatly influences the dynamics of geared systems (e.g. Garcia et al., 2002; He, Gunda, & Singh, 2007a; Henriksson, 2009; Parey & Tandon, 2003; Yang et al., 2013). Furthermore, the gear loading influences its stiffness and friction properties. The effect of these imperfections is a topic of research for many gear specialists and is usually done using a semi-static approach including bearing and axis stiffness (e.g. Kohn et al., 2014; Stahl, Otto, & Zimmer, 2013). Using this approach, it is generally assumed that the gear system is in a steady state. This type of analysis can be used for many systems where the gear velocity is not changing much with respect to time, as for example in automotive- and wind-turbine applications. However, for dynamic positioning systems such as aircraft actuators, the gears seldom move at a constant velocity. In this case, a steady state approach will therefore not be valid. Another topic of research where position dependent effects are of interest, is the analysis of broken gears for the development of health monitoring algorithms (e.g. Mohammed et al., 2015). In most cases, specialized models are developed which describe the dynamic behaviors of the system.

In this chapter, the models developed in Chapter 2 will be extended with a forcing error [1], as well as with position- and load dependent stiffness and friction models. These extensions are developed in such a way that the object-oriented approach introduced in Chapter 2 will be fully exploited. The user can select all the options that are necessary and let the model "grow" as the need for more complexity arises. Models for healthy, as well as broken configurations will be presented. Test rig measurements will be used to validate the models.

This chapter consists of 3 parts: the forcing error which is defined as the no-load forcing error, the load and position dependent stiffness and the load and position dependent friction. Note that no dynamic forcing error will be used, as this forcing error is the cause of a stiffness variation, which is directly taken into account.

4.2 Forcing error

The forcing error in gear systems is caused by eccentricities and misalignment of the gear wheels as well as manufacturing errors. The total forcing error is the sum of the individual forcing errors of the gear wheels. The forcing error of the gears can lead to high dynamic gear contact forces during meshing (e.g. Inalpolat & Dynamics, 2015) and can be a major cause of noise and gear rattle (e.g. Henriksson, 2009; Ottewill et al., 2009). The investigation and modeling of forcing errors is therefore an important aspect to consider for gear systems.

[1] Forcing errors are geometric excitations from eccentricities, misalignments and production errors which lead to transmission errors.

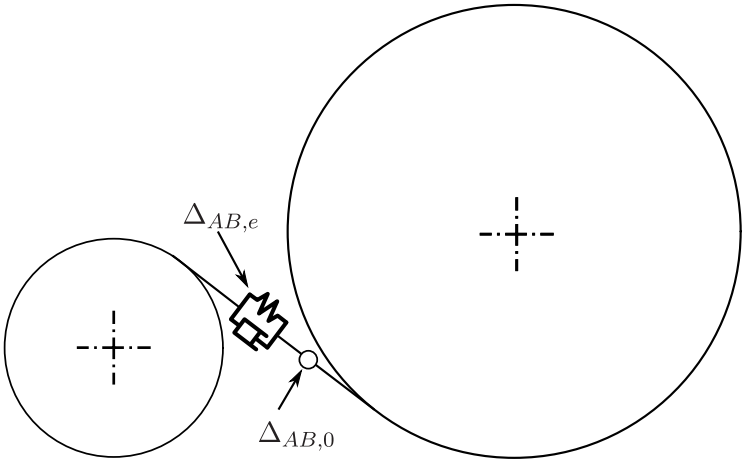

Figure 4.1: Basic gear contact with transmission error.

4.2.1 Modeling

In Chapter 2, the modeling of a gear contact has been described. However, no gear forcing errors have been included. In this chapter, the forcing errors will be included as shown in Figure 4.1. This often used approach (e.g. Kahraman & Singh, 1990) models the forcing error as an additional variable distance element between the gear teeth which can have a positive or negative distance. The forcing error can be included in the models presented in Chapter 2 by modifying Δ_{AB} to accommodate the forcing error as well as the elasticity:

$$\Delta_{AB} = \Delta_{AB,0} + \Delta_{AB,e} \tag{4.1}$$

In this equation, $\Delta_{AB,0}$ is the no-load forcing error and $\Delta_{AB,e}$ the elastic deformation of the gear mesh.

The static forcing error of a gear set is periodic by definition, with a period of the least common multiple of the tooth numbers divided by the greatest common divider of the tooth numbers. To avoid large periodicities, the sum of two series of harmonics can be used to model the forcing error caused by both gear wheels. This has the further benefit that the forcing error amplitudes are a property of the gear wheels which is the case in reality. The forcing error is therefore defined as:

$$\begin{aligned}\Delta_{AB,0} = &\sum_{n\in m} A_{\Delta A,n} \cos\left(2\pi n(\phi_A - \phi_{gear}) + \phi_{\Delta A0,n}\right) \; + \\ &\sum_{n\in m} A_{\Delta B,n} \cos\left(2\pi n(\phi_B - \phi_{gear}) + \phi_{\Delta B0,n}\right)\end{aligned} \tag{4.2}$$

In this equation $A_{A,n}$ and $A_{B,n}$ are the amplitude of the n th harmonic of the set of m elements and $\phi_{A0,n}$ and $\phi_{B0,n}$ are the phase of the harmonics of gear wheel A and B of the same set m. m represents the set of all harmonics which are included in this sum. The amount of harmonics which have to be taken into account depends on the analysis to be carried out. A single eccentricity can be represented by a single harmonics, where a real gear system with a removed tooth needs up to 30 harmonics for a good representation (see Section 4.2.2). These coefficients can be experimentally obtained (see Section 4.2.2), calculated using FEM methods (e.g. Rigaud & Barday, 1999), obtained using specialized methods (e.g. Kissling & Raabe, 2006) or estimated based on experience with similar systems.

4.2.2 Measurements and validation

The test rig presented in Chapter 3 is used in this section to measure the transmission error of the gears. This is done by applying a small load of 0.5 N m to motor 2. Using a small load instead of using a no-load condition avoids wrong measurements due to gear play. The transmission error defined in Chapter 2 is:

$$\Delta_{AB} = \phi_A r_A - \phi_{gear} r_A - (-\phi_B r_B + \phi_{gear} r_B) \tag{4.3}$$

In this equation ϕ_A and r_A are the position and radius of the gear coupled to motor 1 and ϕ_B and r_B the position and radius of the gear coupled to motor 2. ϕ_{gear} is the rotation of the overall gear contact (in the case of a spur gear this is the rotation of the complete transmission). Because of the low loading of the gear contact, the deformation of the train stiffness does not influence the measurements. Therefore it can be assumed that $\Delta_{AB,e} = 0$. From this follows that $\Delta_{AB} = \Delta_{AB,0}$.

Combining the forcing error introduced in Section 4.2 and the mesh deformation in Chapter 3, the measured forcing error is the sum of the elastic deformation and static forcing error.

Healthy gear

The results of the forcing error measurements and Fourier interpolation results of the healthy gear are shown in Figure 4.2. The 99 % confidence interval, represented by the light blue area is very small. Therefore it is concluded that the measurements are reproducible. In the same figure, an approximation of the transmission error using the Fourier series of Equation 4.2 is shown. The approximation is made by a Fourier approximation of the measured signal to select the harmonics with the highest amplitudes. This step is followed by fitting these harmonics to the original signal using an optimization routine (Joos, 2002).

The 54 harmonics (m) with the highest amplitudes are presented in Table 4.1. The standard deviation between measurement and approximation is 0.98 µm. Measurements at a positive and negative load are shown, to show the transmission error of both sides of the gear flanks as these can be different due to geometry differences of the teeth.

The periodicity of the forcing error is shown in Figure 4.3. In this Figure, most of the peaks can be clearly identified using Table 4.1: The peaks with a periodicity of 1 and 3 periods per revolution belong to the dominant peaks of the periodogram, which are caused by an eccentricity of the gear wheels on the axis. Other major peaks are the peaks at 2 and 6 periods per revolution of gear B. They are caused by a misalignment of the gear wheels (skew gear wheels w.r.t. axle). Furthermore a peak can be seen by 60 periods per revolution, which is caused by the 60 teeth of gear wheel B. However, the peaks at 12 and 36 times per revolution cannot be identified directly. These peaks can be caused by production errors of the gears. Small difference between the measurements on both gear sides (positive and negative loading) can be measured, however, the main excitation stays constant, as it is caused by eccentricity and misalignment of the gears.

Broken tooth

A gear with an artificially removed tooth has been used to represent a defective gear. The tooth has been removed using Electrical discharge machining to avoid any introduced stresses on neighboring teeth (see Figure 4.4). Using this pinion, the same test as in the previous Section has been performed.

The results of the forcing error measurements are presented in Figure 4.5. In this Figure, 3 distinct peaks can be identified, which are caused by the missing tooth in combination with the

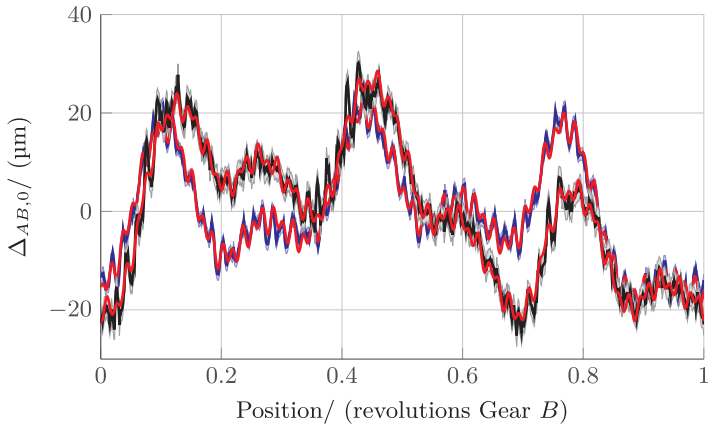

Figure 4.2: Forcing error of the healthy transmission (——). The blue area represents the 99 % confidence interval of the measurements, assuming a normal distribution of the measurement error for a small positive load. The red line (——) is the fitted Fourier approximation of the signal using the 7 harmonics from Table 4.1. The black line (——) and surface represent a measurement with a small negative load. The standard deviation between the mean measurement and the Fourier approximation is 1.26 µm for the positive load.

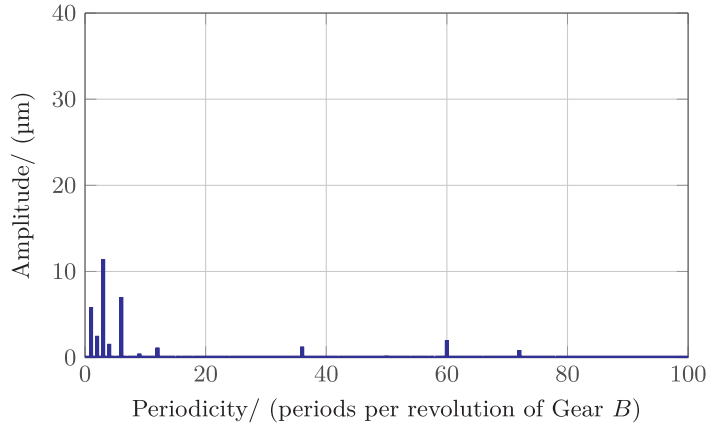

Figure 4.3: Forcing error periodicity of the average healthy transmission for a small positive load. The main periodicities of the signal are shown in Table 4.1

Table 4.1: Main harmonics m of the healthy gear

Periodicity	Description
1	Eccentricity of Gear B
2	Misalignment of Gear B
3	Eccentricity of Gear A
6	Misalignment of Gear A
12	Unknown
36	Unknown
60	Number of engaging teeth

Figure 4.4: Pinion with artificially removed tooth. This pinion is used to measure the effect of a broken tooth.

gear ratio of $i = 3$. The approximation using Equation 4.2 using the largest 54 harmonics[2] is also presented. The approximation fits well to the measurements but is not as good as for a healthy gear. However, the effect of a broken tooth can be clearly identified. The standard deviation between measurement and approximation is 3.34 µm. If a better fit is needed, more harmonics can be included in the approximation.

The periodogram in Figure 4.6 shows the periodicity of the forcing error for a small positive load. In this figure, more harmonics can be observed as in the healthy case (Figure 4.3). Multiples of 3 periods are observed in this periodogram which can be explained by the Gibbs phenomenon (e.g. Hewitt & Hewitt, 1979) caused by the pulse-shaped forcing error of the broken tooth. In contrast to the healthy gear, a large deviation can be observed at the position of the broken tooth for a positive or negative loading. This can be explained by a locally increased play of the gear.

4.2.3 Summary

The forcing error for healthy gears seem to be dominated by the eccentricity and misalignment of the gears as well as the number of teeth. For a broken gear with removed tooth, the forcing error is greatly influenced by the missing tooth. Due to the pulse-shaped forcing error of the missing tooth, the periodogram shows many harmonics of the missing tooth. A Fourier approximation is proposed to approximate the measured forcing error. The healthy gear can be well approximated using 7 harmonics. The broken tooth needs many more harmonics to have a reasonable fit. A fit with 54 harmonics is proposed and shows a good agreement with the measurement data. Using the FaultTriggering toolbox presented in Appendix C, the datasets of the healthy and broken gear can be switched to simulate a broken tooth. The switching is also possible during the simulation, which is important for the development and validation of health monitoring algorithms.

[2] m=[1 2 3 4 6 9 12 15 18 21 24 27 30 33 35 36 39 42 45 48 51 54 57 59 60 61 63 66 69 72 75 78 81 84 87 90 93 96 99 102 105 108 111 114 117 120 123 126 129 132 135 138 141 144]

Figure 4.5: Forcing error of transmission with a broken tooth (——). The blue area represents the 99 % confidence interval of the measurements, assuming a normal distribution of the measurement error. The red line (——) is the fitted Fourier approximation of the signal using the largest 54 harmonics. The black line (——) and surface represent a measurement with a small negative load. The standard deviation between the mean measurement and the Fourier approximation is 2.53 µm

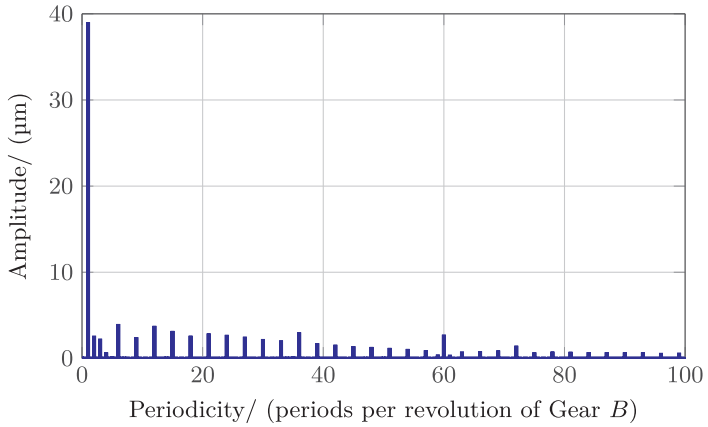

Figure 4.6: Forcing error periodicity of the transmission with a broken tooth. Many distinct peaks can be seen at n times the tooth failure frequency caused by the pulse shaped excitation of the missing tooth.

4.2.4 Discussion

The difference in forcing error between the positive load and negative load which can be best observed with a broken gear is likely to be caused by gear play. Therefore, it seems that also the gear play is a function of the position. Further investigations are needed for a more precise analysis of this phenomenon. If the transmission error as shown in Figure 4.5 is used, care must be taken that traveling through the play is avoided as this invalidates the model. Therefore the loading direction must be the same as used for the measurements.

4.3 Load- and position dependent gear deformation and stiffness modeling

The elasticity of gear contacts varies with the loading of the gear (e.g. ISO 6336-1, 2007; Niemann & Winter, 1989; F. L. J. Van der Linden, 2015), as well as with the meshing position (e.g. Kar & Mohanty, 2008; Kiekbusch et al., 2011). It is important to model the varying gear stiffness, as this stiffness variation causes internal excitation of the system leading to noise and higher loads. Moreover, local stiffness reduction is associated with an incipient gear fault (e.g. Choy et al., 1996).

The modeling of the deformation of the gear contact is beneficial in cases like the assessment of dynamic forces on the teeth, rattling analysis, and the development of health monitoring algorithms.

The load dependency of the deformation and stiffness has been discussed in Chapter 2 and several load dependent stiffness models are presented. In this Section, the load dependent models from Chapter 2 will be extended with a position dependency by changing the nominal stiffness $c(F_n)$ of the gear contact to $c^*\left(F_n, \phi_A, \phi_B, \phi_{gear}\right)$, the local nominal stiffness.

As in Section 4.2.1, the periodicity of the gears is exploited, and a Fourier expansion is used to modify the nominal stiffness c to obtain the local nominal stiffness c^*:

$$\begin{aligned} c^* = \big[\big(&\sum_{n\in m} A_{cA,n} \cos\left(2\pi n(\phi_A - \phi_{gear}) + \phi_{cA0,n}\right) \; + \\ &\sum_{n\in m} A_{cB,n} \cos\left(2\pi n(\phi_B - \phi_{gear}) + \phi_{cB0,n}\right)\big) + 1\big] c \; . \end{aligned} \tag{4.4}$$

In this equation, $A_{cA,n}$ and $A_{cB,n}$ are the amplitude of the stiffness ripple. To set the stiffness ripple to 10 % of the nominal stiffness c, the stiffness amplitude must be set to $A_{cA,n} = 0.1$. $\phi_{cA0,n}$ and $\phi_{cB0,n}$ are the phase angles of the Fourier series. To obtain the stiffness ripple, the gear transmission stiffness can be measured. However, this method is only suitable for single stage gears, as it will be impossible to differentiate between the gear stages if a complete gear is measured. A further possibility is to obtain the stiffness ripple with specialized gear design programs like FVAWorkbench or KiSSoft. This has the advantage that each gear stage can be individually designed and therefore the gear parameters of each gear can be obtained. Values from experience can also be used as a first approximation.

Modeling of broken gears

To model the effect of a broken tooth during the simulation, two sets of amplitudes ($A_{cA,n}$ and $A_{cB,n}$) and phases ($\phi_{cA0,n}$ and $\phi_{cB0,n}$) are defined; one set for the normal behavior and one to model a broken tooth. In case of a fault, the set of amplitudes is replaced, and the effect of a broken tooth will be modeled. The coefficients of a broken gear can, just like for the healthy gear be obtained experimentally (see Section 4.4.3), calculated using specialized methods or estimated based on experience with similar systems. To trigger such faults in Dymola models, the FaultTriggering Library (see Appendix C or (F. L. J. Van der Linden, 2014b)) has been developed. This library systematically introduces the mechanism to enable faults in models. The systematic approach of including faults in a system simulation becomes important if systems with many faults are used.

4.4 Measurement of load- and position dependent gear deformation and stiffness

The measurement of the gear deformation and stiffness is needed to validate the models presented in Chapter 2, and to obtain the behaviour of gear trains on a gear test rig for healthy and defective state. These measurement results can be used to parametrize these simulation models and predict the behavior of similar systems.

Using the test rig presented in Chapter 3, the deformation of the gear contact can be obtained as a function of the load and rotational position of the gears. It is therefore possible to obtain the gear contact stiffness using the same stepped load with constant speed measurements as which are used in Chapter 3.

Note that the elastic contact deformation $\Delta_{AB,e}$ cannot be measured without measuring the forcing error $\Delta_{AB,0}$. Therefore, in the sections below, the total contact deformation including forcing error Δ_{AB} is analyzed.

4.4.1 Contact deformation

To obtain the gear mesh deformation as a function of the load and position of the gear, the gear is running at a constant velocity ($\omega_B = 10\,\mathrm{RPM}$). A series of measurements is carried out at load levels from $-26\,\mathrm{N\,m}$ to $26\,\mathrm{N\,m}$ in steps of $0.25\,\mathrm{N\,m}$. Each measurement consists of 4 rotations of gear wheel B, while measuring the position and load using the installed sensors (see for a detailed sensor description Chapter 3).

The measured deformation between the position sensors 1 and 2, $\Delta_{12} = \phi_{sensor1} r_A - \phi_{sensor2} r_B$ is the deformation of the gear train. This deformation includes the deformation of the couplings and sensors. To obtain the gear mesh deformation Δ_{AB}, the train deformation must be compensated:

$$\Delta_{AB} = \Delta_{12} - \frac{F_n}{c_{train}} \,. \tag{4.5}$$

In this Equation, c_{train} is the apparent stiffness of the train at the contact position. It can be obtained by solving Equation 4.6 for the train stiffness c_{train}:

$$\frac{1}{c_{train}} = \frac{r_A^2}{c_{train,A}} + \frac{r_B^2}{c_{train,B}} \,. \tag{4.6}$$

$c_{train,A}$ and $c_{train,B}$ are the lumped stiffness of the train at the A, respectively B side of the gear. This stiffness is obtained from the data-sheets of the components and stiffness calculations of the shafts. In Chapter 3 the stiffness parameters of the couplings, sensors and axis are presented. It must be noted that the train stiffness is relatively low with respect to the gear stiffness. Therefore the train stiffness must be known accurately since an offset in the train elasticity has a great impact on the measured gear stiffness.

The gear test rig used in this thesis is developed to mimic geared actuators as it is mainly designed for health monitoring applications. In this case the extra elasticity of the system simulates the real life coupling of all parts. Therefore, the position sensors are positioned relatively far away from the gear which is not optimal for stiffness analysis presented in this Section.

Combining the data from the set of measurements at different loading conditions, a 3D map can be created of the deformation $\Delta_{AB}\,(F_n, \phi_B)$. To be able to efficiently process this dataset and suppress noise, the 3D map is gridded to an equidistant surface using the surface fitting algorithm

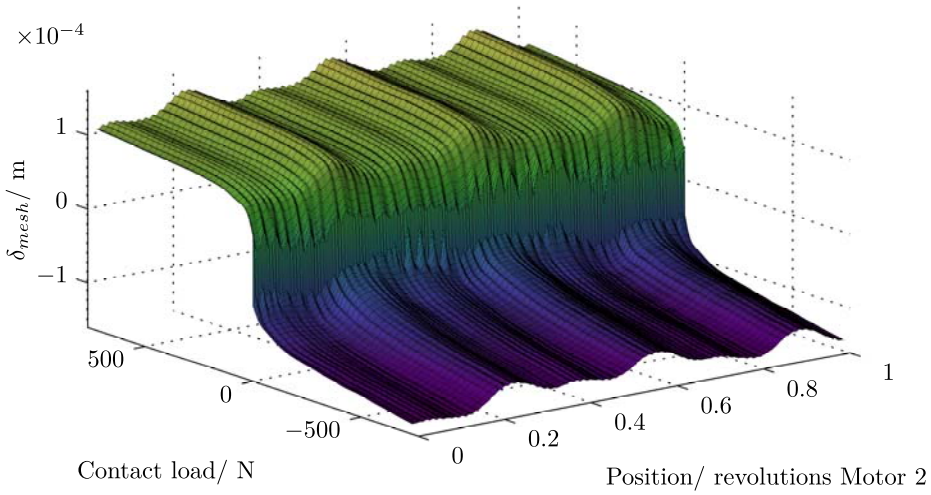

Figure 4.7: Deformation Δ_{AB} of the gear contact as a function of the contact load F_n and gear position ϕ_B. This figure shows the deformation of a typical healthy gear contact, measured at w_A = 10 RPM.

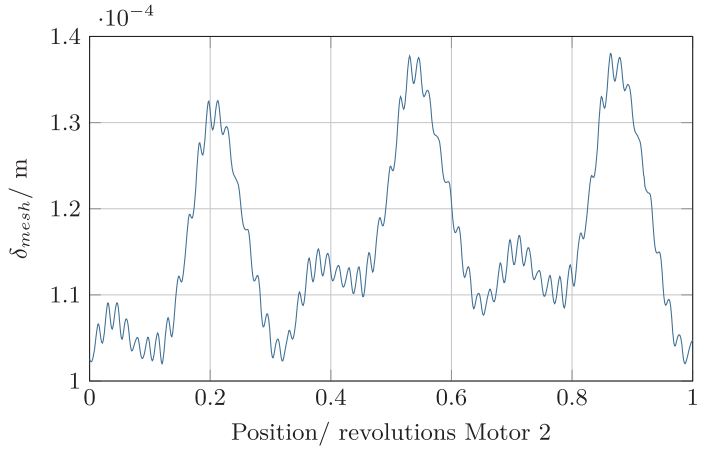

Figure 4.8: Cut of Figure 4.7 at a load of 500 N showing the stiffness ripple of the gear.

`gridfit` by (D'Errico, 2005). Using the "diffusion" interpolation, a gridded surface is approximated. The advantage of this method is that it can handle big data sets with noisy data and multiple entries. Since this gridding algorithm is not optimized for discontinuous surfaces as is the case in the position difference measurements due to the gear play, the surface is gridded in two parts. One part for positive loads and one part for negative loads. After gridding the results for these two sets, the two sets are combined into a single dataset for further processing and displaying. To reduce the noise, the results are smoothed using the smoothing parameter in the `gridfit` algorithm.

In Figure 4.7, the deformation is shown of the same set of gear and pinion as used in Section 4.2.2. An inspection of this surface shows a nonlinear deformation of the surface with respect to the loading condition and the mesh position. The eccentricity and misalignment of the gear as discussed in Section 4.2.2 can be clearly seen in the measurements.

Furthermore, it is possible to observe the effects of the single tooth on the tooth deformation; a

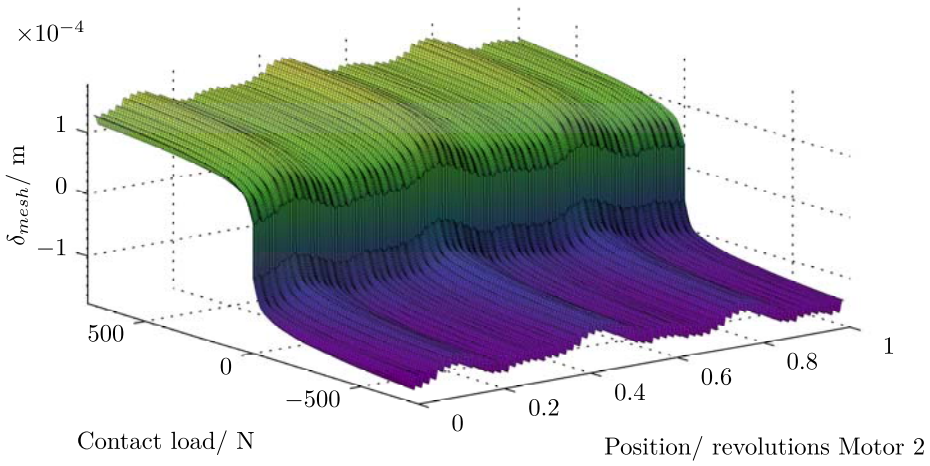

Figure 4.9: Deformation Δ_{AB} of the gear contact as a function of the contact load F_n and gear position ϕ_B. This figure shows the deformation of a simulation of a healthy gear contact with a position depending forcing error, measured at $w_A = 10\,\mathrm{RPM}$.

small periodic deformation can be identified 60 times per revolution, which is the mesh period of the tooth. This is especially visible when only a single load level is observed as shown in Figure 4.8.

Repeated gear deformation measurements can be found in Appendix A.1.1. The results of the repeated measurements show a good agreement between each other.

In Figure 4.9 the results of the same analysis as above are shown with a simulated testrig. Exactly the same "measurements" have been done using these simulations as on the real test rig. The rig has been parametrized with the measured forcing error (Figure 4.2) and a 5 % elasticity ripple. A similar pattern for the gear measurements and gear simulations can be observed, showing that the modeled gear with nonlinear stiffness can represent the behavior of a real gear transmission when it is properly parametrized.

4.4.2 Contact stiffness

The local stiffness of the gear contact can be obtained by differentiating the load with respect to the deformation:

$$c^*\left(F_n, \phi_A, \phi_B, \phi_{gear}\right) = \frac{\delta F_n}{\delta \Delta_{AB}} \ . \tag{4.7}$$

This differentiation is numerically done using an Euler method. This differentiation of the deformation dataset can lead to large outliers in rare cases. Such cases can be caused by unusual high noise or a rare case of local sticking of the gear during the measurements. Since these outliers hinder a good representation of the data, these datapoints have been removed from the graphical representation of the data. Where a datapoint is missing, no data is shown. The results of the local stiffness calculations are shown in Figure 4.10. In Figure 4.11 a two dimensional representation of the data at 4 load levels is shown. In this particular dataset, no missing datapoints are present. However, such missing datapoints can be found in the repeated measurements provided in Appendix A.2.1. The mean stiffness as discussed in Chapter 2, increases linearly with the contact load (see Figure 4.10). The two dimensional representation of the stiffness in Figure 4.11 shows a stiffness variation between the teeth: 60 times per revolution of gear B the stiffness varies with an amplitude of

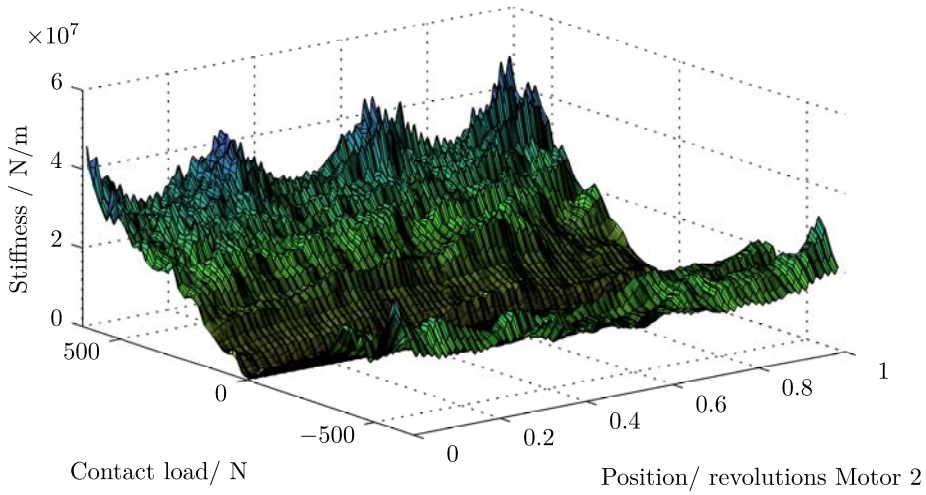

Figure 4.10: Local stiffness c^* of the gear contact as a function of the contact load F_n and gear position ϕ_B. This figure shows the stiffness of a typical healthy gear contact, measured at $w_A = -10\,\mathrm{RPM}$. The deformation of this measurement set is shown in Figure 4.7

Figure 4.11: Normalized stiffness at different load levels extracted from Figure 4.10, measured at $w_A = 10\,\mathrm{RPM}$.

approx 2.5 %. It can be further noticed that the stiffness is mostly independent of the transmission error as the characteristics of the forcing error are not represented in the measurements. This is also expected, because the forcing error is by definition assumed to be independent on the loading.

Repeated stiffness measurements can be found in Appendix A.2.1. The results of the repeated measurements show a reasonable agreement between each other. The differentiation of the measurement results leads to a noisy dataset and especially at higher loads, the gear stiffness is increasing very rapidly. This might be caused by an insufficient accurate gear train stiffness. When the gear train stiffness estimate is too low, the deformation of the train is estimated too high resulting in a too low gear deformation which leads to an apparent stiff gear connection.

The same stiffness analysis as used for the measurement results has also been performed on the simulation results. The position- and load dependent stiffness of the testrig is indicated in

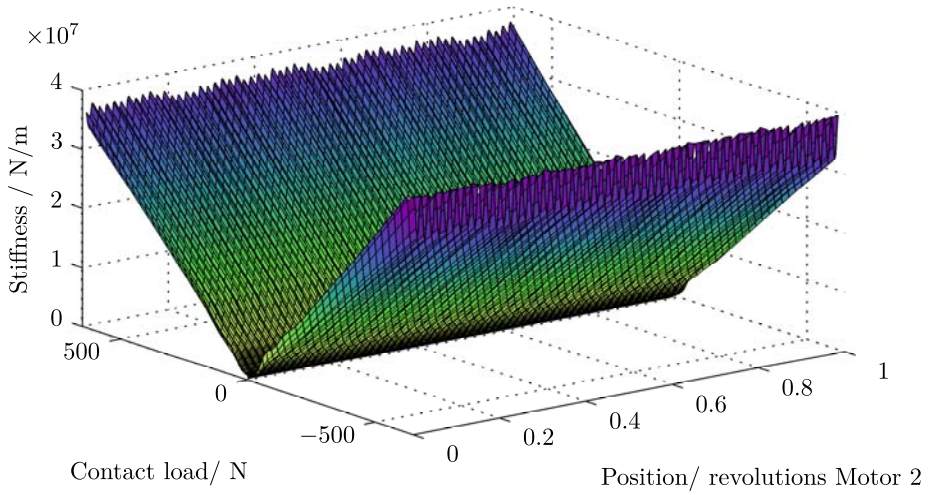

Figure 4.12: Local stiffness c^* of the gear contact as a function of the contact load F_n and gear position ϕ_B. This figure shows the stiffness of a the simulation of a healthy gear contact at $w_A = 10\,\mathrm{RPM}$.

Figure 4.12. The behavior represented by the simulation is also found in a real gear transmission (compare Figure 4.10 and Figure 4.12).

Check of the stiffness measurement

A plausibility check of the analysis method used in Section 4.4 can be carried out. The prescribed stiffness ripple in the simulations was ±5 %. Careful study of figure 4.12 shows that at 550 N and a positive speed of wheel A ($\omega_A > 0$), the stiffness varies with ±6 %. This is slightly higher as expected. At −550 N, the stiffness variation is ±11 % which is much higher as expected. These deviations seem to be slightly influenced by the friction in the gear, as an analysis of a simulation without friction yields a variation ±5 % for a positive load of 550 N and ±9 % for negative load of −550 N. Using the same, but negative speed of motor 2, a different stiffness profile is obtained as presented in Figure 4.13. A comparison of Figures 4.12 and 4.13 shows that for an opposite gear rotational direction, the load variation at a positive load changes from ±7 % to ±15 %. Is it assumed that this variation is caused by dynamic effects during the rotation of the gear. It can be concluded that the variable stiffness cannot be perfectly represented using the presented method. However, the method can represent the absolute gear stiffness very well.

4.4.3 Deformation and stiffness of gear contact with broken tooth

From the results of the mesh deformation Δ_{AB} (Figure 4.14) and stiffness (Figure 4.15) the eccentricity and misalignment of the gear can be identified. The deformation and stiffness reduction at the broken tooth can be clearly identified by the local variations at approx 0.12, 0.45 and 0.78 revolutions of Motor 2.

The increased deformation in Figure 4.14 can also be observed in the Figure 4.15. At the position of the broken tooth a reduction of the stiffness can be observed.

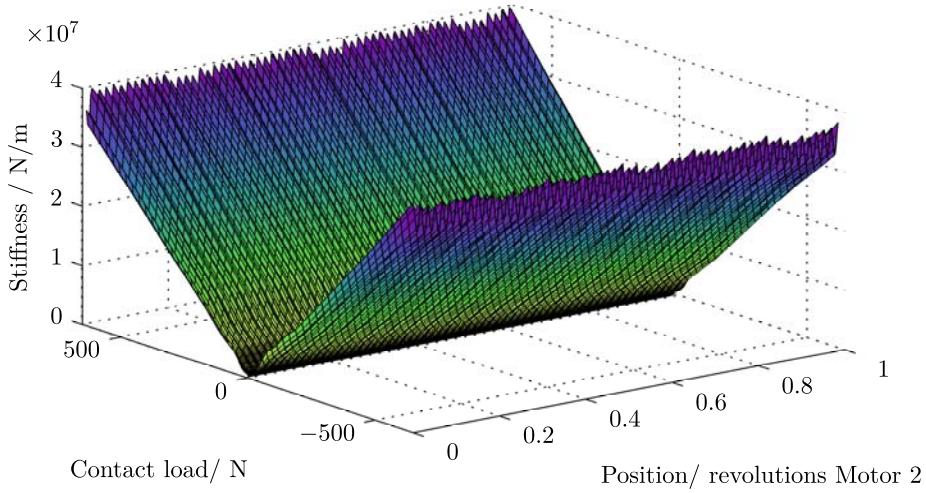

Figure 4.13: Local stiffness c^* of the gear contact as a function of the contact load F_n and gear position ϕ_B. This figure shows the stiffness of a the simulation of a healthy gear contact at $w_A = -10\,\mathrm{RPM}$.

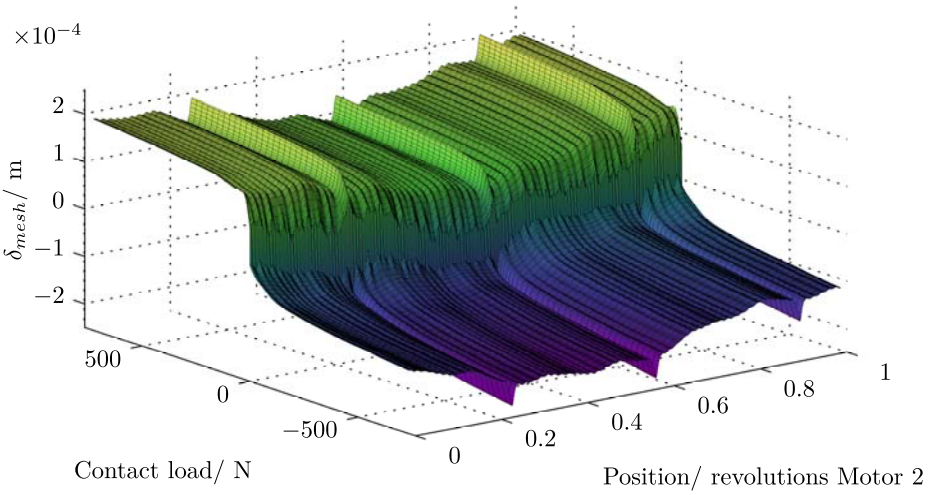

Figure 4.14: Forcing error of the transmission with a broken tooth, measured at $w_A = 10\,\mathrm{RPM}$.

In Figure 4.16, the stiffness of the gear at different load levels is presented. It can be seen that at the position of the gear fault, the stiffness is reduced with approximately 20 %.

Further repeated measurements can be found in Appendix A.1.

4.4.4 Summary

The load- and position dependent gear deformation and stiffness of gears can be measured and simulated. For the used straight cut gear wheel, the stiffness variation between the teeth is measured to be approx 2.5 %. The stiffness reduction of a missing gear tooth is around 20 %. This stiffness reduction leads to a deformation under load, which can be detected using health monitoring

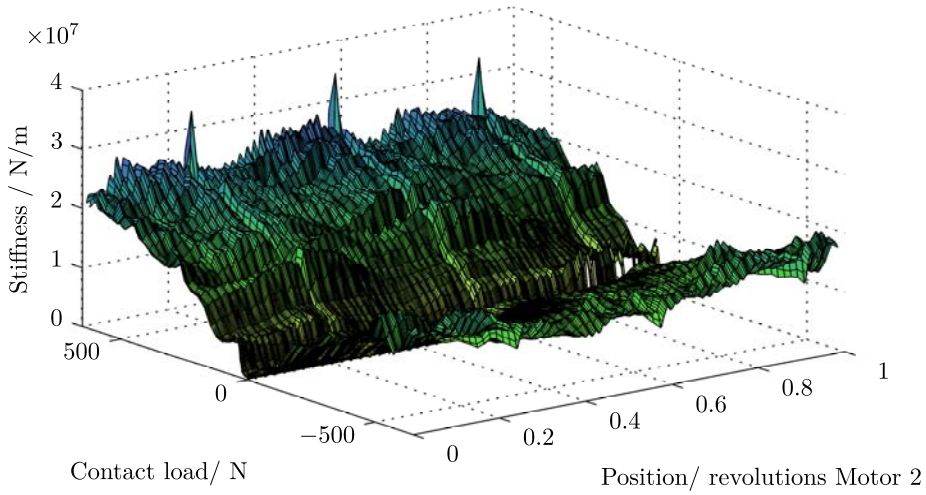

Figure 4.15: Local stiffness c^* of the broken gear contact as a function of the contact load F_n and gear position ϕ_B, measured at $w_A = 10\,\mathrm{RPM}$. This figure shows the stiffness of a typical gear with a broken tooth. The deformation of this measurement set is shown in Figure 4.14

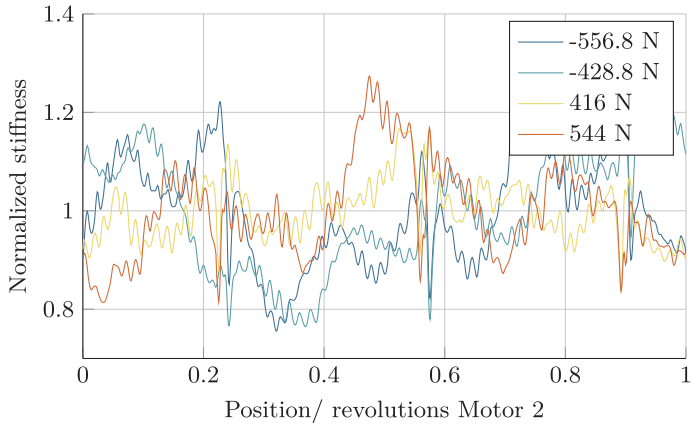

Figure 4.16: Normalized stiffness of a gear with a broken tooth at different load levels extracted from Figure 4.15, measured at $w_A = 10\,\mathrm{RPM}$.

applications. Further work from the author (F. L. J. Van der Linden, Dreyer, & Dorkel, 2016) has shown that this is not only theoretically possible in simulations or on a specialized test rig, but can also be detected on real aircraft actuators.

4.5 Load and position dependent friction modeling

For a complete description of a gear contact dependent on the position and loading, not only the forcing error and deformation of the gear contact are important, but also the friction in the gear contact. A good example is Garcia et al. (2002), who propose a position and mesh speed dependent friction. However, many friction models (e.g. DIN 3990 Teil 4, 1987; Niemann & Winter, 1989) also include a dependency on the gear loading. In this work, a combined approach is proposed: The

load dependent friction coefficients as presented in Section 2 will be extended with a sinusoidal component as used by (Garcia et al., 2002). This position dependent friction is important since it can self-excite the gear wheels leading to vibrations. Furthermore, the sticking-behavior of a gear is position dependent leading to positions where the stiction force can be easily overcome and positions where a high breakout force is required.

4.5.1 Modeling

The friction modeling is based on the friction introduced in Chapter 2. In that chapter, load and velocity dependent friction models have been introduced. In this Section, the friction coefficient $\mu(v_{mesh})$ will be extended to a position dependent friction coefficient $\mu^*(v_{mesh}, F_n, \phi_A, \phi_B, \phi_{gear})$. To add a position dependent variation of the friction, the same approach as used for the stiffness variation (see Section 4.3) will be used. A Fourier expansion will be used to be able to introduce as many terms as needed to correctly model the variation of the friction coefficient:

$$\begin{aligned}\mu^* = \big[\big(\sum A_{\mu A,n} \cos\left(2\pi n(\phi_A - \phi_{gear}) + \phi_{\mu A0,n}\right) \; + \\ \sum A_{\mu B,n} \cos\left(2\pi n(\phi_B - \phi_{gear}) + \phi_{\mu B0,n}\right)\big) + 1\big]\mu \; .\end{aligned} \tag{4.8}$$

In this Equation, $A_{\mu A,n}$ and $A_{\mu B,n}$ are the normalized amplitude of the friction variation. Setting $A_{\mu A,n}$ to 10 % will lead 10 % variation of the friction coefficient μ^*. $\phi_{\mu A0,n}$ and $\phi_{\mu B0,n}$ are again the phase angles of the Fourier series.

4.5.2 Measurements

The test rig (Chapter 3) has been used again for measurements to create a 3D map of the friction, dependent on the gear loading (F_n) and gear position (ϕ_B). The same measurements as used in the contact deformation- and stiffness measurement can be applied, as for the friction measurements also a stepped load at constant velocity is needed.

The gear friction has been defined as in Chapter 2:

$$\tau_{friction} = \tau_A + \tau_B \frac{r_A}{r_B} \; . \tag{4.9}$$

The results of the friction measurement of a healthy gear at ω_A =10 RPM is presented in Figure 4.17. These measurements show that the friction varies substantially over the position of the gear. The position dependent part of the friction of the gear is of the same magnitude as the average friction. Thus, to accurately model the gear friction, the position dependency of the friction must be taken into account. The friction variation is a well known effect and is caused by the different positions on the line of contact. A single contact at the pitch point is subject to plain rolling which has a very low resistance. Further away from the pitch point the friction forces increase. It can be seen that the friction is at certain positions positive which is suspected to be an artifact of the dynamic response of the system.

4.5.3 Friction of gear contact with broken tooth

Friction measurements have also be carried out for a broken gear tooth and are presented in Figure 4.18. As can be seen in this figure, the friction forces are large when the broken tooth is in contact, exceeding 400 % of the normal friction. When developing health monitoring algorithms for electromechanical actuators, the friction spike can lead to position dependent motor current

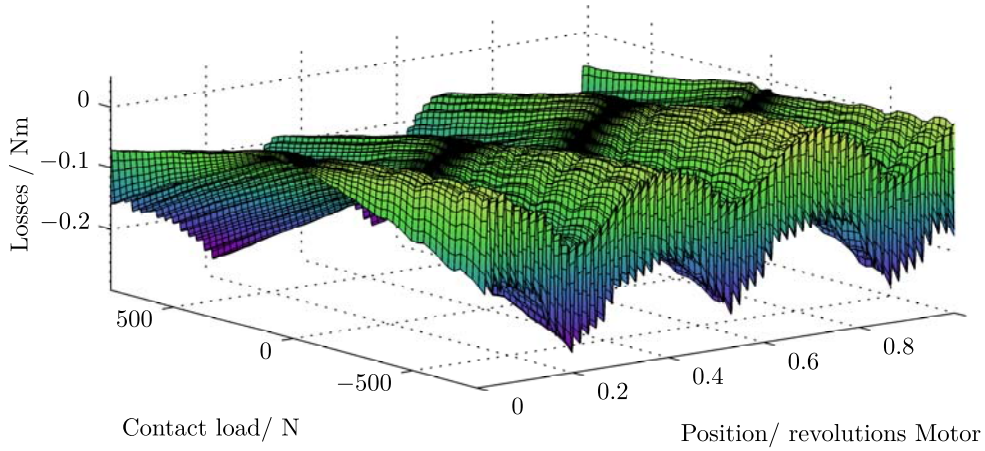

Figure 4.17: Local friction of the healthy gear contact as a function of the contact load F_n and gear position ϕ_B. This figure shows the friction of a typical healthy gear contact, measured at w_A = 10 RPM. The deformation of this measurement set is shown in Figure 4.7

increases in a closed loop system as the speed control loop compensates the position dependent friction. This effect will be mainly visible at low speeds with high load as no dynamic forces can compensate the increased friction.

4.5.4 Model validation

Using the position dependent friction modeling as presented in Section 4.5.1, it is possible to achieve the same behavior as the measured gearset in simulation. A Fourier analysis of the scaled friction has been made of the measurements, to obtain a load-independent friction scaling function which can be used in Equation 4.9. The results of this position dependent friction is shown in Figure 4.19. Using the fitted friction variation, the model can reproduce a very good matching friction profile when compared with the measured friction (Figure 4.18).

4.5.5 Summary

Position dependent friction modeling can prove a useful tool for simulation of friction self excitation as well as for the development and testing of health monitoring algorithms. The proposed approach which scales the load dependent friction coefficient dependent on the rotational position of the gears can represent a real gear transmission system well.

4.5.6 Discussion

It has been shown that dynamical effects play a role in the measurement of the stiffness. To avoid such dynamical issues, it has been tried to perform the same measurements at lower motor speeds. However, at these motor speeds, a stick-slip phenomenon is observed which invalidates the measurements. This stick-slip problem can probably be avoided by using dynamic motors, lower latency hardware and a tighter control loop. Using the hardware used for this analysis, a performance increase was not possible.

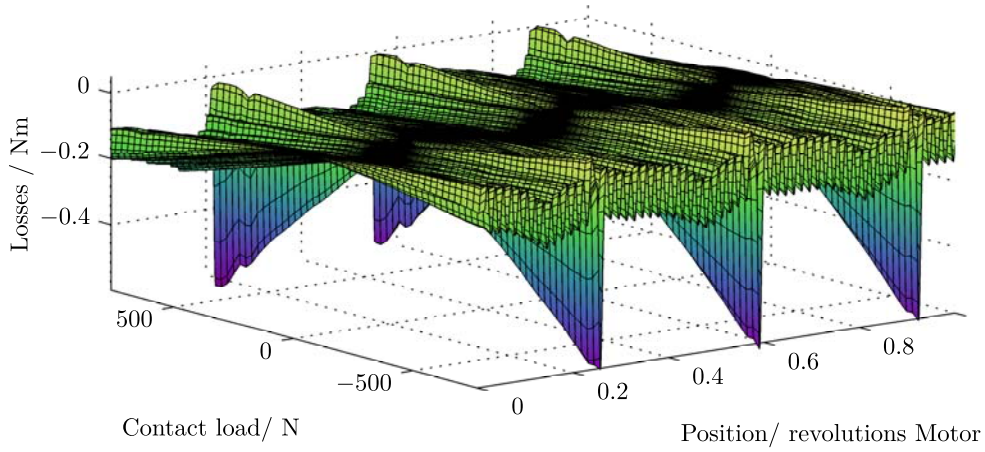

Figure 4.18: Local friction of the broken gear contact as a function of the contact load F_n and gear position ϕ_B, measured at $w_A = 10\,\mathrm{RPM}$. This figure shows the friction of a typical broken gear contact. The deformation of this measurement set is shown in Figure 4.14

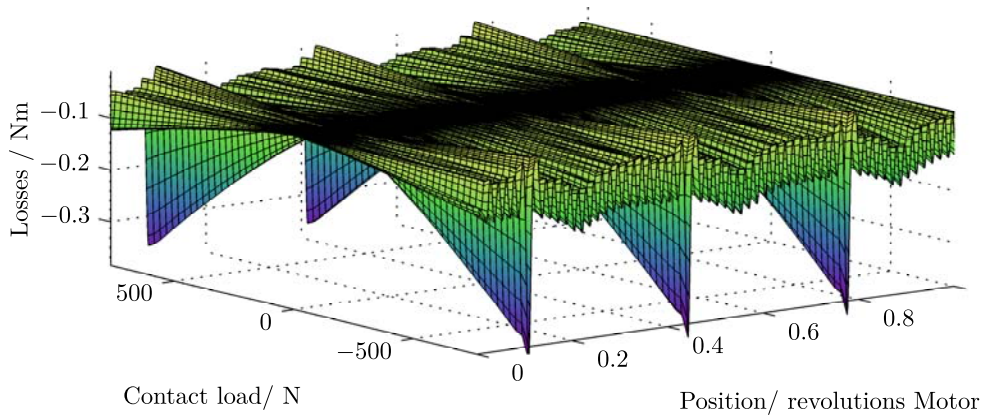

Figure 4.19: Local friction of a simulated broken gear contact using the proposed gear models as a function of the contact load F_n and gear position ϕ_B, measured at $w_A = 10\,\mathrm{RPM}$.

4.6 Conclusion of periodic effects with gear systems

By measuring the forcing errors as well as load and position dependent stiffness and friction of a gear transmission, it is found that for straight cut gears the position dependent variation is substantial for a healthy gear set. For a broken gear set, the position dependent variation of the stiffness is found to be approximately 20 % and the friction variation peaks over 400 %. The stiffness and friction variation are of greatest influence in slow moving systems. A local friction increase can stop a slowly moving system, putting it into the stuck phase. This effect introduces a position dependent stick-slip problem. This phenomenon has also been observed during tests at very low speeds. Moreover the stiffness variation of the gear is the most prominent at low speeds

as the inertia of the system only plays a small role at such speeds. Therefore, the speed variation of the gear wheels, leading to vibration will be high.

Moreover the forcing error can play an important role in the self-excitation of the system. Especially at higher speeds, this forcing error can lead to high dynamic tooth forces. Dependent on the needed analysis, the position dependent effects discussed in this section have to be included in the system. The presented model includes these effects using a modular approach, giving the user maximal design freedom.

5 Example implementation of torque-vectoring drives for electric vehicles

In this chapter, a practical example of a complex gearing system using the methods from Chapter 2 is presented. To show that the models can not only be used for actuator design, an example from the automotive industry is chosen. This chapter is based on the paper *Modeling of Torque Vectoring Drives for Electric Vehicles: a Case Study*, presented in 2015 at the *International Modelica Conference* in Paris (F. L. J. Van der Linden & Tobolár, 2015).

For the presented example, a powertrain configuration with controlled torque vectoring device for an electric vehicle was selected. It represents a future-oriented solution particularly suitable to actively influence the dynamic behavior of the vehicle, such as using active yaw rate control. Such a torque vectoring drive (TVD) configuration is used e. g. in experimental cars like the VISIO.M (Gwinner et al., 2014) and allows for very high vectoring torques with a small electric motor. A graphical overview of this TVD is shown in Figure 5.1. In this chapter, Jakub Tobolář has contributed to this research with a vehicle model with realistic properties.

This specific TVD example was selected as it shows the use of the presented gear models from Chapter 2 in a complex complete model where the TVD is in the stuck mode when driving straight ahead, making it a very interesting candidate to test the capabilities of the models. The combined planetary differential and superimposing unit make this example a very challenging test for numerical soundness of the gear models as multiple stages of this TVD can have a locked state at the same time. Furthermore, the interaction of the gear with the car highlights the need for a detailed analysis of the gear in a complete system simulation.

Since no measurement data of this example vehicle are available, the example studied in this chapter can be seen as the first steps of the design of a new electric car with a new driveline concept. The goal of such studies is to find any potential problems in the design and find possible solutions to these problems.

5.1 Gear model description

The gear models used in this analysis are based on the Modelica implementation of previous work which consisted of the simulation of elastic ideal gears (see Appendix B). These models have been extended with various loss models and elasticity models that are presented in Chapter 2 and 4. An overview of the forces and torques are shown in Figure 5.2 (identical to Figure 2.5 but repeated here for convenience). Since the derived model of gear teeth contact is purely planar, it is implemented using the PlanarMechanics Modelica library (Zimmer, 2012). This allows the use of standard planar parts and enables the transfer of forces and torques to full 3D models using a standardized interface.

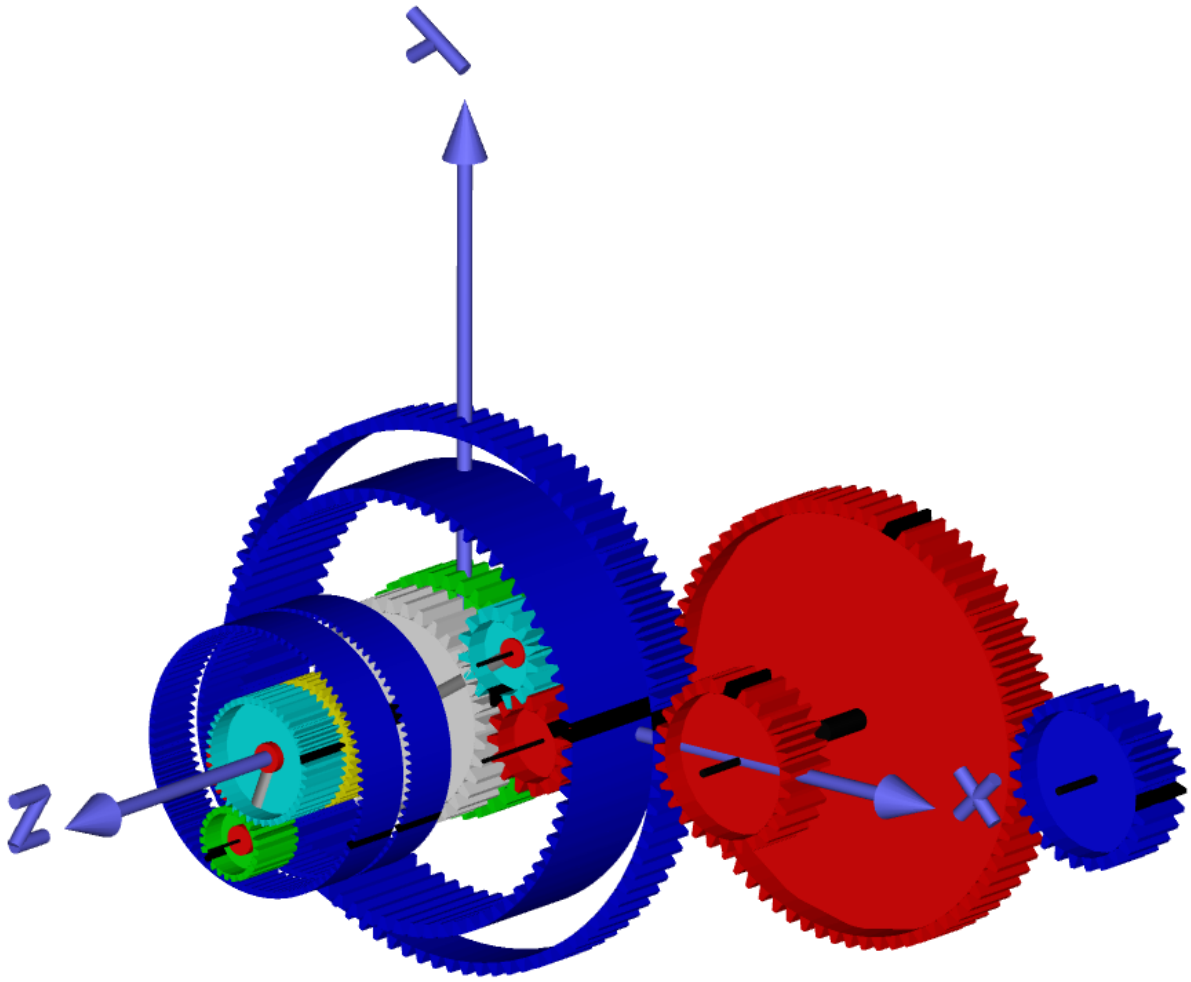

Figure 5.1: Torque vectoring drive consisting of a differential, superimposing unit and spur gear train. Note that only single planets are shown for simplification of the calculations.

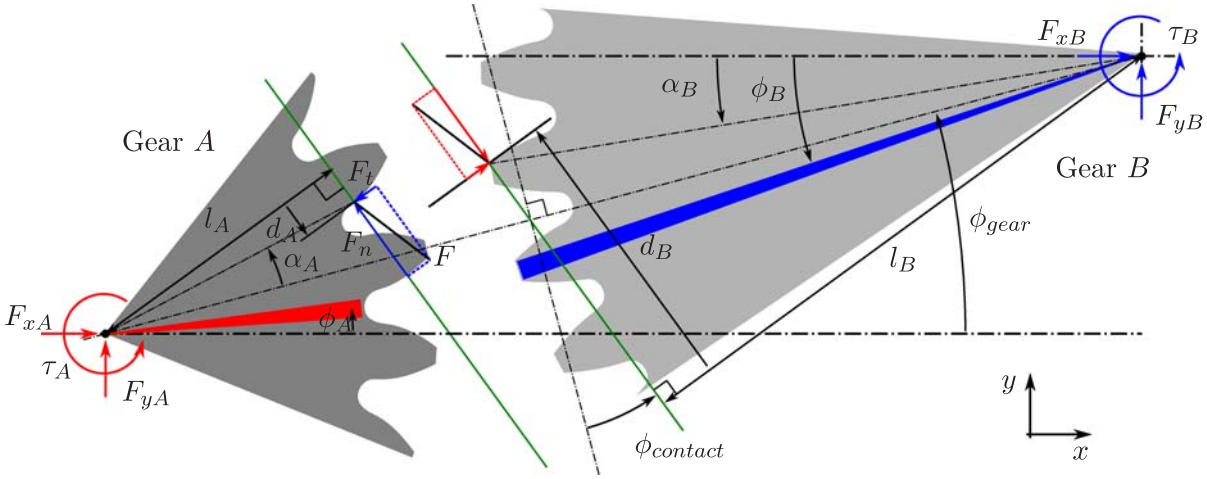

Figure 5.2: Free body diagram of two involute gears. In the figure $\omega_A < 0$ and Gear A drives Gear B.

5.1.1 Friction force implementation

Since in gear dynamics different friction models are often used, a decision was made to implement the friction using a replaceable function structure.

The friction is implemented using a state machine to be able to handle friction during the `Forward`, `Backward` and `Stuck` mode. To switch between these modes, two transition modes are used: `StartForw` and `StartBackw`. A tearing variable `sa` is used in the Stuck mode to calculate the forces to keep the model stuck. This approach is similar to the friction implementation of (Otter et al., 1999). The gear friction force F_t is calculated using specialized functions based on e. g. gear meshing speed, operational mode of the gear contact, contact angle and the radii of the gear wheels.

The concept of replaceable functions allows for a quick selection between the different friction models: no friction, viscous friction, specified efficiency, Coulomb friction, friction according to the DIN 3990 specifications (DIN 3990 Teil 4, 1987) and a friction implementation from Niemann and Winter (1989). The DIN 3990 friction and the friction to Niemann and Winter both define the friction as a function of the speed and loading of the gear.

Furthermore, a continuous friction model which is not based on a state machine is implemented. This implementation uses a regularized friction model to smooth the discontinuity of the gear friction. It is implemented using

$$F_t = \mu |F_n| \tanh \frac{|v_{mesh}|}{v_{mesh,0}}. \tag{5.1}$$

In this equation, v_{mesh} is the relative speed of the gears at the meshing point and $v_{mesh,0}$ the characteristic meshing speed which is chosen small compared to the nominal meshing speed. Using this regularization, event chattering of gear systems with many gear contacts can be avoided. However, it must be noted that in this case no stiction can take place, as the friction is zero at zero speed.

In this paper, a fixed friction coefficient will be used as this method is heavily used in the design of gear transmissions for powertrain analysis, together with the friction implementation to the DIN 3990 norm due to a good match with measured friction results from Chapter 4.

5.1.2 Elasticity implementation

Similar to the variability of friction methods used in the modeling of gears, also the gear elasticity is described in many ways. In most cases, a nonlinear relation between normal forces F_n and deformation of the gear at contact is present. To incorporate the different stiffness models known from literature, also the elasticity is implemented using another set of replaceable functions. These functions calculate the normal contact force F_n from multiple model inputs like the mesh deformation and speed, gear radii, thickness of the wheels and wheel positions. The position of the gear wheels makes it possible to include a position dependent gear stiffness which can be used to simulate the effect of meshing teeth or the effect of a damaged tooth.

5.1.3 Forcing error implementation

To simulate forcing errors like misalignment of the gear wheels, manufacturing errors or damaged teeth, a position dependent forcing error is added to the overall gear deformation. In Figure 5.3 (repeated from Figure 4.1), the deformation between the gears is given by $\Delta_{AB} = \Delta_{AB,0} + \Delta_{AB,e}$.

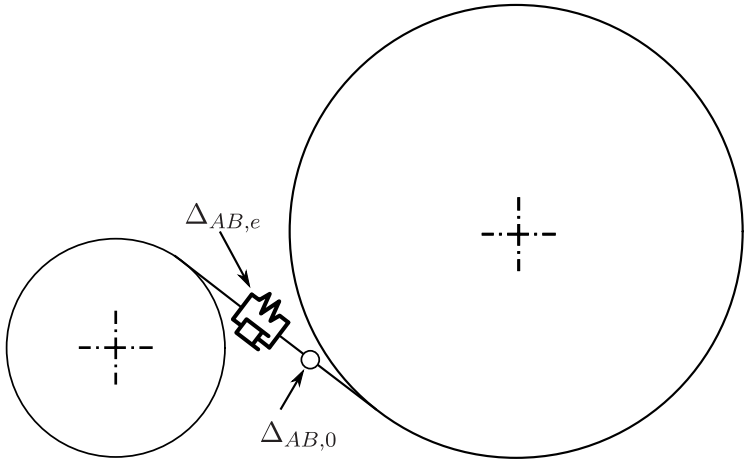

Figure 5.3: Forcing error excitation using a position dependent forcing distance $\Delta_{AB,0}$

In this equation, $\Delta_{AB,e}$ is the elastic deformation of the gear contact as discussed in Section 5.1.2. Adding the forcing distance $\Delta_{AB,0}$ gives the total gear deformation.

Also in this case, replaceable functions are used to implement several cases: a forcing error defined by the misalignments of the gears, a forcing error defined by a Fourier-series and a table-based interpolation. All these methods define the forcing error as a function of the position of each gear wheel.

5.1.4 Graphical representation of gears

The graphical representation of the gears is an important way to check proper geometry of the gear. Therefore, visualizers from `Modelica.Mechanics.MultiBody.Visualizers` are used to visualize the gear wheels. The results of such exemplary 3D representations can be seen in Figure 5.1 and Figure 5.5. The parameters needed for the visualization, such as gear radius or thickness, are directly taken from the gear model parameters.

5.1.5 Implementation of constraint equations

The gear model as depicted in Figure 5.2 needs a defined distance between the centers of the gear wheels for a correct calculation of the forces and torques. However, when a constraint equation is defined in each gear contact model, epicyclic gear sets result in modeling problems since the planet–sun distances and sun–ring distance is defined double, thus leading to an overconstrained system. Therefore, these constraints cannot be defined in the model itself, but must be defined using the `PlanarMechanics` library. This mimics the behavior of real gears: a gear connection itself has no constraining equations. The gear wheel positions are defined by the bearing arrangement of the transmission.

An example of a simple epicyclic gear set is shown in Figure 5.4 and Figure 5.5. The structure of the model is similar to the gear construction. Hence, each bearing, mass and carrier is modeled in Modelica just like in a real system.

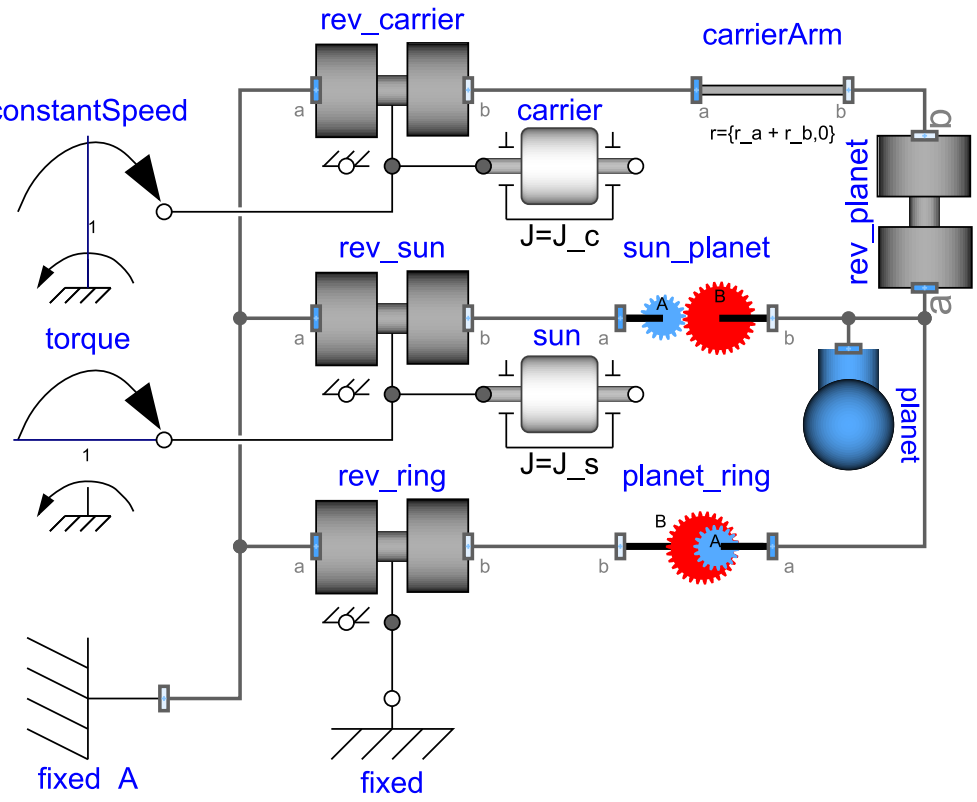

Figure 5.4: Modelica model of simple epicyclic gear configuration

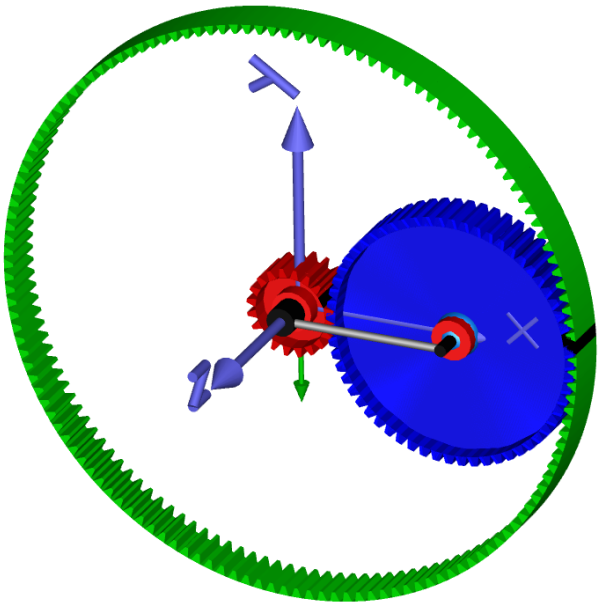

Figure 5.5: Graphical representation of the epicyclic gear configuration shown in Figure 5.4.

5.2 Construction of a torque vectoring drive in Modelica

The models as described in Section 5.1 are used to build a complete torque vectoring drive consisting of a Ravigneaux differential, superimposing gear and spur gear train.

5.2.1 Ravigneaux differential

The Ravigneaux differential is used to allow for different speeds of the car tires. Compared to common open differentials with bevel gears, using a Ravigneaux differential allows for a smaller construction envelope combined with lower losses. The Modelica representation of the differential is shown in Figure 5.6. The Ravigneaux differential uses four gear instances, together with a carrier which houses two connecting planets.

For simplicity reasons, only one set of planets is used in this analysis. When using all planet sets of a full Ravigneaux gear, the system would – in the case of rigid gear connections – lead to an over-determined system. In the case of elastic gears, the different gear stages which can switch between friction modes can lead to heavy event chattering of the planets.

To compensate the stiffness reduction caused by the lower number of modeled planets, thicker gears with higher masses are incorporated.

The reduction of the number of planets would lead to an unbalanced gear model as long as the masses of the planets are considered as well. But since the model in Figure 5.6 is purely rotationally coupled (see rotational flanges on both left and right side), this effect does not apply. On the contrary, if the bearing forces are studied, this planet number reduction will lead to wrong results. In this case, all planet masses should be added to balance the system and they must be rotationally coupled with the planet which is driven by the gear connections.

5.2.2 Superimposing gear

The superimposing gear uses the input torque to create a torque difference between the output flanges. Also in this case, only a single planet is modeled instead of all planets. The stiffness and mass are compensated to mimic all planets as depicted in Section 5.2.1. In Figure 5.7, the setup of the gear is shown. For the superimposing gear, four gear instances are needed.

5.2.3 Overall TVD model

Connecting the Ravigneaux differential, superimposing gear and spur gear train together, a complete TVD is generated as shown in Figure 5.8. To represent the connection elasticity between the drives, rotational stiffness-damping elements are added from the Modelica Standard Library.

In the overall TVD model, ten gear connection models are used for a representation of the complete drive.

In the simulations which are presented in Section 5.4, three different configurations are analyzed according to Table 5.1.

The spring constant of the gear instances is set to 20×10^6 N/m/mm (Newton per meter per millimeter gear width), and the gear damping to 20×10^3 Ns/m/mm for all gear connections. The coupling between the superimposing gear, Ravigneaux gear and spur gear train have a stiffness of 10^7 Nm/rad and a damping of 10^5 Nms/rad, respectively.

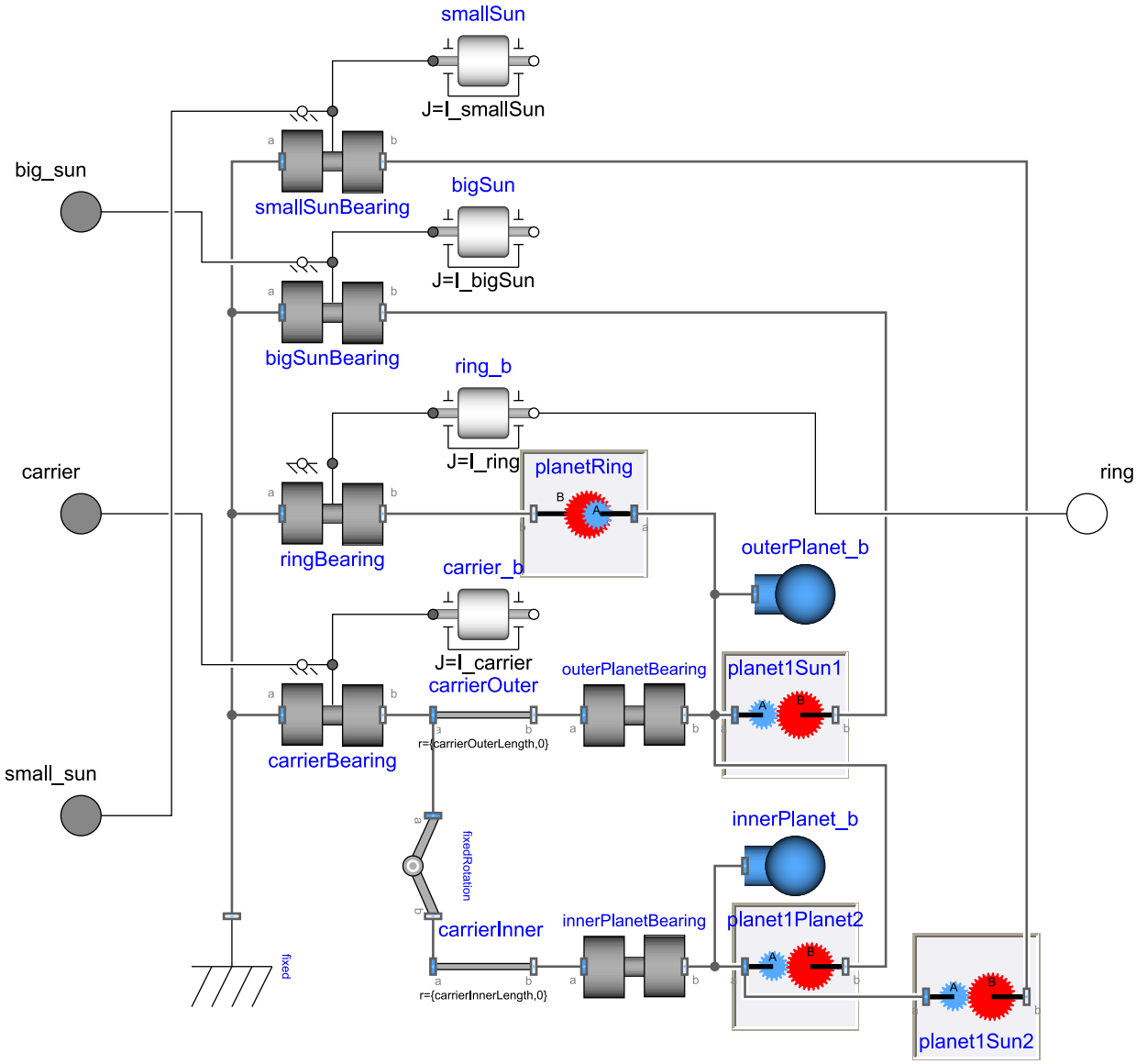

Figure 5.6: Ravigneaux differential

Table 5.1: TVD model configurations under investigation

Configuration	Description
Fixed eta	Constant spring constant, constant gear efficiency
Fixed eta with Backlash	Nonlinear spring constant and backlash, constant gear efficiency
DIN 3990 eta with Backlash	Nonlinear spring constant and backlash, efficiency using to DIN 3990

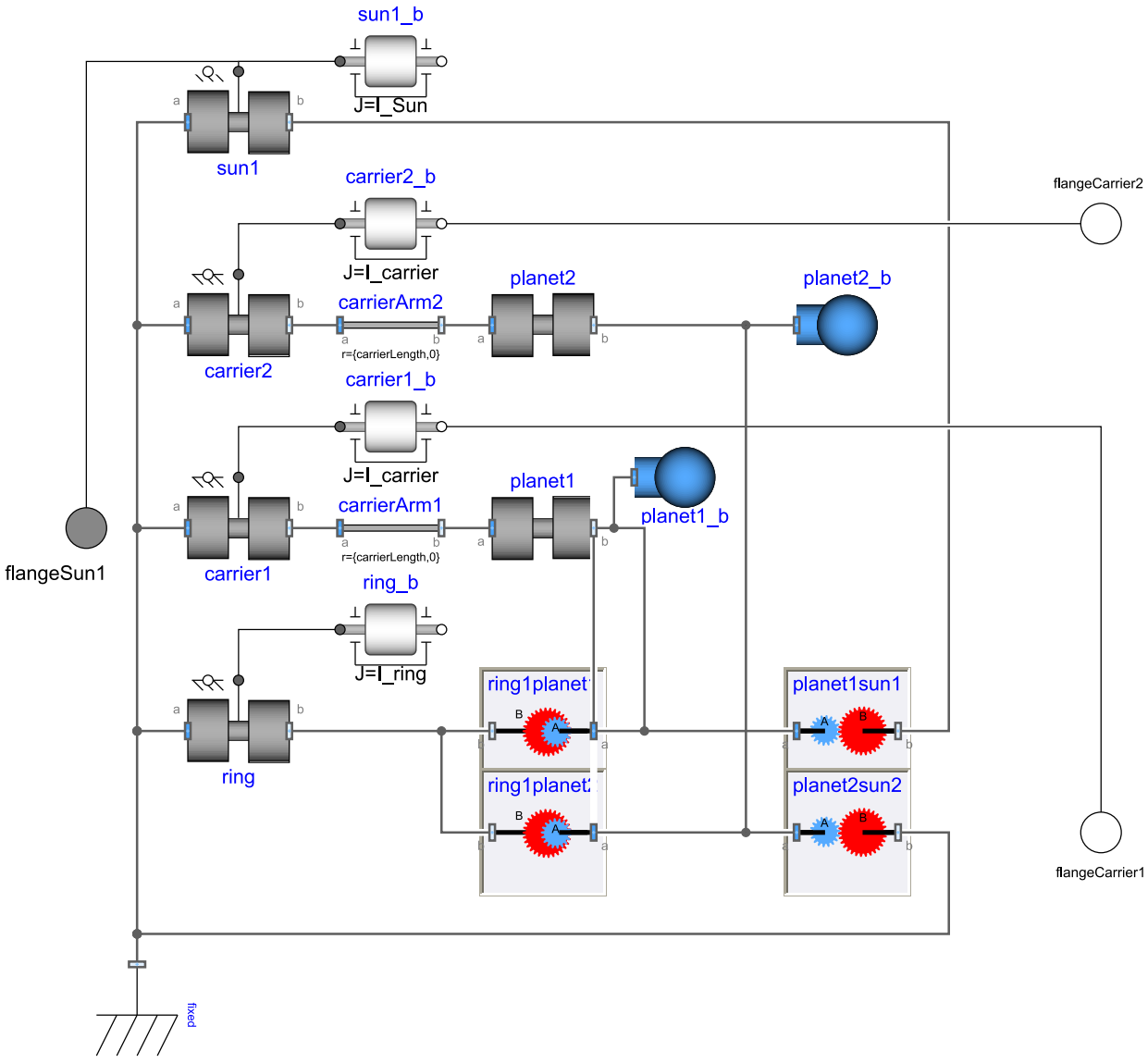

Figure 5.7: Superimposing gear

5.3 Vehicle model

To analyze the TVD model in typical vehicle driving maneuvers, a vehicle model has to be utilized. For the sake of simplicity, a planar vehicle model was introduced which moves in the horizontal plane, thus only enabling longitudinal, lateral and yaw motion. Additionally, a six degrees of freedom mass (i. e. three positions and three rotations) was joined to the planar vehicle body. By taking into account the forces on this mass, wheel load variation due to vehicle mass transformation between wheels during braking, accelerating and cornering are enabled. The tire models allow slip and are based on the work of Zimmer and Otter (2010).

A small size electric vehicle with rear-wheel drive is considered for simulation. Its mass is about 1000 kg with wheelbase of 2.6 m and track of 1.45 m.

The powertrain of the vehicle consists of the TVD as described above, the main motor which applies the main driving torque, and a differential motor which divides torques to the wheels of

one axle. Utilizing the differential motor control, the torque vectoring functionality can be realized. Finally, driveshaft elements are considered as well to additionally incorporate their elasticity. An overview of the model is shown in Figure 5.9. To mimic the electrical time constant of the motors, a first order system with a time constant of 10^{-3} s for both motors is used.

5.4 Simulation results

Using the vehicle model with a free steering setup (free steering wheel), an acceleration maneuver is simulated. The main motor torque is given as a ramped signal, and the differential motor torque as a changing signal as shown in Figure 5.10.

5.4.1 Elastic drive shafts

The wheel torque of the right driveshaft during the maneuver is shown in Figure 5.11. It can be observed that the results of the constant efficiency and the DIN 3990 efficiency differ significantly. The fixed efficiency cases (97% per gear stage) show a behavior which is intuitively expected by the TVD: the differential torque of the differential motor is amplified and split between the two axles.

Introducing the DIN 3990 friction model, the results yield – in contrast to the constant efficiency – an oscillating output torque. This is caused by the fact that due to the pre-load of the differential, combined with low rotational velocities, high friction between the teeth occurs. Due to this high friction, the gear can get in the stuck mode (this phenomenon is also described and measured for air path actuators by Ahmed et al. (2012)).

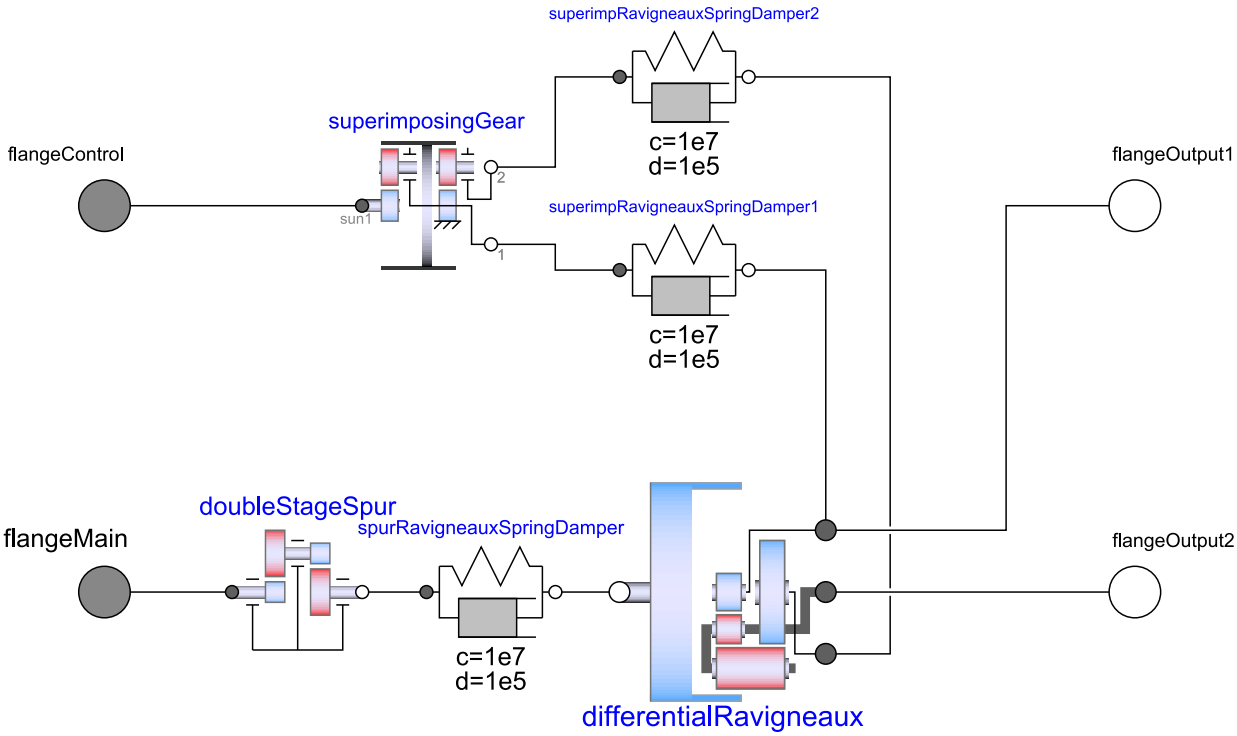

Figure 5.8: Complete TVD consisting of Ravigneaux differential, superimposing gear and spur gear train

The combination of the drivetrain elasticity with high friction leads to a stick-slip problem resulting in highly varying torques. Note that without further measurements and / or experience with a TVD, it cannot be concluded which of the friction models correctly represents the real system.

Analyzing the speed of the differential motor depicted in Figure 5.12, the stick-slip problem is also evident. High rotational accelerations are caused by the fast variation of the motor speed, which can lead to high loads on the rotor of the motor. This can lead to fatigue damage of the motor.

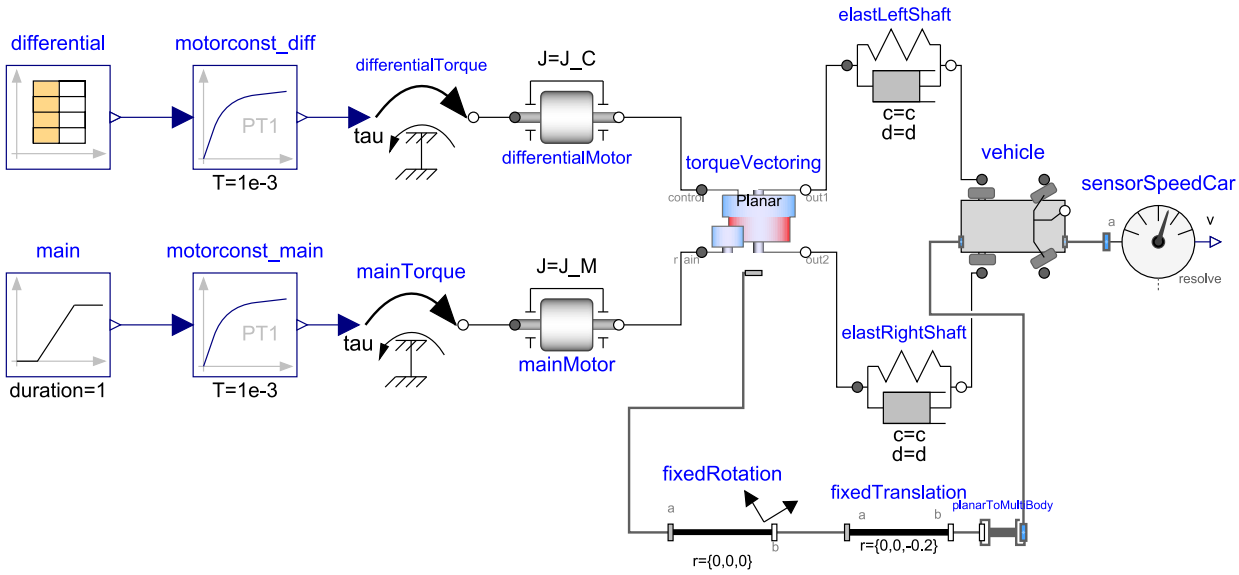

Figure 5.9: Vehicle model with motor configuration and driveshaft elasticity. The right bottom section of the diagram (with the planarToMultibody element) enables an animation where the drive is fixed to the car.

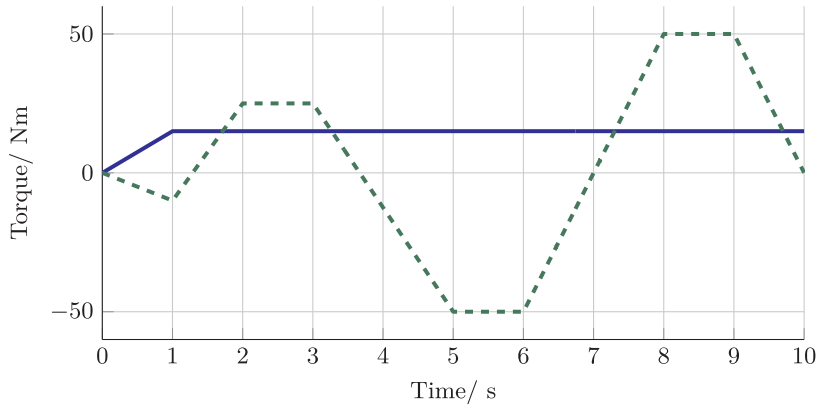

Figure 5.10: Motor torques during maneuver. The main motor torque (——) has a ramp of 1 s to 15 N m , the differential motor (- - -) is controlled with a changing reference torque.

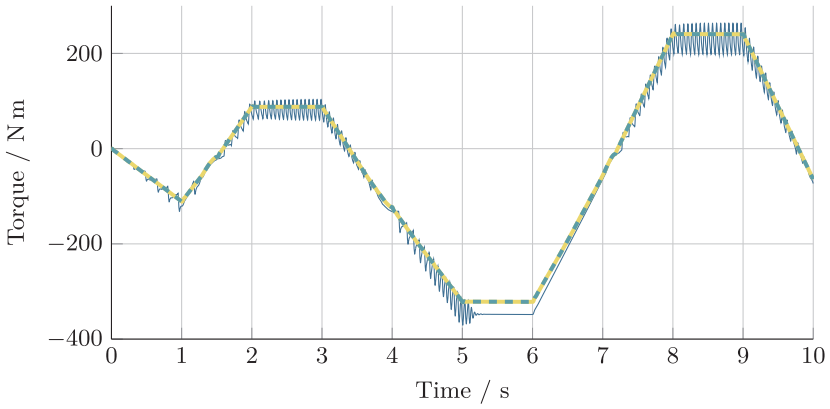

Figure 5.11: Wheel torques of the right driveshaft (reference stiffness) with different friction and elasticity models: A fixed efficiency without backlash (- - -), fixed efficiency with backlash (——) and a friction law according according to the DIN 3990 standard (——).

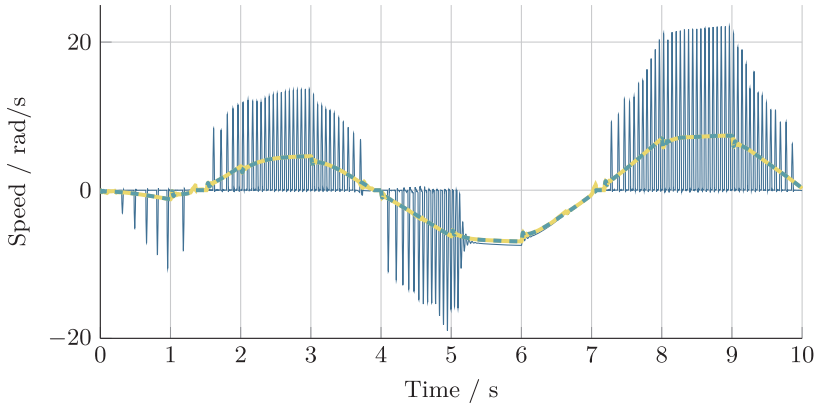

Figure 5.12: Speed of the differential motor using driveshafts with the reference stiffness. Different friction and elasticity models are shown: A fixed efficiency without backlash (- - -), fixed efficiency with backlash (——) and a friction law according to the DIN 3990 standard (——).

5.4.2 Stiff driveshafts

Using driveshafts with a significant higher stiffness and damping, the stick-slip problems described in Section 5.4.1 can be avoided. In the presented example with increased stiffness, a ten times higher friction and damping has been used with respect to the nominal situation. The wheel torques of the right rear wheel (see Figure 5.13) behave as expected, also for TVD using the DIN 3990 friction model. Moreover, the high peaks in motor velocity of the differential gear are eliminated, cf. Figure 5.12 and Figure 5.14.

5.4.3 Simulation of eccentricities

Eccentricities are common in most gear wheels and are often caused by manufacturing tolerances. To simulate a non-perfect drive, an eccentricity of 10 µm is added to both gear wheels of the first stage of the spur gear train. This eccentricity excites the gear train leading to vibrations. In this simulation, a constant torque of 5 N m is applied to the differential motor to keep the Ravigneaux

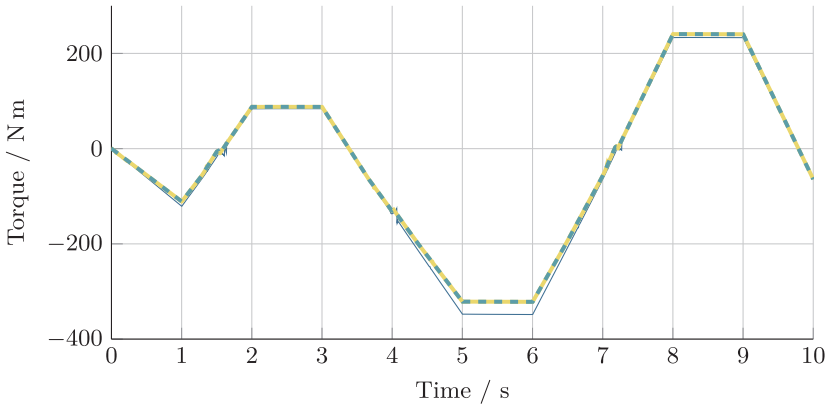

Figure 5.13: Wheel torques of the right driveshaft with different friction and elasticity models. A ten times increased stiffness of the driveshafts is used. A fixed efficiency without backlash (- - -), fixed efficiency with backlash (——) and a friction law according according to the DIN 3990 standard (——).

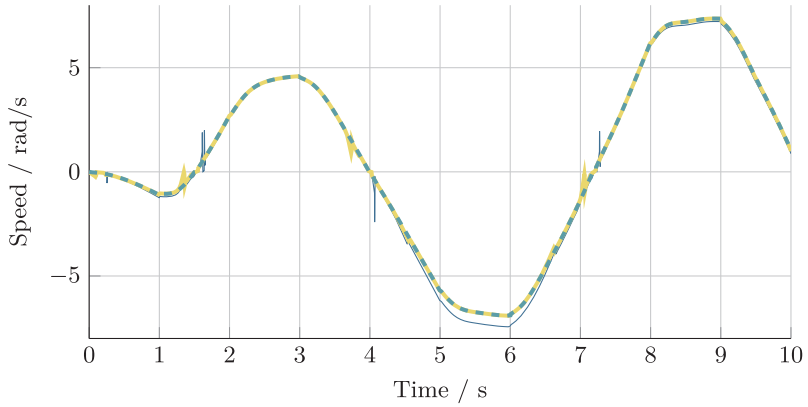

Figure 5.14: Speed of the differential motor using driveshafts with ten times increased stiffness. Different friction and elasticity models are shown: a fixed efficiency without backlash (- - -), fixed efficiency with backlash (——) and a friction law according according to the DIN 3990 standard (——).

differential out of the stuck mode. The main drive motor is driven with a constant load for a constant acceleration.

In Figure 5.15, the wheel torques of a simulation with a stiff driveshaft with eccentricity, an elastic driveshaft with eccentricity and an elastic driveshaft without eccentricity are given. Analyzing the simulation results, it is clear that this eccentricity has a high-frequency impact on the wheel torques. With a nominal driveline, the torque variations are lower at high velocities as for a stiff driveline. A detailed view of this vibration is shown in Figure 5.16. The high frequency vibrations of the gear seem to excite the drivetrain for the nominal stiffness drivetrain.

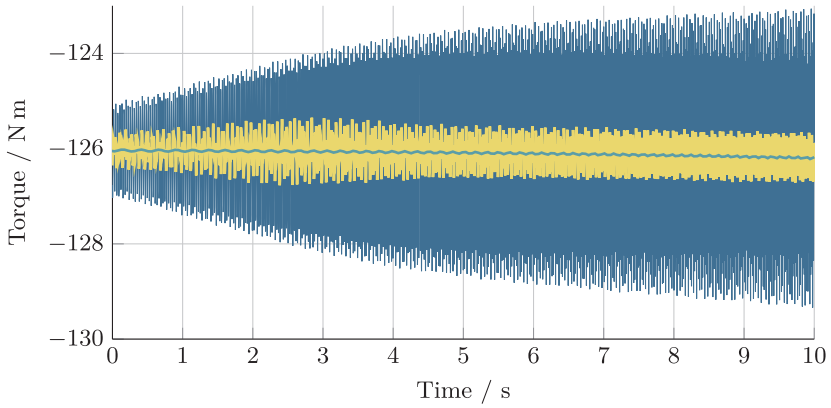

Figure 5.15: Wheel torques of right rear wheel with and without gear eccentricities: All simulation results have a fixed efficiency and a nonlinear stiffness. The different lines show a simulation without eccentricity(——), simulation with the nominal stiffness (——) and a simulation with an increased stiffness(——).

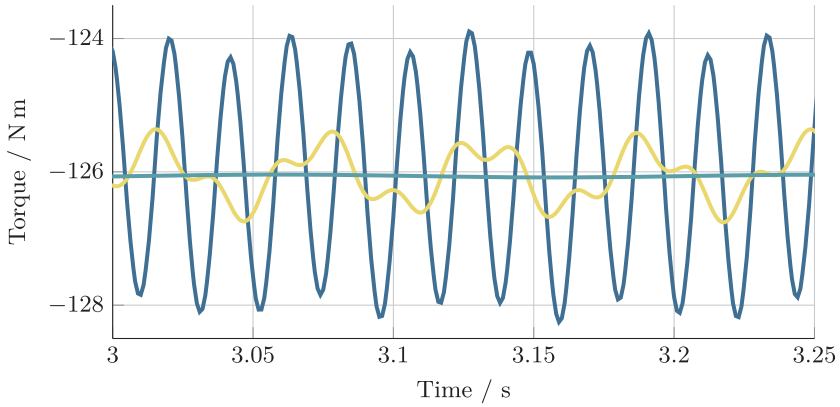

Figure 5.16: Wheel torque of right rear wheel with and without gear eccentricities: All simulation results have a fixed efficiency and a nonlinear stiffness. This figure shows a detail of Figure 5.15. The different lines show a simulation without eccentricity(——), simulation with the nominal stiffness (——) and a simulation with an increased stiffness(——).

5.5 Discussion

During performed simulations, it was realized that – due to the large number of switching components and high gear stiffness – the proposed model challenges common numerical solvers like DASSL or Radau IIA. Finding consistent restart conditions after an event can be hard, since this often directly triggers a next event in an adjacent gear connection.

In some cases, it is therefore advisable to use a regularized friction model as presented in Section 5.1.1. Such friction models can help to avoid events and make a simulation progress even if very complex gearing configurations are analyzed. However, most of these problems can be avoided by modeling the real-life world more accurately. As an example, spring-damper models between the differential, superimposing gear and spur gear train have been added to mimic the stiffness of the connections. This avoided many problems with the simulation.

5.6 Summary

In this chapter, different techniques for gear modeling were presented and adopted for a torque vectoring drive which was analyzed in simulations of a complete car model. Applying such gear modeling techniques, which include losses, nonlinear elasticity and forcing errors, at a varying level of gear detail. These different detail levels can be user-selected and have shown to significantly influence the simulation results.

The higher level of modeling detail is particularly important when investigating torque and speed oscillation issues which can be useful for e. g. driveline design. Then, simple fixed efficiency based friction models are insufficient. In contrast, DIN 3990 or similar friction models are required to capture such effects. Furthermore, it was shown that both insufficient torsional stiffness of the drive shafts and stick slip in the gear lead to large torque oscillations within a complete driveline.

The influence of gear eccentricities on the driveline was shown for driveshafts of different elasticity. It is shown that a higher stiffness of this shaft increases the load on this axle. This shows that a trade-off must be made between the load caused by eccentricities and the load caused by the stick-slip effect, as a high driveshaft elasticity lowers the load caused by stick-slip effects, but increases the load caused by a stiffer shaft.

The drawback of some of the presented models can be an increased simulation effort due to large number of state events triggered during the simulation of stick-slip phases. For such cases, a regularized friction model proved to be a possible alternative.

It is worth mentioning that the model and the simulation results were not validated so far. Especially, the damping coefficient is largely unknown and not well researched at the moment. It is advisable to push the experimental research to get a usable estimate of the gear damping properties in the future.

6 Summary, conclusions and recommendations

6.1 Summary

Currently gear transmissions and complete systems are designed by different groups of engineers. However the simplified models of system designers cannot represent the effects of detailed models of gear designers. This complicates the integrated design of transmission and system and hinders collaboration between system and gear designers.

This thesis presents models with a good balance between simulation speed and accuracy leading to the main contribution of this thesis: the development of a set of models that bridge the gap between fast, but inaccurate models currently used for system design and highly detailed models for gear design.

A set of models have been created which include forcing errors, nonlinear tooth stiffness, position dependent tooth stiffness and position dependent friction models. Measurements on a dedicated gear test bench have shown that the behavior of a gear set can be well represented with the developed models. Furthermore, it has been shown using the example of a Torque-Vectoring-Drive (TVD) in an electric car that these models can be used in complex system simulations for the assessment of vehicle dynamics.

6.1.1 Gear modeling

A planar description of gear wheels has allowed a correct representation of the friction and elastic forces in a gear contact. Furthermore, the planar description has proved to be a flexible way to handle arbitrary gear problems. The simple configuration of the gear model combined with good visualization capabilities helps engineers to quickly setup simulations and to check for potential modelling errors. The possibility to gradually increase model complexity has proved to be valuable, especially when large complex gear systems are modeled. This avoids the tedious debugging processes when modeling faults have been made.

The pre-calculation of the friction has proved to be a valuable tool to represent the friction as a computational efficient method that describes the behavior of gear wheels in contact. Various friction models have been implemented which can be easily interchanged.

By including only the effect of the position dependence of the gear contact, the computational costs of the models have been kept low. Position dependent forcing errors, stiffness and friction have been implemented and compared with semi-static measurements. The developed models can represent the position dependence of the models of healthy and damaged gear transmissions.

6.1.2 Gear measurements

A testrig has been built to analyze straight cut spur gear transmissions. Healthy gear wheels as well as a set of gear wheels with a single missing tooth have been analyzed. The transmission error, elasticity and losses of these gear transmissions have been obtained for these two gear sets. These measurements have been used to validate the system models.

Healthy gear transmission

The stiffness of the measured healthy gear has been measured to be linear dependent on the contact load. Therefore it can be best described by the stiffness model of Niemann and Winter (1989). The friction of the gear contact can be well approximated by the friction model according to the norm DIN 3990 Teil 4 (1987).

It has been found that gear wheel misalignments lead to a non-even load distribution on the gear flanks causing large stiffness reductions at low loads. The effective tooth width of the testrig was estimated to be only 28 % of the available tooth contact.

The load- and position depending measurement of the transmission error, stiffness and friction show that the transmission error is mainly caused by eccentricities and misalignments of the gear wheels. The stiffness of the analyzed gear varies only marginally with the position.

Gear transmission with missing tooth

A gear wheel with an artificially removed tooth has been analyzed to obtain realistic data for a damaged gear. The measurements have shown that a missing tooth locally reduces the gear stiffness by 20 % and increases the gear friction at the position of the missing tooth by over 400 %. These large position dependent changes of the stiffness and friction enable the detection of such faults by health monitoring algorithms. The quantification of these faults are a valuable input to be able to simulate similar systems with failures.

6.1.3 Implementation

The object-oriented language Modelica has been used to implement the models. By exploiting the strength of the object-oriented approach of this language, a set of models have been developed that are modular and can be simply understood and extended. The possibility that the model complexity can be increased as a higher modeling accuracy is needed, helps to keep the simulation detail at the optimum of computational efficiency and model accuracy. A complex gear model of a torque-vectoring drive has been developed and implemented in a dynamic car simulation to perform analysis on the drive during test maneuvers. It has been shown that the model can predict stick-slip behavior in the gear train when the parameters of the drive axles are unfavorable. This has highlighted the importance of complete system simulations since only the complete system lead to stick-slip problems. Such a simulation can therefore prevent design mistakes by early highlighting potential problems.

6.2 Conclusions

After studying the topic of gear contact modeling for system simulations and their application for the design of vehicle drivelines and aircraft actuators, following conclusions can be drawn:

- The modeling level of the complete system should be in line with the needed accuracy to optimize the modeling efforts.
- For an optimal design of a mechanical system, the transmission must be an integral part of the design process.

- The proposed gear description can represent the behavior of gears with usual manufacturing errors and also damaged gear wheels within simulation times that are acceptable for system designers.
- The proposed gear description can help the system designer to better communicate their needs to gear designers, as these models can represent real-life behavior of gear transmissions.

6.3 Recommendations

6.3.1 Gear modeling

For the modeling of gear connections, it is crucial to understand the goal of the research problem. The approach presented in this thesis is optimal for integrated, dynamic systems such as electromechanical aircraft actuators, torque-vectoring drives for automotive applications or the design of health monitoring systems. The simulation capabilities of the method have been demonstrated with an example of an electric vehicle with torque-vectoring drive. Contrasting to the design of complex integrated systems, is the design of simple systems with basic requirements. For such systems, low fidelity models are often sufficiently accurate to represent the system. In these cases, the complexity of a planar approach with nonlinear effects is sometimes not needed, deeming the use of the presented gear model not to be the best available option. Furthermore, for the design of (semi) stationary systems, methods are available that exploit this stationary condition to increase the simulation speeds. Since these methods are integrated in software packages for the gear design of the gear flanks, better results can be expected when such design methods are used.

6.3.2 Gear measuring

Carrying out the measurements on the healthy and broken tooth gearsets in this thesis proved to be difficult with very low velocities as local friction peaks can easily engage a stuck mode. As the processing of the measurements assume that no stiction takes place, the measurement becomes corrupted. Adding flywheel masses to the side of the gear which is speed-controlled could avoid the aforementioned problems as the flywheel counteracts speed changes. Furthermore, by using a load-motor with a low inertia can help to keep the prescribed load moment better at the set-point, as the lower inertia does not counteract the fast moment control. The changes described before could enable the possibility to do similar tests as discussed in this paper for a wider range of velocities. This enables the possibility to study the friction of very slow turning gears, thereby obtaining better very low speed friction data which can be used to improve the friction models in the low speed regime. Such friction models are needed for a better description of stick slip problems.

6.3.3 Open research questions

The implementation of a state machine to represent the stiction yields correct results, but can lead to a high simulation time. The gear contacts can enter a stick-slip phenomenon between multiple gear contacts. The triggering of a stuck phase can cause chattering of state transitions on all adjacent gear connections. It is unclear if this phenomenon happens in real transmissions and should be further investigated. For a more computational efficient approach, it can be considered to add a "cool-down penalty" on the stuck mode to avoid this very high frequency chattering. The

advantages, but also the impact on the accuracy of such a cool-down penalty should be thoroughly invested.

In this thesis, the speed of the contact position is assumed to be constant over the line of contact to simplify the calculations as this avoids the need for contact finding algorithms. This simplification removes the position dependence of the friction on the line of contact. Further research is needed to prove that it is possible to use a pre-processing method to generate a lookup table which takes into account the varying friction on the line of contact.

The measurements of stiffness and friction can be well represented with the developed gear models. Furthermore, these measurements also show that the gear play seems to be dependent on the mesh position. It should be investigated if a position dependent gear play could be used to replace the forcing error. This could further increase the model accuracy and potentially simplify the system models.

Currently there is hardly any information available about the damping of gears. However, in test simulations, the damping of the gear contact plays a large role on the stick-slip behavior of a gear transmission. More research is needed to better understand the damping of the gear contact to allow for more precise simulations.

Integration of gear-design software and system-design software

The parameters needed for the presented gear model are no parameters which can be readily found in other gear design programs such as FVAWorkbench. The different approach of these programs to tackle similar problems avoids a direct exchange of parameter data at the moment. To use the results of the high fidelity calculations of these specialized gear design programs, efforts should be made to create a standardized exchange format between specialized gear programs and the methods as developed in this thesis. A generalized position dependent play, stiffness and friction could be calculated and can serve as a source of high quality input for the gear models as designed in this thesis.

A good example of a comparable collaboration between specialist and system engineers, is the collaboration of system engineers and FEM specialists. A standard to introduce reduced FEM models in multi-body programs enables the use of flexible bodies in system models, thereby increasing the model accuracy.

In Figure 6.1 an example work flow that relies on the transfer of the gear properties from the gear designer to the system designer using a standardized gear property file is shown. Such an interaction enables the use of reduced gear models in system simulation using the models presented in this thesis, increasing the simulation accuracy of the complete system design.

An example design could be as following: A first set of requirements is given to the gear designer by the system designer. This set of requirements can be more detailed than before, as the detailed models presented in this thesis allow for good estimation of the gear properties. The gear designer can now create a full gear design based on these specifications. The design is reduced and exported to a file which defines the standardized gear properties. The system designer can now integrate this data into the full system model and check if the behavior of the designed gear transmission in the complete system is satisfactory. If problems arise, the gear design can be optimized in cooperation with the gear designer. A second design optimization loop must be made to allow for a correct system behavior. It must be noted here that these reduced gear parameters need not to include the exact gear corrections and therefore the intellectual property of the gear designer can be guaranteed.

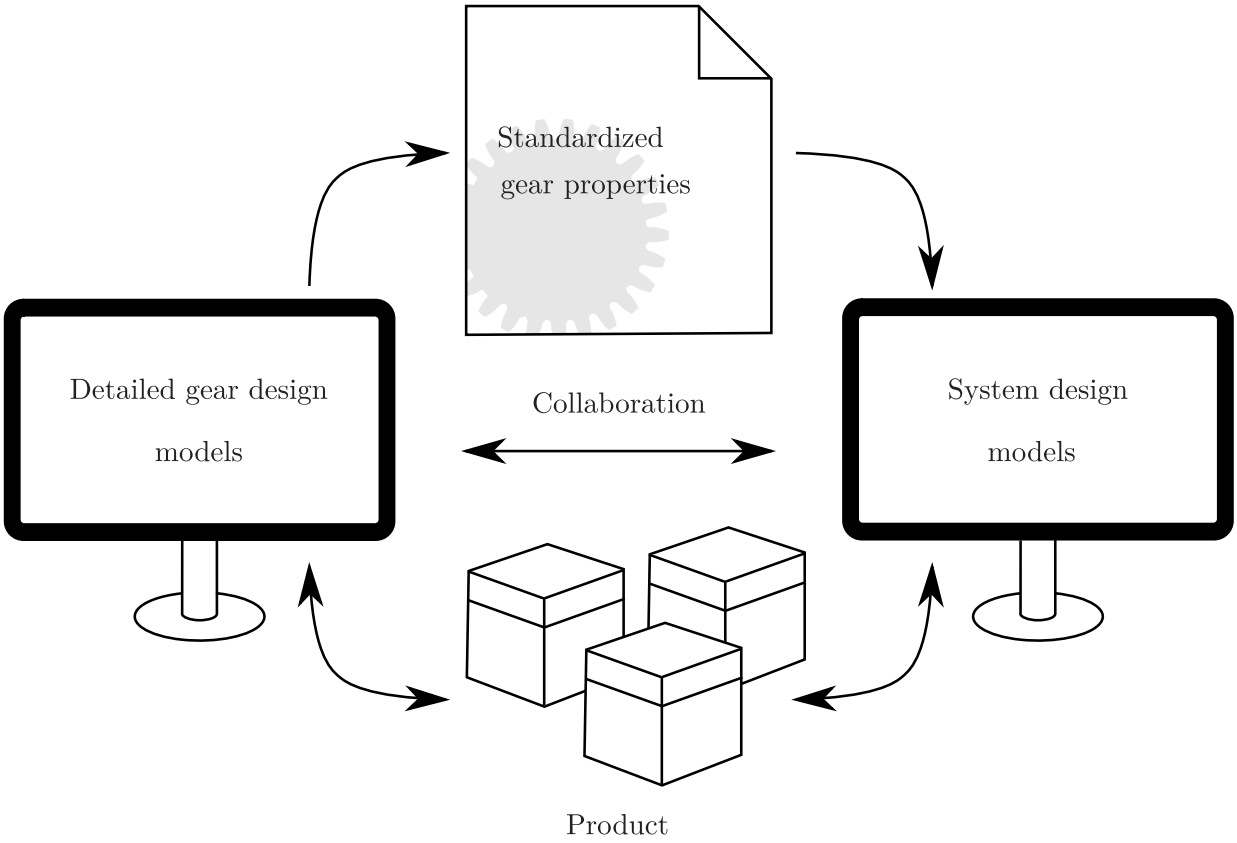

Figure 6.1: Interaction between gear designer and system designer

The main contribution of this thesis: *Models that bridge the gap between fast, but inaccurate models currently used for system design and highly detailed models for gear design* can be brought to perfection by realizing this coupling. Gear designer and system designer can collaborate, allowing a direct integration of the specialized gear models in the overall system models.

A Measurement results

In this appendix, repeated measurements are shown to assess the repeatability of the measurements.

A.1 Deformation measurements

A.1.1 Healthy

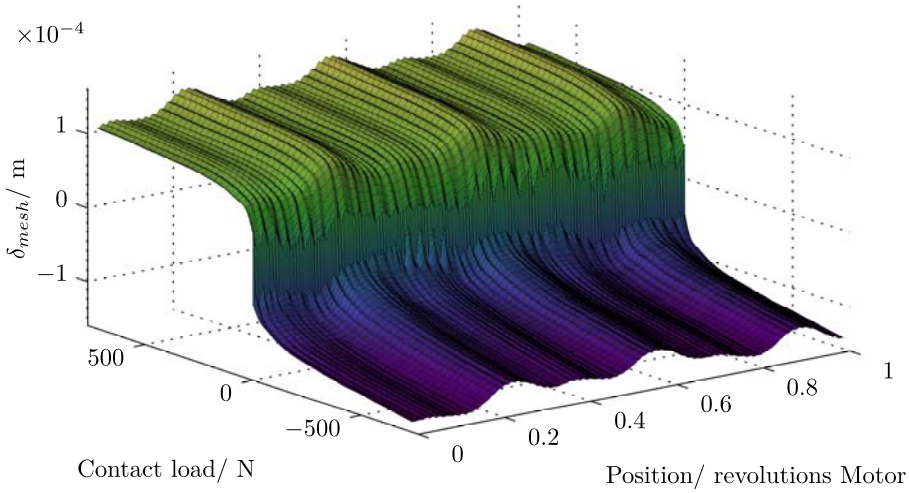

Figure A.1: Deformation Δ_{AB} of healthy gear contact as a function of the contact load F_n and gear position ϕ_B. Gear set I, $\omega_A = 10\,\mathrm{RPM}$. Measurement 2.

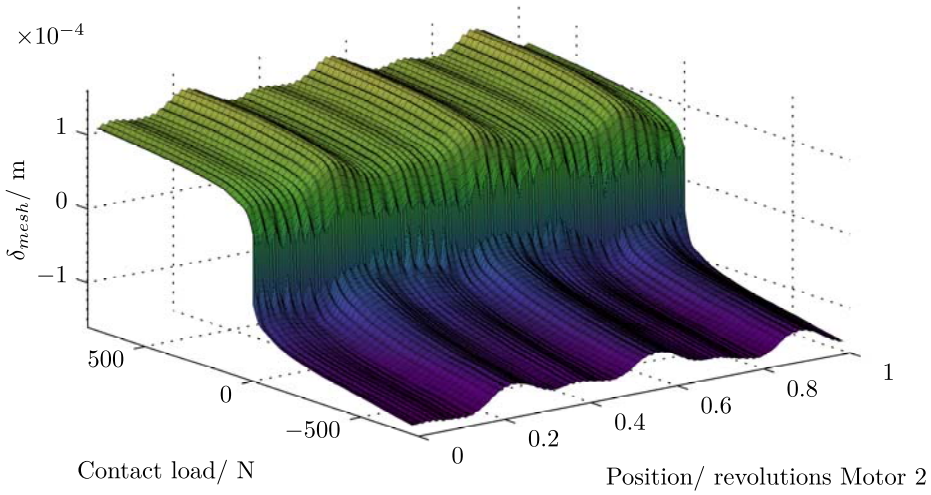

Figure A.2: Deformation Δ_{AB} of healthy gear contact as a function of the contact load F_n and gear position ϕ_B. Gear set I, $\omega_A = 10\,\mathrm{RPM}$. Measurement 3.

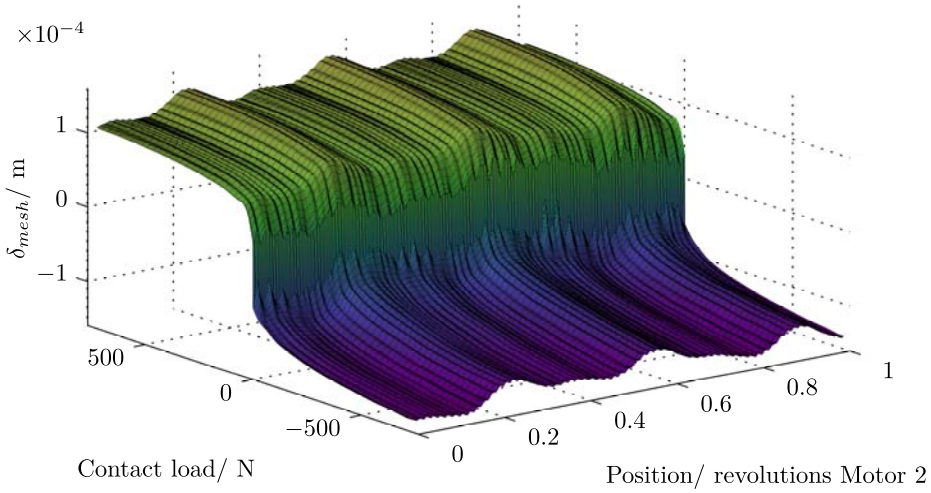

Figure A.3: Deformation Δ_{AB} of healthy gear contact as a function of the contact load F_n and gear position ϕ_B. Gear set I, $\omega_A = -10\,\mathrm{RPM}$. Measurement 2.

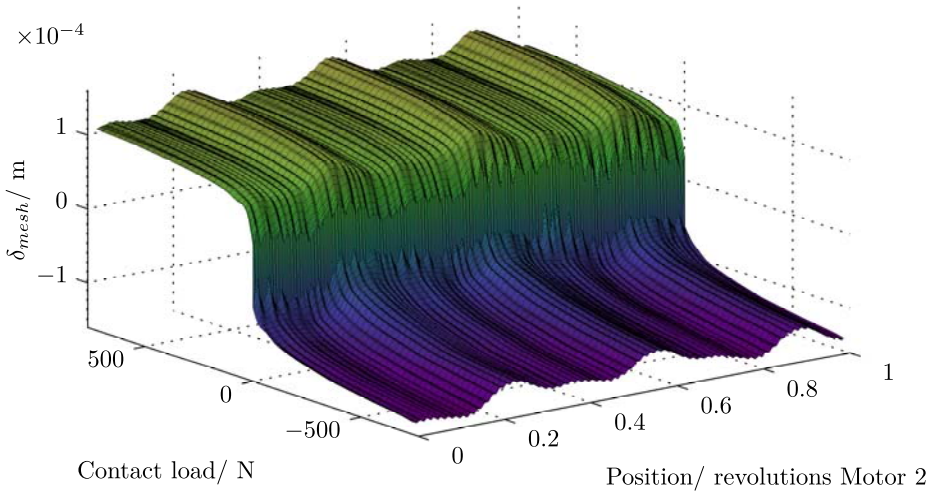

Figure A.4: Deformation Δ_{AB} of healthy gear contact as a function of the contact load F_n and gear position ϕ_B. Gear set I, $\omega_A = -10\,\text{RPM}$. Measurement 3.

A.1.2 Artificially removed tooth

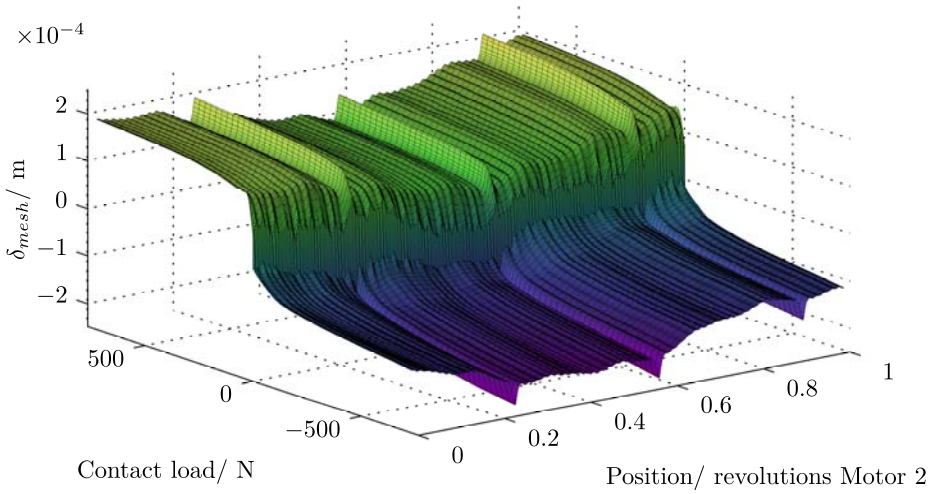

Figure A.5: Deformation Δ_{AB} of broken tooth gear contact as a function of the contact load F_n and gear position ϕ_B. Gear set II, $\omega_A = 10\,\text{RPM}$. Measurement 2.

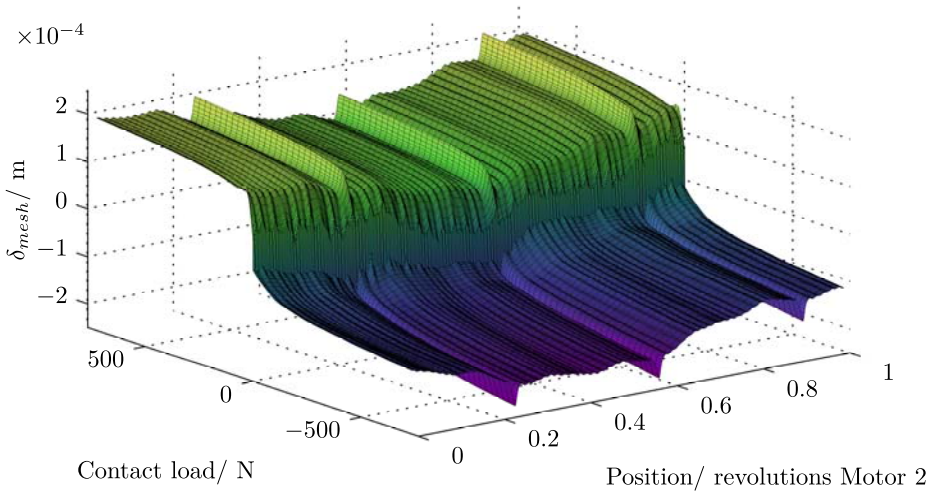

Figure A.6: Deformation Δ_{AB} of broken tooth gear contact as a function of the contact load F_n and gear position ϕ_B. Gear set II, $\omega_A = 10\,\mathrm{RPM}$. Measurement 3.

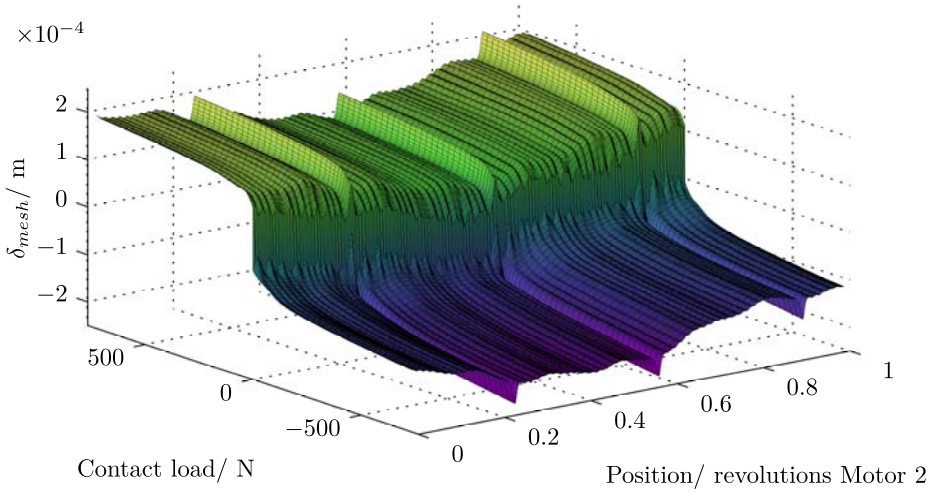

Figure A.7: Deformation Δ_{AB} of broken tooth gear contact as a function of the contact load F_n and gear position ϕ_B. Gear set II, $\omega_A = -10\,\mathrm{RPM}$. Measurement 2.

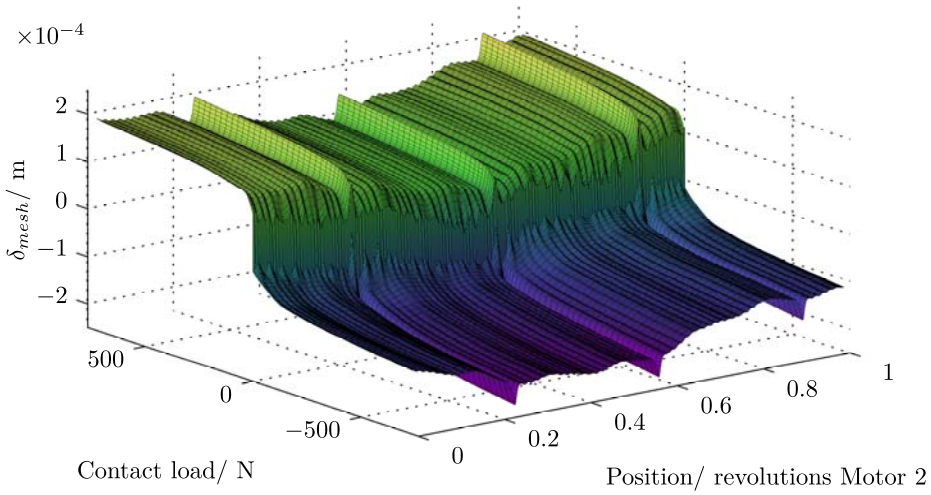

Figure A.8: Deformation Δ_{AB} of broken tooth gear contact as a function of the contact load F_n and gear position ϕ_B. Gear set II, $\omega_A = -10\,\mathrm{RPM}$. Measurement 3.

A.2 Stiffness measurements

A.2.1 Healthy

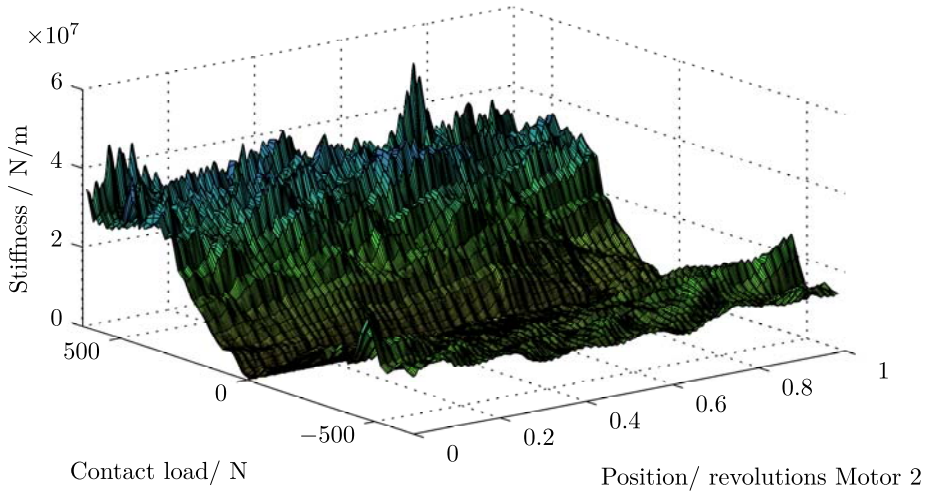

Figure A.9: Stiffness of healthy gear contact as a function of the contact load F_n and gear position ϕ_B. Gear set I, $\omega_A = 10\,\mathrm{RPM}$. Measurement 2.

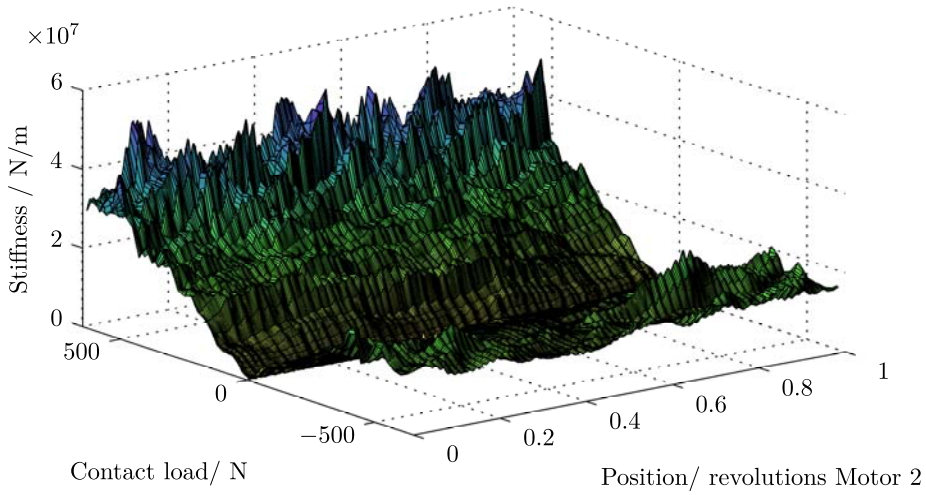

Figure A.10: Stiffness of healthy gear contact as a function of the contact load F_n and gear position ϕ_B. Gear set I, $\omega_A = 10\,\mathrm{RPM}$. Measurement 3.

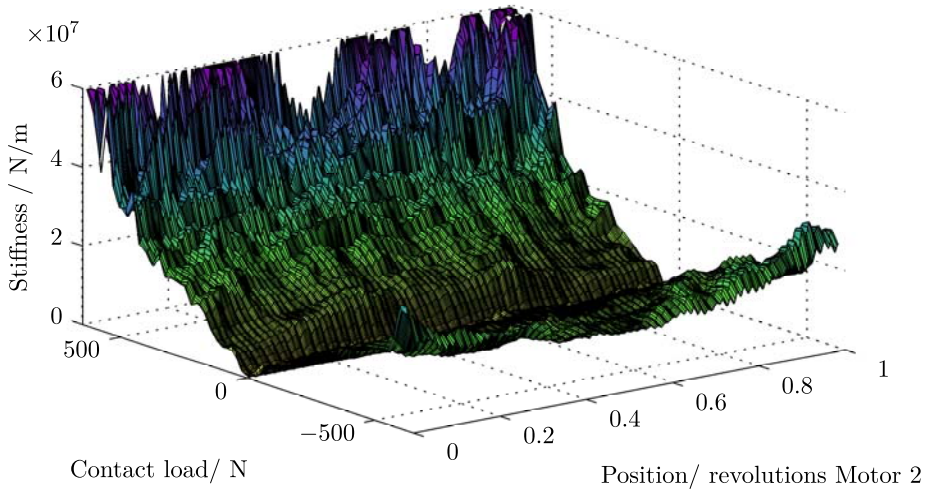

Figure A.11: Stiffness of healthy gear contact as a function of the contact load F_n and gear position ϕ_B. Gear set I, $\omega_A = -10\,\mathrm{RPM}$. Measurement 2. To be able to compare the stiffness between the measurements, the stiffness is capped at $6 \times 10^7\,\mathrm{N\,m}$.

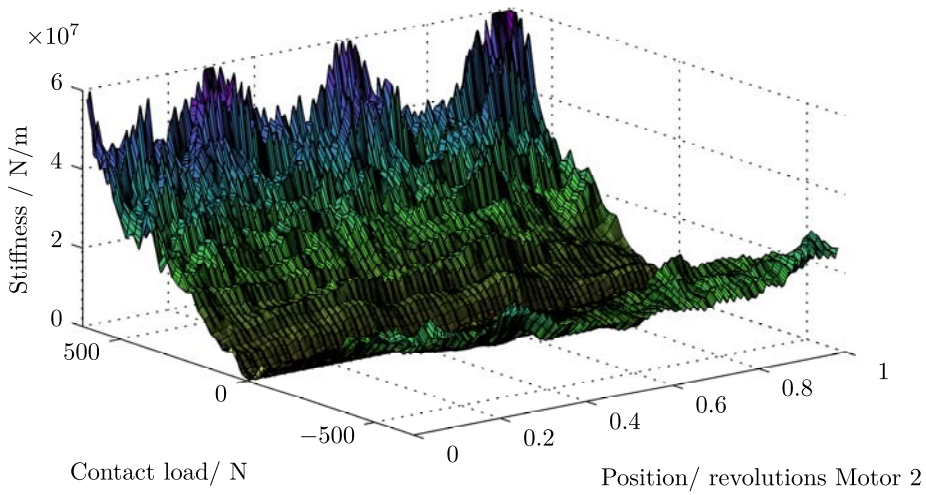

Figure A.12: Stiffness of healthy gear contact as a function of the contact load F_n and gear position ϕ_B. Gear set I, $\omega_A = -10\,\mathrm{RPM}$. Measurement 3. To be able to compare the stiffness between the measurements, the stiffness is capped at $6 \times 10^7\,\mathrm{N\,m}$.

A.2.2 Artificially removed tooth

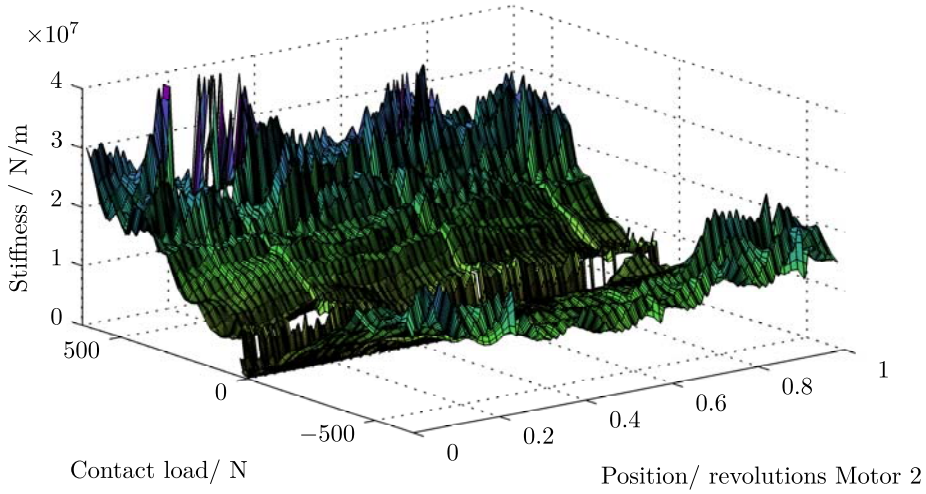

Figure A.13: Stiffness of gear contact with artificially removed tooth as a function of the contact load F_n and gear position ϕ_B. Gear set II, $\omega_A = 10\,\mathrm{RPM}$. Outliers marked by gaps in the surface have been removed to be able to see the results. Measurement 2.

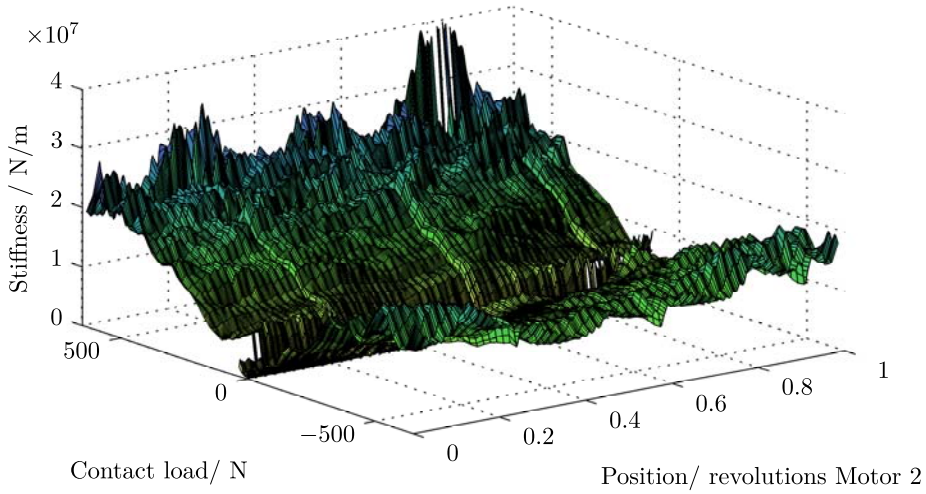

Figure A.14: Stiffness of gear contact with artificially removed tooth as a function of the contact load F_n and gear position ϕ_B. Gear set II, $\omega_A = 10\,\mathrm{RPM}$. Outliers marked by gaps in the surface have been removed to be able to see the results. Measurement 3.

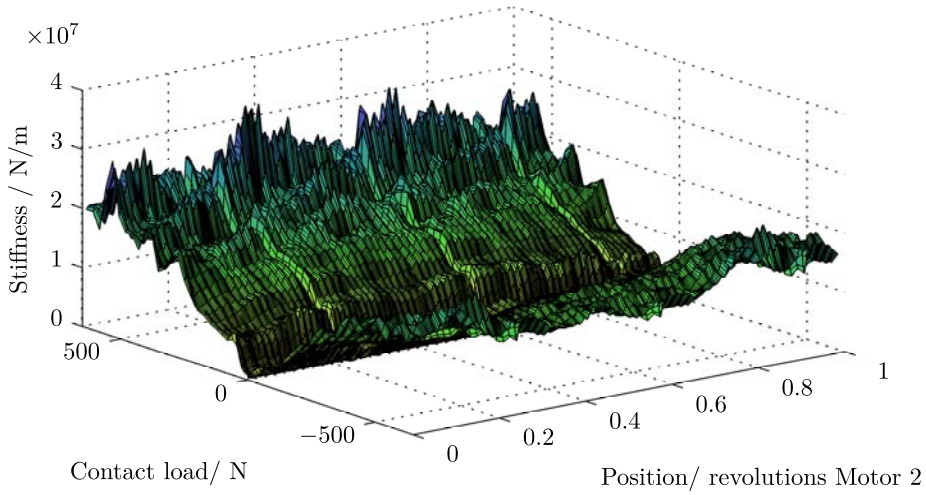

Figure A.15: Stiffness of gear contact with artificially removed tooth as a function of the contact load F_n and gear position ϕ_B. Gear set II, $\omega_A = -10\,\mathrm{RPM}$. Outliers marked by gaps in the surface have been removed to be able to see the results. Measurement 2.

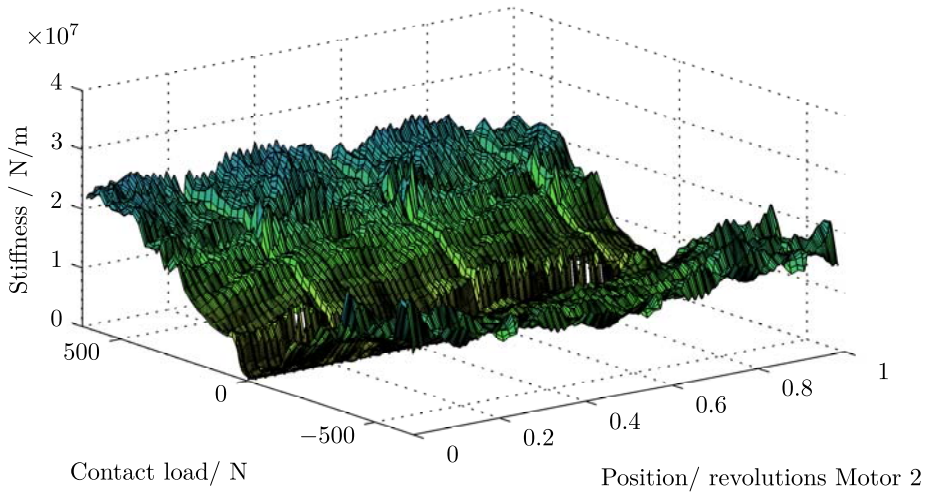

Figure A.16: Stiffness of gear contact with artificially removed tooth as a function of the contact load F_n and gear position ϕ_B. Gear set II, $\omega_A = -10\,\mathrm{RPM}$. Outliers marked by gaps in the surface have been removed to be able to see the results. Measurement 3.

A.3 Friction measurements

A.3.1 Healthy gear

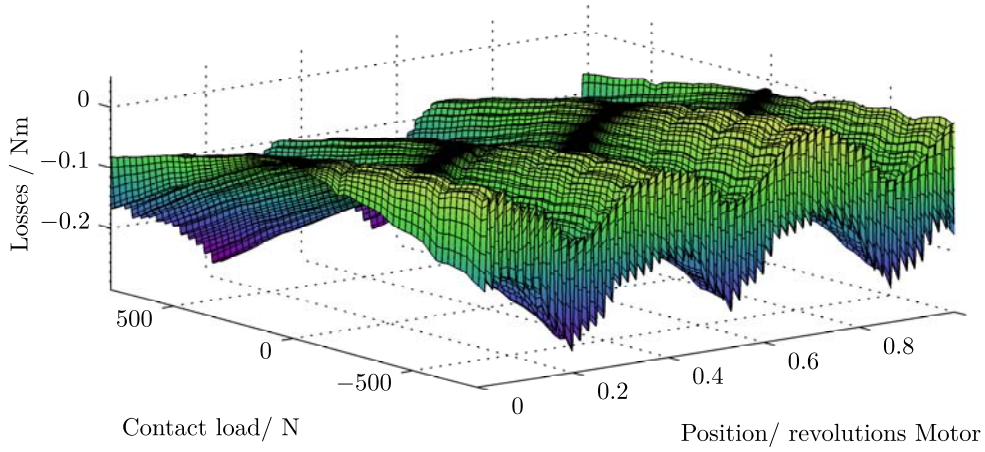

Figure A.17: Local friction of a healthy contact as a function of the contact load F_n and gear position ϕ_B at $\omega_A = 10\,\mathrm{RPM}$. Gear set I, Measurement 2.

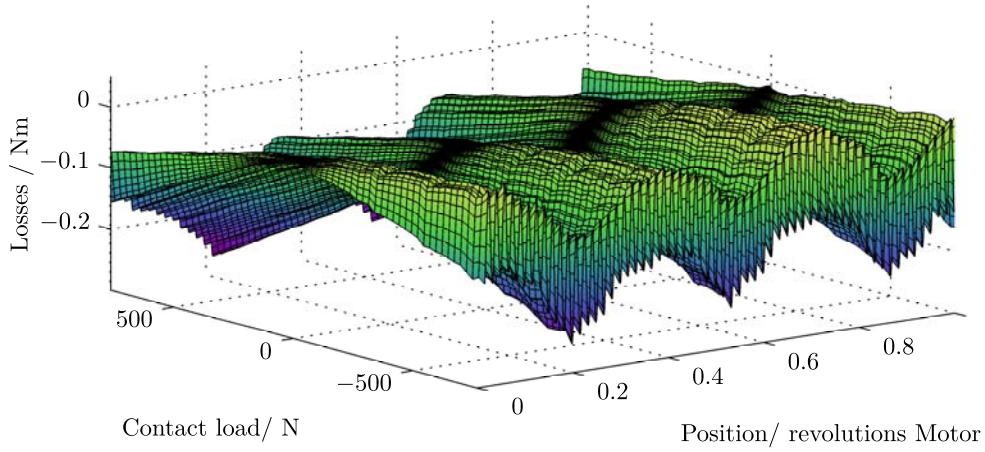

Figure A.18: Local friction of a healthy contact as a function of the contact load F_n and gear position ϕ_B at $\omega_A = 10\,\mathrm{RPM}$. Gear set I, Measurement 3.

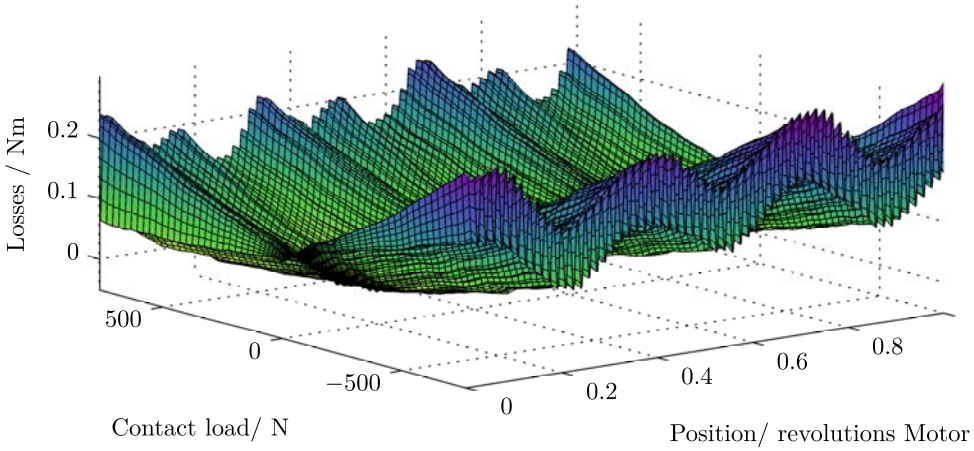

Figure A.19: Local friction of a healthy contact as a function of the contact load F_n and gear position ϕ_B at $\omega_A = -10\,\mathrm{RPM}$. Gear set I, Measurement 2.

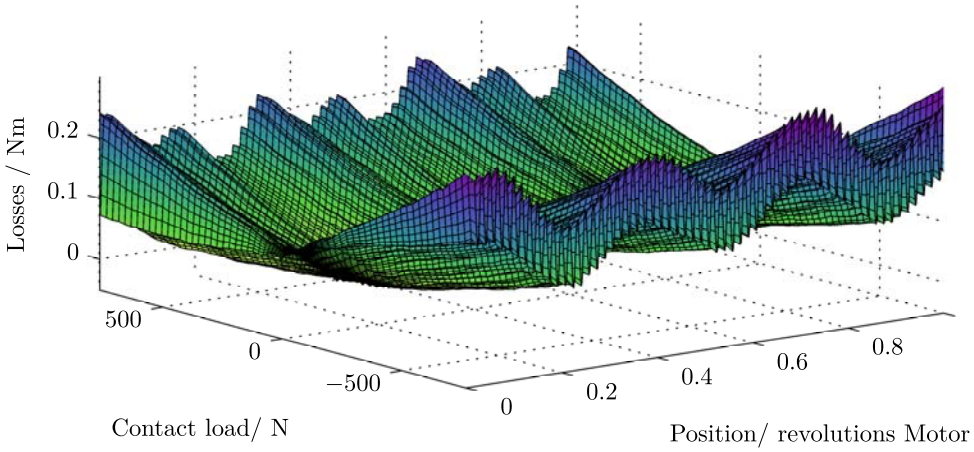

Figure A.20: Local friction of a healthy contact as a function of the contact load F_n and gear position ϕ_B at $\omega_A = -10\,\mathrm{RPM}$. Gear set I, Measurement 3.

A.3.2 Artificially removed tooth

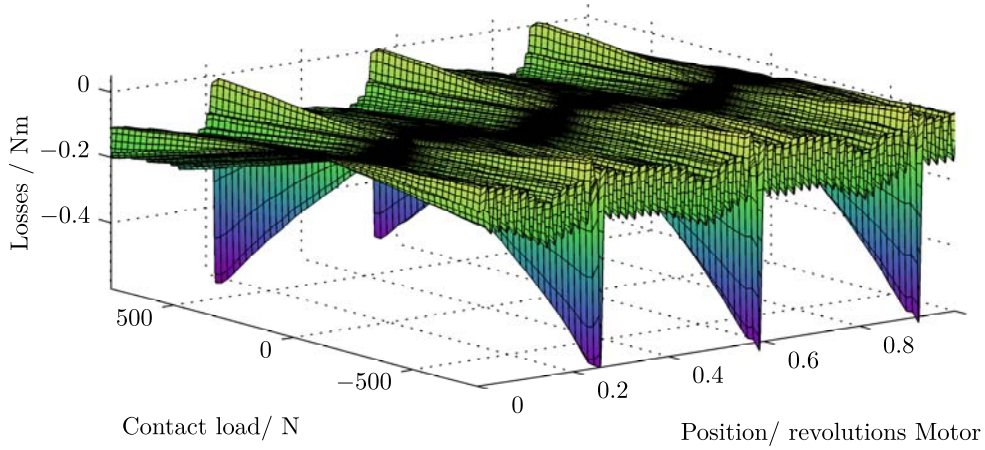

Figure A.21: Local friction of the broken gear contact as a function of the contact load F_n and gear position $\phi_B$at $\omega_A = 10\,\mathrm{RPM}$. Gear set II, Measurement 2.

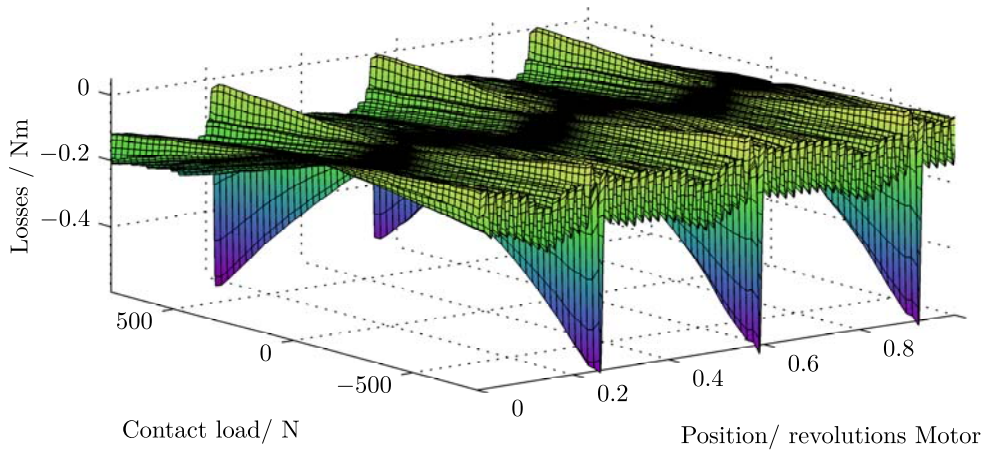

Figure A.22: Local friction of the broken gear contact as a function of the contact load F_n and gear position $\phi_B$at $\omega_A = 10\,\mathrm{RPM}$. Gear set II, Measurement 3.

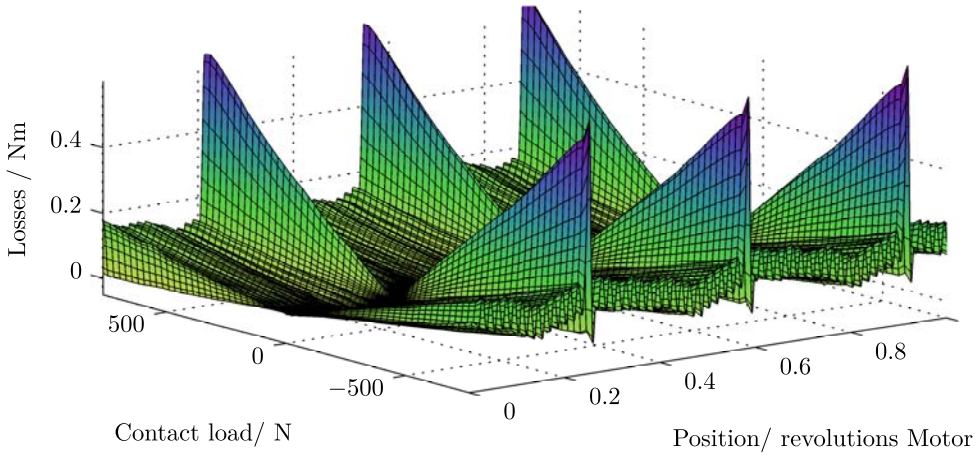

Figure A.23: Local friction of the broken gear contact as a function of the contact load F_n and gear position $\phi_B$at $\omega_A = -10\,\mathrm{RPM}$. Gear set II, Measurement 2.

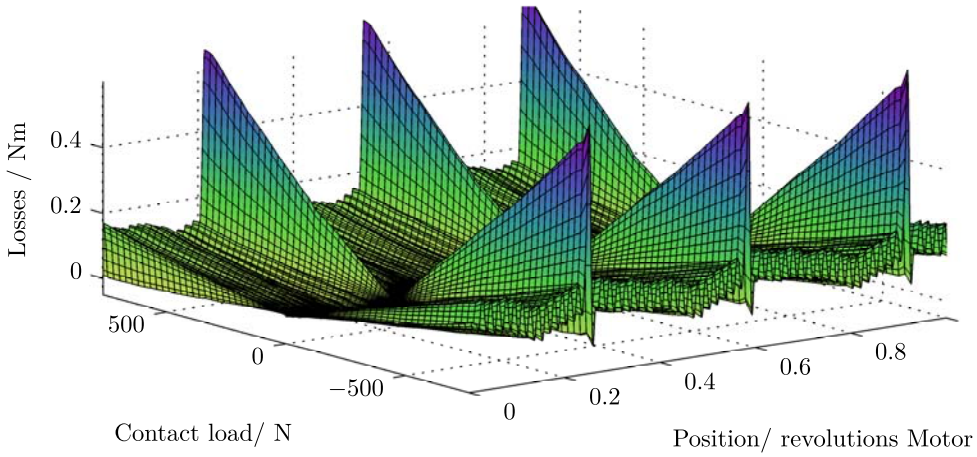

Figure A.24: Local friction of the broken gear contact as a function of the contact load F_n and gear position $\phi_B$at $\omega_A = -10\,\mathrm{RPM}$. Gear set II, Measurement 3.

B Modeling of elastic gear contacts in Modelica

This Appendix represents the paper *Modelling of Elastic Gearboxes Using a Generalized Gear Contact Model* presented in 2012 at the *international Modelica conference* in Munich (F. L. Van der Linden, 2012).

B.1 Introduction

The object of this section is to present an universal model that describes the gear contact between two gears in a planar environment. The model includes elastic effects between the gear wheels. Using this model it is possible to create arbitrary spur gear connections as well as all kinds of epicyclic gearing configurations by supplying the proper external constraints. The presented model is implementated in the Modelica language and Dymola is used for the simulations. The models presented here can simulate an arbitrary elastic gearbox configurations by relying on a planar library. This approach makes it very easy to evaluate several model configurations without a lot of design work. To keep the simulation time low, the presented model does not include any friction effects, since they are often not directly necessary in the pre-design stage.

B.2 Gear forces and equations

In this chapter the forces and torques on the gear wheels are evaluated. Since these forces and torques differ for internal- and external teeth, these aspects are treated as separate cases.

B.2.1 Force and moment balance of external teeth

In Figure B.1 a schematic overview of two gear wheels in contact are shown. The rotation of the gear wheels are ϕ_A and ϕ_B, shown by the angles to the body-fixed red and blue markers on the gear wheels.

The gear ratio is defined by:

$$\frac{r_A}{r_B} = -i \tag{B.1}$$

This ratio is constant for each gear angle and position.

Figure B.2 shows a free body diagram of the two gears in contact. The forces of only one contact point are displayed.

Using Figure B.2, it is possible to create the torque and force balances of each gear wheel for external teeth configurations. These forces and torques are resolved in the fixed coordinate system shown in Figure B.2. The use of a fixed coordinate system and gear angle ϕ_{gear} makes it possible to use the contact model also in more complex gear systems (e.g. all kinds of Epicyclic gearing configurations).

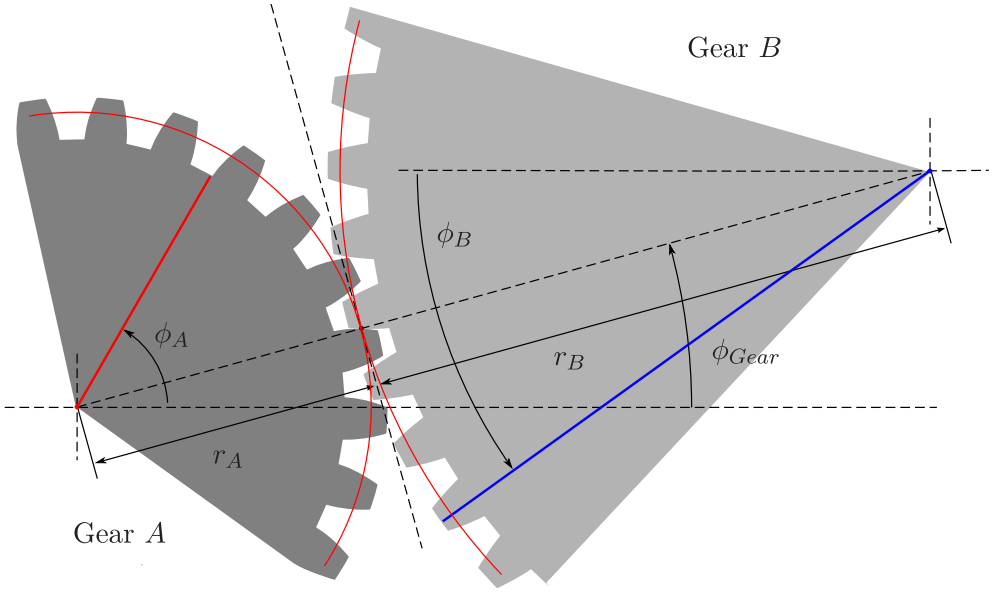

Figure B.1: Schematic overview of two gearwheels in contact. The blue and red line are fixed markers on the gear wheels. In the figure $\dot{\phi}_A > 0$ and Gear A drives Gear B.

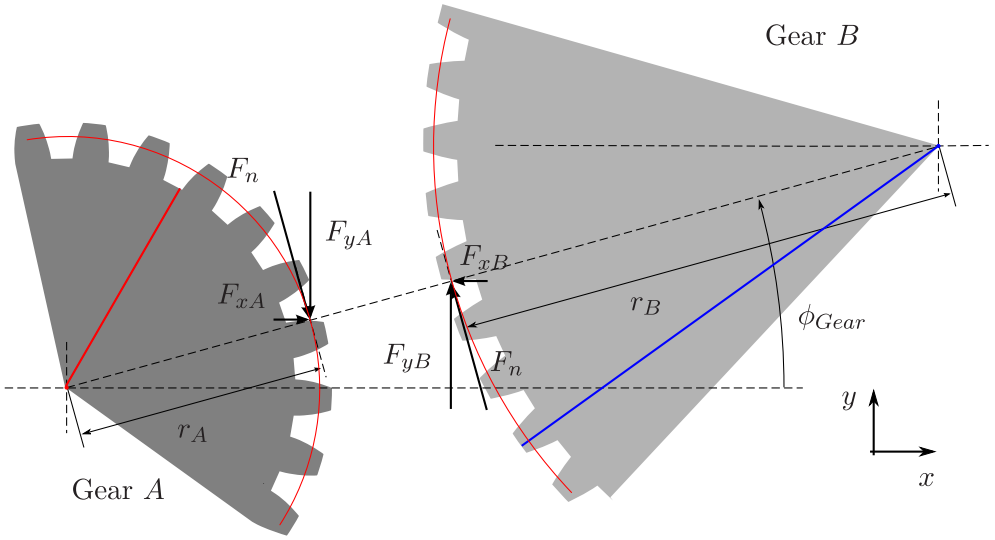

Figure B.2: Free body diagram of the two gearwheels from Figure B.1.

$$\tau_A = F_n r_A \tag{B.2}$$
$$\tau_B = F_n r_B \tag{B.3}$$
$$F_{xA} = -\sin(\phi_{gear}) F_n \tag{B.4}$$
$$F_{yA} = \cos(\phi_{gear}) F_n \tag{B.5}$$
$$F_{xB} = -F_{xA} \tag{B.6}$$
$$F_{yB} = -F_{yA} \tag{B.7}$$

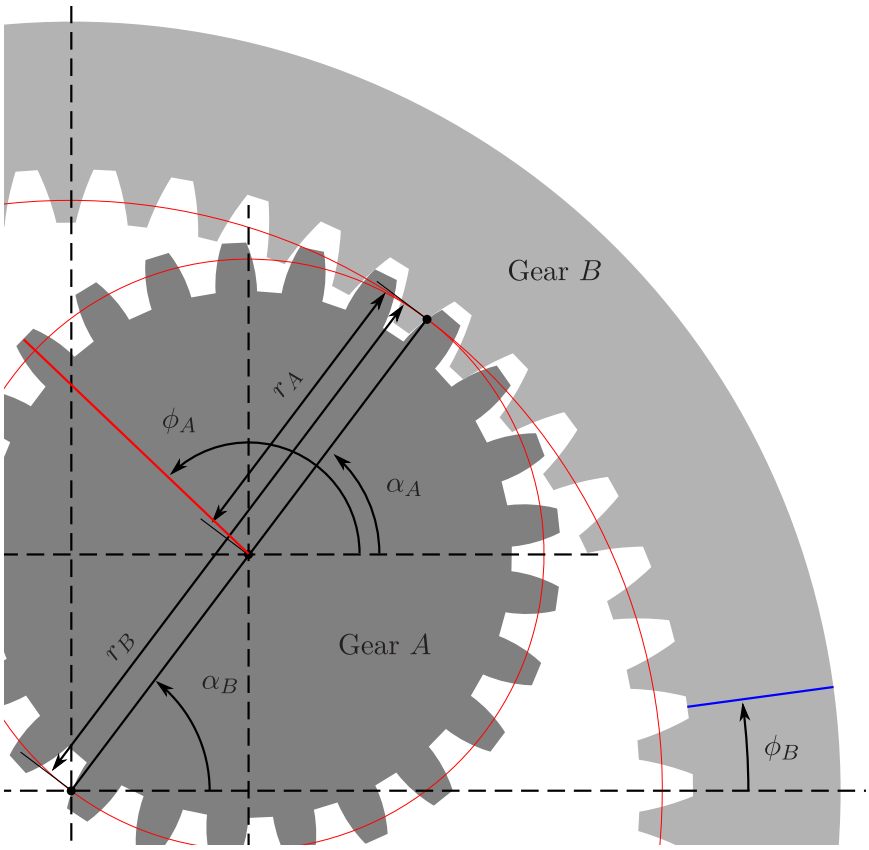

Figure B.3: Schematic overview of two gearwheels in contact. The blue and red line are fixed markers on the gear wheels. In the figure $\omega_A > 0$ and Gear A drives Gear B.

B.2.2 Force and moment balance of internal teeth

Just like in Section B.2.1, the force and moment balance can be created by examining Figure B.3 together with Figure B.4:

$$\tau_A = F_n r_A \tag{B.8}$$
$$\tau_B = -F_n r_B \tag{B.9}$$
$$F_{xA} = -\sin(\phi_{gear}) F_n \tag{B.10}$$
$$F_{yA} = \cos(\phi_{gear}) F_n \tag{B.11}$$
$$F_{xB} = -F_{xA} \tag{B.12}$$
$$F_{yB} = -F_{yA} \tag{B.13}$$

B.3 Meshing distance

To keep track how the gear wheels move with respect to each other, the mesh distance x_{mesh} is introduced. This distance is defined as the distance the gear has traveled through the meshing point and can be calculated for both gear wheels. For the complete description of the mesh position the following assumption is postulated:

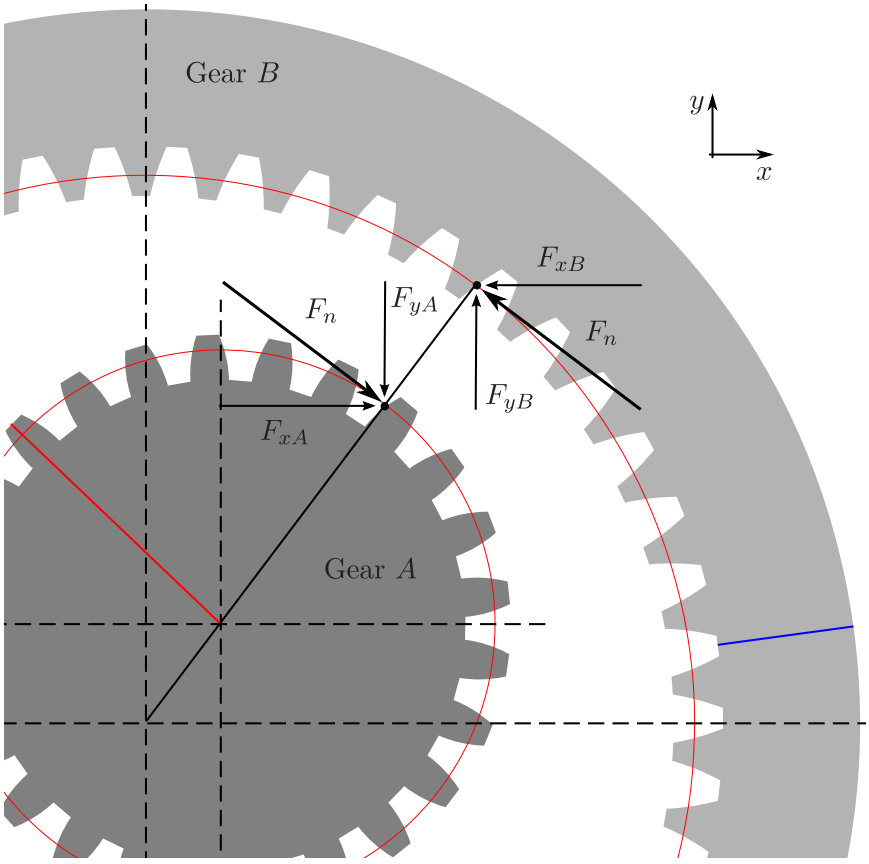

Figure B.4: Free body diagram of the two gearwheels from Figure B.3.

Assumption B.1 *The mesh contact position is on the direct connection between the center of gear A and B at a distance r_A from the center of A*

This assumption is valid for all cases in which the deformation of the teeth is small. In all engineering applications this must be the case for gearwheels under normal loading conditions.

B.3.1 Mesh distance external teeth

For external teeth, the mesh distance can be calculated as follows using the geometry and definitions from Figure B.1.

$$x_{mesh,A} = \phi_A r_A - \phi_{gear} r_A \tag{B.14}$$

$$x_{mesh,B} = -\phi_B r_B + \phi_{gear} r_B \tag{B.15}$$

From this equation it becomes clear that the mesh distance ($x_{mesh,A}$ or $x_{mesh,B}$) can be constant although the gear wheels are rotating. This is the case if $\phi_A = \phi_{gear}$ or $\phi_B = \phi_{gear}$. This is not only a theoretical implication; in e.g. bicycle gear hubs this is often the case.

The difference between the mesh positions is the elasticity of the gear contact:

$$\Delta_{AB} = x_{mesh,A} - x_{mesh,B} \tag{B.16}$$

Assuming the meshing position is always halfway the elastic deformation, together with using the equations B.14 to B.16 the mesh velocity is:

$$v_{mesh} = \dot{x}_{mesh,A} - \frac{\dot{\Delta}_{AB}}{2} \tag{B.17}$$

B.3.2 Mesh distance internal teeth

The same analysis method can be applied to the internal teeth:

$$x_{mesh,A} = \phi_A r_A - \phi_{gear} r_A \tag{B.18}$$
$$x_{mesh,B} = \phi_B r_B - \phi_{gear} r_B \tag{B.19}$$

The difference between the mesh positions is as mentioned above the elasticity of the gear contact:

$$\Delta_{AB} = x_{mesh,A} - x_{mesh,B} \tag{B.20}$$

Assuming the meshing position is always halfway the elastic deformation, together with using the equations B.18 to B.20 the mesh velocity is:

$$v_{mesh} = \dot{x}_{mesh,A} - \frac{\dot{\Delta}_{AB}}{2} \tag{B.21}$$

B.4 Gear wheel coupling

The gear wheels A and B are coupled by a spring-damper combination. This yields:

$$F_n = \Delta_{AB} c(\phi_{gear}, \phi_A, \phi_B) + \dot{\Delta}_{AB} d(\phi_{gear}, \phi_A, \phi_B) \tag{B.22}$$

In this equation $c(\phi_{gear}, \phi_A, \phi_B)$ is the angle dependent spring constant and $d(\phi_{gear}, \phi_A, \phi_B)$ is the angle dependent damping constant.

B.4.1 Position dependent stiffness

The angle dependency can be used to simulate a non constant teeth stiffness. The total teeth stiffness is the combined stiffness of both gearwheels. Since the circumference of a gearwheel is periodic by definition, the following assumption can be postulated:

Assumption B.2 *The position dependent stiffness and damping of a gearwheel can be described by a Fourier decomposition.*

One of the most basic forms of Assumption B.2 is a single harmonic with zero phase offset that represents the teeth of the gear wheel. The stiffness over the circumference of a gearwheel can therefore be written as:

$$c_A(\gamma_A) = c_{const} + c_{\Delta,A} \sin(2\pi n_{tooth,A} \gamma_A) \tag{B.23}$$
$$c_B(\gamma_B) = c_{const} + c_{\Delta,B} \sin(2\pi n_{tooth,B} \gamma_A) \tag{B.24}$$

In this equation γ_A is the angle which describes the position of the material on the gear wheel. The stiffness at the contact position however, is dependent on which part of the gearwheel is in contact. The local stiffness can be obtained for an external gear by using:

$$\gamma_A = \phi_A - \phi_{gear} \tag{B.25}$$
$$\gamma_B = -\phi_B + \phi_{gear} \tag{B.26}$$

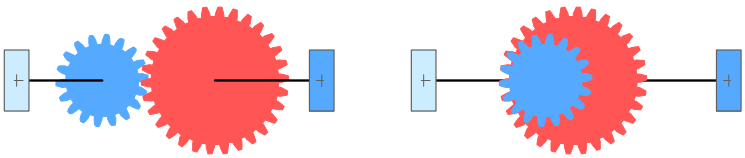

Figure B.5: Modelica Icon of the inner and outer gearwheel connections

Substituting Equations B.25 and B.26 into Equations B.23 and B.24 leads to the stiffness at the contact position.

$$c_{cont,A} = c_{const} + c_{\Delta,A} \sin(2\pi n_{tooth,A}(\phi_A - \phi_{gear})) \tag{B.27}$$
$$c_{cont,B} = c_{const} + c_{\Delta,b} \sin(2\pi n_{tooth,B}(-\phi_B + \phi_{gear})) \tag{B.28}$$

An internal gear configuration would yield:

$$\gamma_A = \phi_A - \phi_{gear} \tag{B.29}$$
$$\gamma_B = \phi_B - \phi_{gear} \tag{B.30}$$

leading to a contact stiffness of:

$$c_{cont,A} = c_{const} + c_{\Delta,A} \sin(2\pi n_{tooth,A}(\phi_A - \phi_{gear})) \tag{B.31}$$
$$c_{cont,B} = c_{const} + c_{\Delta,B} \sin(2\pi n_{tooth,B}(\phi_B - \phi_{gear})) \tag{B.32}$$

The overall stiffness can be calculated by putting both springs in series:

$$c = \left(\frac{1}{c_{cont,A}} + \frac{1}{c_{cont,B}} \right)^{-1} \tag{B.33}$$

B.5 Modelica implementation

The presented gear contact model must be supplied by constraints in the x, y and ϕ direction (standard planar constraints). The PlanarMechanics Library from D. Zimmer (Zimmer, 2012) is used to supply these constraints. Features like (rotational) bearings, connection rods, inertias e.g. are all represented. The library will be used to create the total gearbox setup.

Implementation of the gear model in Modelica is straightforward using the sections above. The gear model is implemented with 2 planar interface connectors; each with 3 degrees of freedom (x,y,ϕ). These connectors are the connections to the gearwheels A and B. To sense the total revolution angle ϕ_{gear} ($\phi_{gear} \in \mathbb{R}$), the atan3 function is modified to supply a continuous and differentiable angle.

In Figure B.5 the icons of the gear models are shown. No inertia's or constraints are included in the model.

Using the planar library, it is possible to create all kind of different gear configurations. Everything between simple spur gears models (Figure B.6 and B.7) up to complex epicyclic gearing configurations (Figure B.8 and B.9) is easily generated. In these models, the gearbox models (Figure B.5) are defined as described in this paper, all other components are components of the PlanarMechanics Library (see Zimmer, 2012).

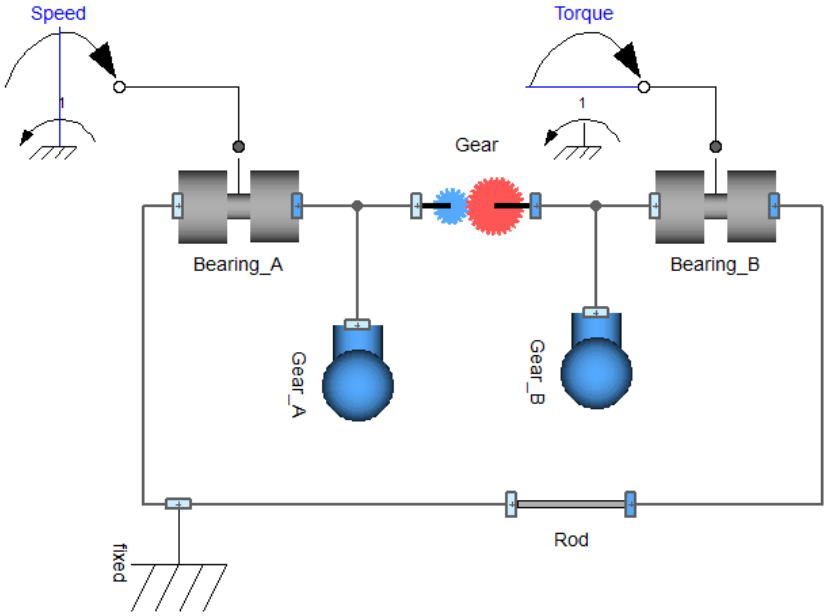

Figure B.6: Spur Gear in Dymola

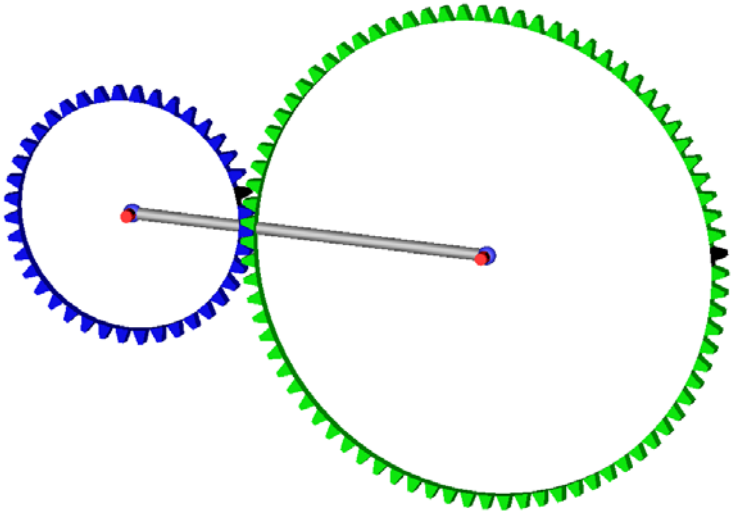

Figure B.7: Spur Gear in Dymola

B.6 Simulation results

B.6.1 Eigenfrequency analysis

Using the Modelica LinearSystems2 library, it is possible to create a Bode-Diagram of a linear system. Since a linear spring and damper are used for the contact stiffness, is is possible to use this toolbox. Using an eigenfrequency analysis it is possible to check the behavior of the models.

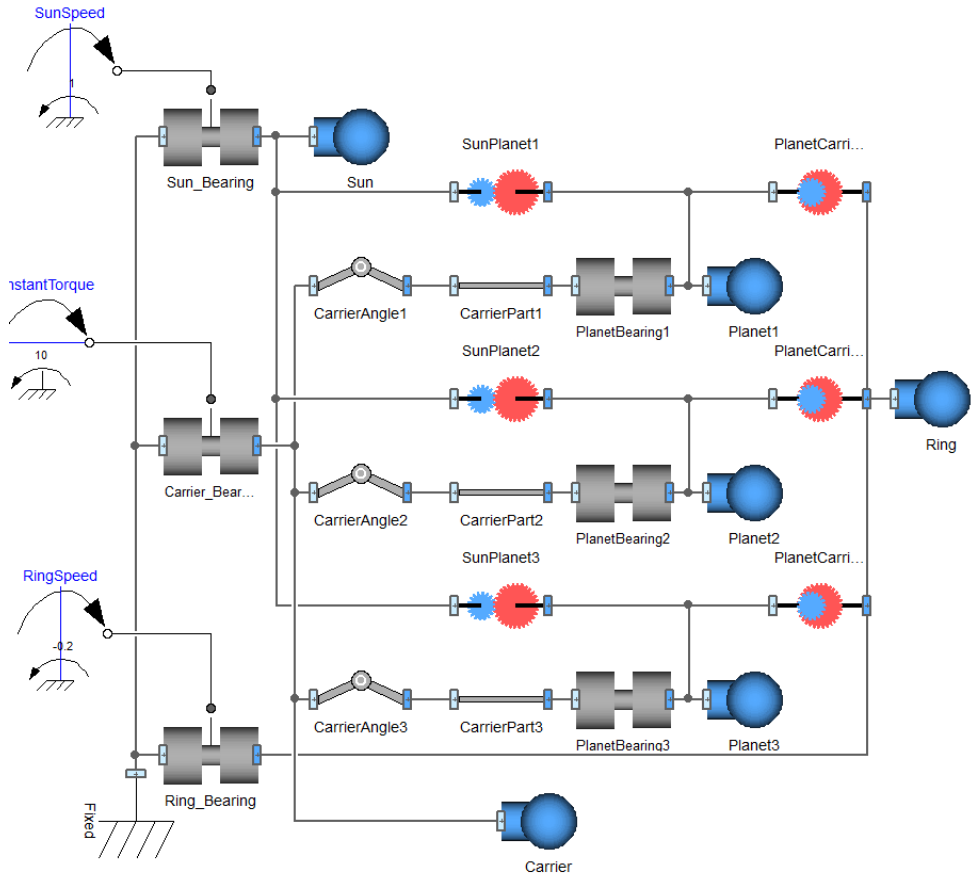

Figure B.8: Epicyclic Gear

Spur gear analysis

A Single Input Single Output (SISO) system of a simple spur gear model (as shown in Figure B.6) is generated by applying a torque input on gearwheel A, and using the angular position of gearwheel B as output. The Bode-Diagram of this system[1] is shown in Figure B.10. In the diagram a clear peak can be found at 0.225 Hz. This is exactly the expected frequency $\omega = \frac{\sqrt{\frac{k}{m}}}{2\pi} = \frac{\sqrt{\frac{2}{1}}}{2\pi} \cong 0.225\,\mathrm{Hz}$. The stiffness $k = 2\,\mathrm{N/m}$ and mass m 1 kg have to be used since the system is a symmetrical system using only one spring (e.g. Kelly, 2000). Lowering of the eigenfrequency due to damping can be neglected due to the low damping coefficient.

Epicyclic gear analysis

A SISO system is created by defining an input torque on the sun (middle (blue) gear in Figure B.9), as output the angular position of the carrier (grey structure). The Ring (red) is fixed, thereby eliminating vibrations of the ring structure. Each small planet is coupled to the planet rotating on the same axis. All bodies have the following properties: Mass 1 kg, Inertia 1 $\mathrm{kgm^2}$. All gear connections have a stiffness of 1 N/m, and a damping coefficient of $1 \times 10^{-3}\,\mathrm{N\,s/m}$. The radius of

[1] The bodies have a rotational inertia of 1 $\mathrm{kgm^2}$, the spring constant of the gear is 1 N/m, and a damping coefficient is $1 \times 10^{-3}\,\mathrm{N\,s/m}$. Both gearwheels have a radius of 1 m.

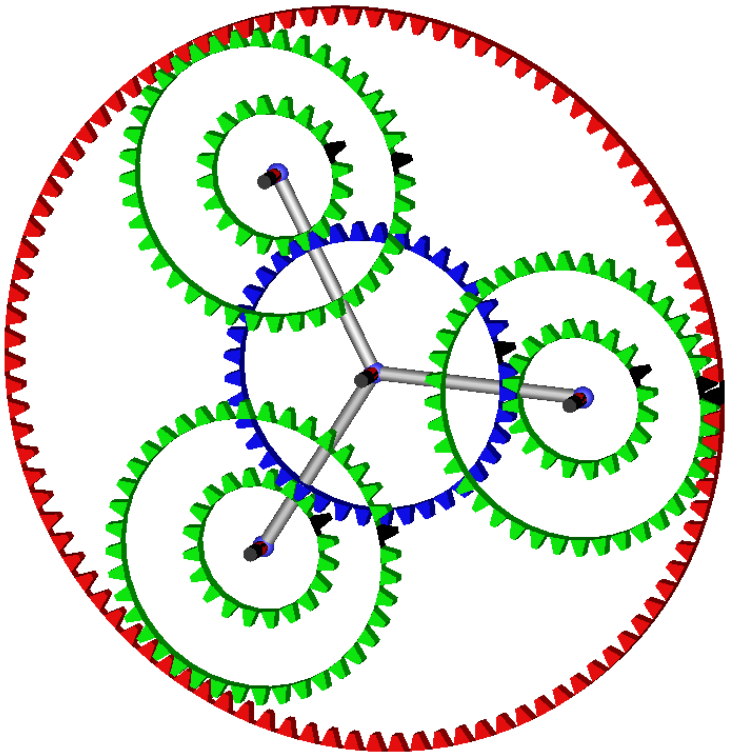

Figure B.9: Epicyclic Gear

the sun is 1 m, the connecting planet has a radius of 0.5 m. The other gear part of the stepped planet has a radius of 1 m. The ring has a diameter of 2.5 m. Using this set up, a Bode-Diagram is made (see Figure B.11). When evaluating the Bode diagram, two peaks and a single dip can be found in the magnitude diagram. These features correspond to the 3 eigenfrequencies of the system. The fact that only 3 peaks can be found in the Bode diagram is due to the fact that the planets all have the same masses and stiffnesses. When the stiffness of one of the Sun-Planet gear connections is lowered to 0.5 N/m, another peak and dip in the magnitude diagram occurs, since now one of the planets will swing in an other frequency as the others (see Figure B.12).

B.6.2 Internal vibrations

In Section B.4.1 the possibility of an internal excitation of the gear through varying stiffness is shown (to simulate gear mesh effects). A demonstation of this excitation is shown for a simple spur gear. Gear A is accelerated from 0 rad/s to 1 rad/s with a constant acceleration. A radius of 1 m and 10 teeth for both gearwheels are assumed for this calculation. The constant teeth stiffness in the simulation is 1 N/m, the stiffness ripple on both wheels is assumed to be 0.1 %. Using a damping coefficient of 0.2 N s/m this yields a lightly damped system with a damping ratio $\varsigma \approx 0.071$. In Figure B.13 the elastic deformation (Δ_{AB}) of the gear is shown.

Figure B.13 also shows that the system is excited by the internal mesh stiffness variation. The response of the system is the largest when the eigenfrequency of the system approximates the excitation by the stiffness variation.

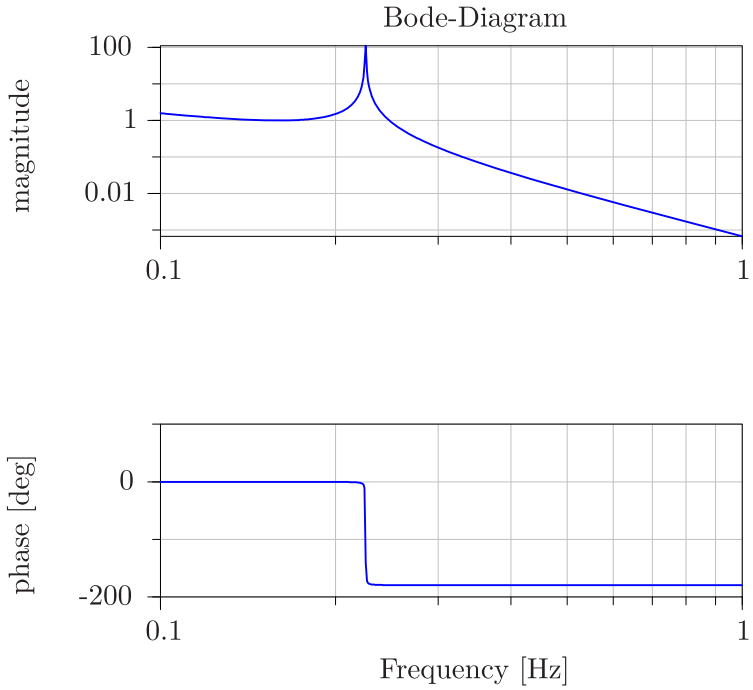

Figure B.10: Bode-Diagram of the spur gear from Figure B.6

B.7 Conclusion

In this paper a model is presented to describe the contact between two gear wheels. Using an external planar library, it is possible to model arbitrary gear configurations ranging from simple spur gears up to complex epicyclic gear configurations. An option to simulate gear meshing effects by varying the stiffness of the gear contact is presented. The presented models make it possible to analyze complex gear configuration by means of time simulations as well as eigenfrequency analyses. The presented simulation results show the power of the method, and illustrate the capability of the model.

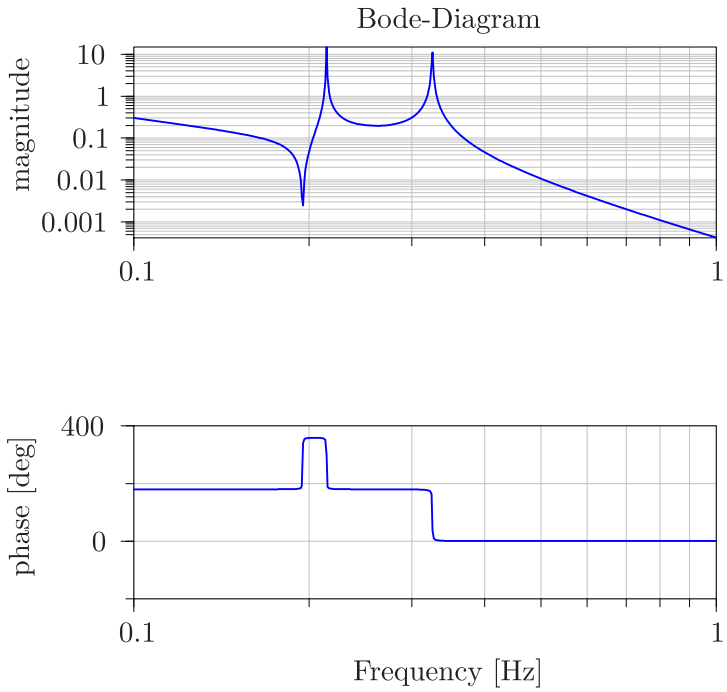

Figure B.11: Bode-Diagram of the epicyclic gear from Figure B.8

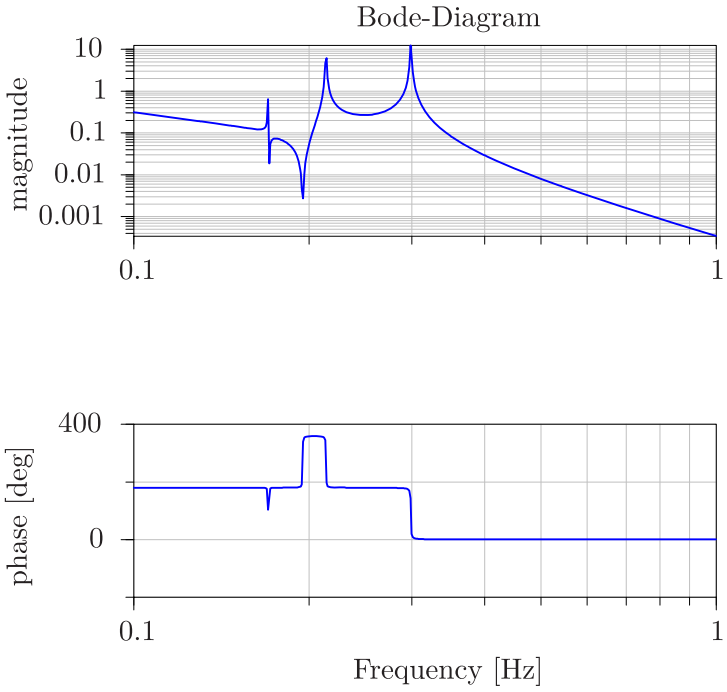

Figure B.12: Bode-Diagram of the epicyclic gear from Figure B.8 with reduced stiffness of one of the gear contacts.

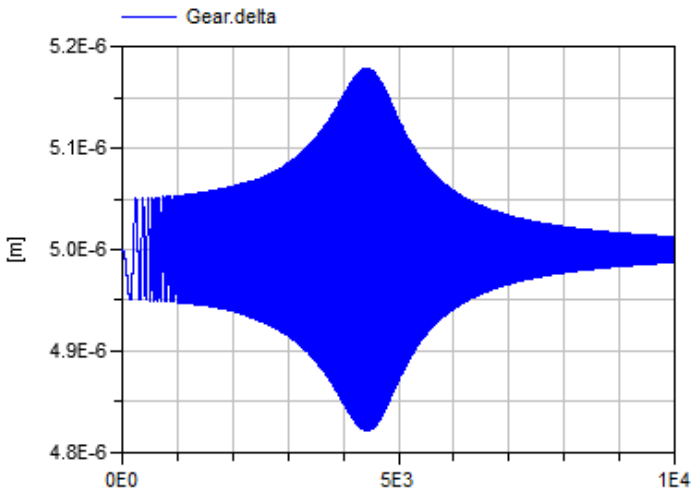

Figure B.13: Time simulation of an elastic spur gear with increasing velocity.

C Modeling faults in Modelica using a standardized blockset

In this thesis, much attention is paid to the modeling and validation of gears in a damaged state. Experience with larger models with many faults has shown that the modeling overhead to connect faults quickly rises with the number of implemented faults and the object oriented approach used in the modeling of such parts is often lost. Since the modeling of damaged components is more common nowadays, this problem is becoming widespread. As each engineer implemented his own solutions to implement faults, collaboration between colleagues was hindered.

To solve this problem, a method to implement faults has therefore been developed that allows a standardized method to implement faults. At the moment the proposed method is used at DLR for multiple projects, including a library for modeling of electromechanical actuators (F. L. J. Van der Linden et al., 2014) and an electrical vehicle with over 300 Faults (Lenz, 2014). Furthermore, the method is nowadays also used by Fraunhofer ISE for building management and the University of Nottingham for triggering of faults in electrical systems (e.g. Hill et al., 2014). This shows that the solution presented in this section is a very general solution and can be used in very different fields.

This Appendix represents the paper *General fault triggering architecture to trigger model faults in Modelica using a standardized blockset* presented in 2014 at the *international Modelica conference* in Lund (F. L. J. Van der Linden, 2014b).

C.1 Introduction

Failure detection and health monitoring systems to improve reliability and lower maintenance costs become increasingly important. Therefore the design and testing of these algorithms need good prediction models combined with an efficient way to trigger all fault cases.

Implementing faults in Modelica models is no new terrain. Many different implementations of real systems have been made. For example Schallert (Schallert, 2011) did a reliability and safety assessment. The faults are automatically identified based on parameter names. To set the parameters of the failed parts, a function is used which automatically sets the parameters before simulation. Gao et al. (J. Gao et al., 2012; M. Gao et al., 2008) did a fault analysis of electrical systems. To trigger the faults, two different methods are used; hard coding a fault in the model as well as creating a completely new model for a fault. Cui et al. (Cui, Ma, & Zeng, 2011) modeled an actuator system with automatically triggered faults. This automatic triggering is based on the predefined fault probability, but cannot be directly controlled. These works are all examples where faults are triggered in a Modelica implementation. However, all of these implementations use different ways to trigger the faults. Since there is a lack of standards implementation ways, all users must find a way for them self to trigger the faults.

Another approach for model-based diagnosis is used by RODON (Lunde, 2000). Uncertainty intervals for the model parameters combined with behavioral models are used to trigger faults. However, time simulations are not supported which limits its use in many applications. Also FaultWeaver (Junghanns, Mauss, & Tatar, 2008) can be used to trigger faults in Modelica. It

uses a set of models in Modelica. An external (non-Modelica) program is used to set the faults in Modelica and simulate the results.

In this section, a set of **standardized** fault-output blocks is proposed in Section C.3. These blocks use a designated data type to clearly identify these blocks as special fault blocks for further processing. Using these blocks, it is possible to create component models which include optional faults by the user. Care has been taken to make sure that all possible faults can be modeled by a single or a combination of standardized fault blocks. By analyzing the complete model, built from individual sub-models, a wrapper package can be automatically generated which can be used to activate all faults (Section C.5). Care has been taken that it is possible to completely eliminate the fault code from a model to increase simulation performance if not all faults are triggered. Furthermore, also quick model testing without a fault setup is possible.

The proposed implementation is based on a Dymola implementation making use of the Abstract Syntax Tree (AST) functions from the `ModelManagement` library. By using the proposed **open** and **standardized** fault blocks with a specialized fault type, it is possible to create similar functionalities in all Modelica solvers.

C.2 Fault injection demands for Modelica

To create a general environment to trigger faults in Modelica, care must be taken that all possible faults can be modeled using the proposed blocks. To make sure all possible faults are covered, a trade off study has been carried out. Fault implementations in the Modelica language can be generalized into classes. The following sections will highlight the different fault classes.

C.2.1 Fault variability classes

For Modelica usage, two different classes of faults can be identified:

1. Faults that have a very low time constant with respect to the simulation horizon and can be considered constant.
2. Faults with time constants faster than the simulation horizon which will cause transient behavior.

To further clarify the classes, a more detailed description including examples of each fault class is given.

Parameter faults

The parameter fault class consists of faults that have a low time constant compared with the simulation horizon. Usually these faults are characterized by slow changes in time such as the variation of the viscosity of oil due to an aging process in a transmission application. Another example of a fault with a slow time constant compared to the simulation time are some high frequency electronics simulations. In these simulations, the temperature of the environment can often be characterized as constant. Some examples of parameter faults are:

- Gear play
- Degradation of capacitors or batteries
- Oil viscosity degradation in a transmission
- Environment temperature increase in a fast switching application

Due to the very slow nature of these faults with respect to their simulation time, it is not necessary to have the possibility to model fault transients.

Variable faults

The second class of faults are variable faults. These faults are characterized by the possibility that they can significantly change during a typical simulation. Quite often the study of a transient response is one of the main purposes of the simulation of such faults. Some examples are:

- Semiconductor short circuit
- Breakage of hydraulic oil line
- Gearbox tooth breakage
- Screw jam

The faults in this class can vary during a simulation run, and can cause a dynamic system response which might be of interest for the engineer.

C.2.2 Fault data type classes

The faults of both classes described in Section C.2.1, can be divided into three types to represent the different cases needed to model faults.

"On-Off" faults (Boolean)

On-off faults are marked by having only two discrete states. Examples are jamming of a nutscrew and disconnection of electrical cables.

Case faults (Integer)

Case faults are marked by having multiple discrete failure modes. A good example is a semiconductor failure:

- Normal operation
- Short circuit
- Open loop

Continuous fault (Real)

A continuous fault is a fault without an explicit discrete value. Examples are:

- Oil degradation
- Increased friction in a bearing
- Capacitor degradation

Combining the fault classes (Section C.2.1) and the fault class properties (Section C.2.2), six different combinations of faults are identified (see Table C.1). These possibilities can model all general and advanced faults. In the next sections, the implementation as well as some extra features for easier fault handling and simulation performance are discussed.

Table C.1: Combined fault possibilities for Modelica models with examples. The choice between a variable and parameter fault is not always directly clear, and may need to be chosen as constant or variable based on the length of the simulation

	Constant	**Variable**
On-Off	Increased friction	Screw jam
Mode	Bearing fault mode	Transistor
Continuous	Gear play	Oil loss

Table C.2: Variable mode selection flag

Flag value	**Description**
0	fault deactivated
1 (default)	standard fault mode activated
2,3,...	optional extra fault modes

C.2.3 Variable mode selection

To accommodate the reconfiguration of a model with a variable fault, a mechanism to decide if the fault can be activated during simulation must be implemented. This reconfiguration can be necessary to increase simulation speed in case of no failure or to switch between different failure modes. In the case of a parameter fault, this is known by definition. However in the case of a variable fault, this is not known. To be able to reconfigure such a model, it is therefore necessary to add a parameter signal flag which can be used to reconfigure the model. For maximal flexibility, it is chosen to add a mode selection using an integer constant as a flag. This flag can be used to reconfigure a model to include or exclude a fault. How to use the values of the flag can be seen in Table C.2.

The same effect as the mode selection is possible by combining a parameter integer fault with an variable fault. However, combining two fault inputs for one fault makes it hard to use consistent naming.

C.3 Fault triggering standardisation architecture

Defining faults types is not sufficient to define a usable Modelica implementation. For a good user-friendly implementation a well designed architecture is vital. Different ways to set up a fault triggering method are analyzed and their benefits compared.

C.3.1 Fault architecture

Controlling of the faults in a global model using components with faults can be done in many different ways. Different ways are studied in this section and it is decided which methods are selected for the proposed standard.

To assess the overall performance of these methods, a set of criteria is defined to evaluate several important aspects for fault triggering. The implementation effort of setting up the general architecture is not evaluated as this effort has to be invested only once in the generation of the fault library.

These criteria are:

(a) **Non physical connections**: The connections between the models should be based on physical quantities. Faults do not have a physical connections as they are triggered by wear, or external influences which are usually not modeled.

(b) **Ease of implementation**: Effort for user to create a model from instances using faults (e.g. the development of a multistage gearbox using predefined faulty gearbox instances)

(c) **Maintainability**: Effort to maintain a set of models with faults. Typical tasks would be adding or removing fault cases, restructuring models and keeping a well documented set of models

(d) **Standardization**: Standardization effort to keep models compatible between different business partners.

(e) **Transients**: Possibility to model transients used for variable faults (see for a description Section C.2.1).

Four methods to implement faults in Modelica have been tried out and analyzed. The results are assessed using the criteria (a through e).

1. **Model parameters**: Each fault is controlled by a parameter in the model. It is possible to "pull" these parameters up to the top level model. Also direct changing of the instance parameter in the model is possible. If the parameter is flagged appropriately, it is possible to create a system with automated parameter detection and central setting of the parameters. Such a structure does not need non-physical connections, is easy to implement for the user and, if a proper automation is used, can be well maintained. Also standardization using the proposed flag methods is possible. Since in this method it is only possible to handle parameters, no transients can be used.

2. **Model inputs**: Inputs are used to control faults in the models. By connecting the input connectors, it is possible to create a central element to control all faults. This method is often used for small fault systems. However, it leads to non physical connections between the models. Due to the high customization, maintainability and standardization cannot be guaranteed. The ease of implementation is good in small systems maintained by a single person, but quickly becomes more and more problematic as the model grows. Transients can be handled well.

3. **Bus system**: A bus system to connect faults. All fault signals are connected to a bus system. This way is similar to the model inputs, except that all faults are organized in one block. A bus system leads to non physical connections. The ease of implementation and maintainability depends highly on the complexibility of the model, small systems can be easily implemented and managed, but it becomes quickly confusing. The standardization is better than using a direct model input since all faults are now marked in one faultbus. However, still no automated algorithms can be used as it is impossible to properly define a standard input. Transients can be handled well as it is possible to connect variables to a bus.

4. **Broadcasting**: Using an inner-outer structure, the fault models can obtain their values from a centralized point in the global model. Using an automated routine, all appropriate flagged

Table C.3: Fault triggering approaches. A detailed description of the criteria can be found in Section C.3.1

Description	(a) Non physical connections	(b) Ease of implementation	(c) Maintainability	(d) Standardization	(e) Transients
(1) Model parameters	+	+	+	+	-
(2) Model inputs	-	±	-	-	+
(3) Bus system	-	±	±	±	+
(4) Broadcasting system	+	±	+	+	+

faults can be found and managed in one central point. No non-physical connections are needed. If standardized, flagged and predefined fault blocks are used, the ease of implementation and maintainability is high. Also the standardization can be guaranteed by flagging the models. Using an inner-outer structure it is also possible to use transients. However, when only parameter Faults are used, this way of modeling is over complex and will always need a full setup of the variable faults. In contrast, it is possible to leave most parameter faults at their standard value and set only one fault without setting up a complete fault system.

In Table C.3, the previously discussed four different approaches (1:4) are assessed using the criteria (a:e). From this analysis follows that the usage of model parameters (1) and a broadcasting system (4) have most advantages. It is therefore chosen to use following architecture:

- **Model parameters** to handle **constant** faults
- **Broadcasting system** for **variable** faults

C.4 Standardized fault class definition

All faults in a model must be recognized by automated scripts, while at the same time the user should have the freedom to name the model faults arbitrarily. To do so, special fault classes have been designed. This has the advantage that a fault is identified by the class name, and can be integrated without special care of instance names by the user. These fault classes are released under the Modelica 2 License.

Below, all fault classes are defined. For a parameter fault of the type Real, the type is defined in Code C.1.

Code C.1: Real parameter fault

```
type Parameter_Fault_Real =
        Real "Value of the Real Fault";
```

Using this special fault class for each Real fault, it is possible to clearly identify each instance of this model as a Real parameter fault.

The same is done for variable faults. Since these faults are more complex, a record with three parameters is used. In Code C.2 the definition of this Fault is shown.

Code C.2: Real variable fault

```
record Variable_Fault_Real
   "External Fault Triggering parameters"
  Boolean externalFaultOn=false
   "External fault controlling
                (true = global)";
  Integer faultIndex = 1
   "External fault index";
  Integer faultMode = 1
   "Optional fault mode for model
                reconfiguration";
end Variable_Fault_Real;
```

The first Boolean `externalFaultOn` is used to switch between the local default fault definitions and external global control. The integer `faultIndex` is used to set the channel in the external global fault triggering (see Section C.5). The integer `faultMode` is used to set the optional fault mode selection as discussed in Section C.2.3.

The examples given in this section are for Real faults. The code for Integer and Boolean faults can be found in Section C.8.

Using these class definitions, it is possible to set up a complete fault triggering system. In Section C.5 an implementation for Dymola using the ModelManagement toolbox is presented. Since these defined faultclasses are open and standardized, algorithms or plug-ins for programs can be developed by users, also for other Modelica solvers.

C.5 FaultTriggering library

Beside the definition of a standard, a library has been built to support the user with implementing faults. Using the definitions from Section C.4, blocks are created which simplify the implementation of faults in a model. Two versions of these outputs are made; one for textual modeling and one for usage in the diagram layer. Also a method to manage the fault signals in a single block is proposed.

In Figure C.1, an overview of the final fault setting structure is given. In the generated wrapper model, it is possible to set the parameter and variable faults. The parameters are set in an automatically generated structure (see Section C.5.3) and the variable faults are handled using a generated bus system (see Section C.5.3).

C.5.1 Parameter fault modeling

The textual modeling block for a parameter fault is a simple block with a parameter of type `Parameter_Fault_Real` (for Real faults). By extending this block in the model, a parameter fault is directly correctly implemented and its name is `constRealFault`.

In Code C.3 the code for the Real parameter fault is given. Parts of the complete path to the components are abbreviated for a better overview. Integer and Boolean faults are implemented using the same approach.

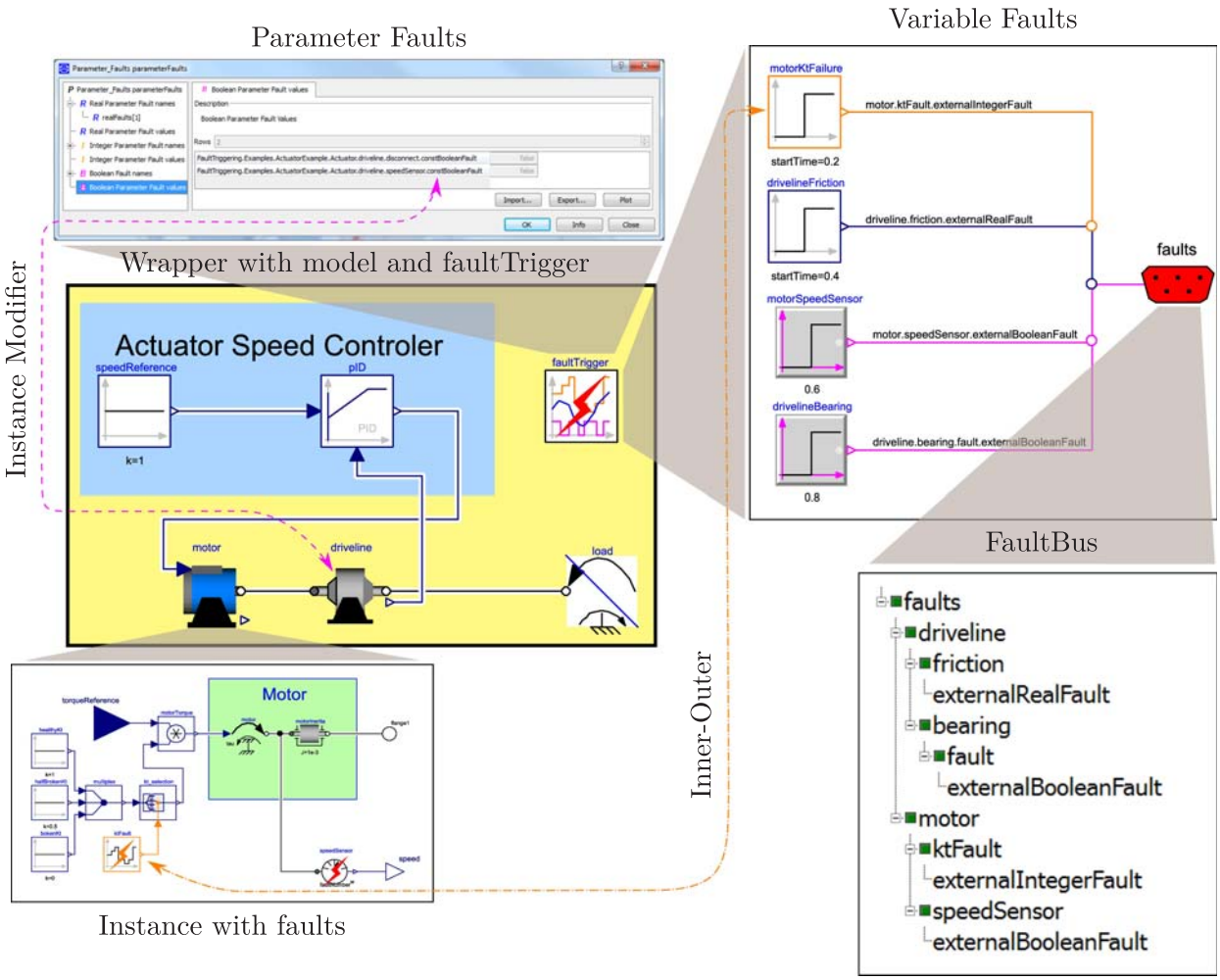

Figure C.1: Automatically generated wrapper model (yellow) which contains the extended original model and the block `faultTrigger`. In this block all parameter and variable faults can be set. The parameter faults communicate directly with the model instances using instance modifiers (pink dash-dotted line), the variable faults using a bus system connected to a global inner/ outer system (orange dashed line).

Code C.3: Real parameter fault for textual modeling

```
block InternalConstantRealFault
 "Generate constant Fault of type Real"
 extends ...Icons.RealFault;
 parameter ...Types.Parameter_Fault_Real
      constRealFault= 1
      "Constant output value";
end InternalConstantRealFault;
```

The blocks for graphical modeling environment are extensions of the discussed textual modeling approach and the interface `Modelica.Blocks.Interfaces.SO` . This creates a block (see Code C.4) with a single Real output whose value is set by the fault parameter.

Code C.4: Real parameter fault for graphical modeling

```
block ConstantRealFault
  "Generate constant signal of type Real"
  extends Modelica.Blocks.Interfaces.SO;
  extends ...InternalConstantRealFault;
equation
  y = constRealFault;
end ConstantRealFault;
```

C.5.2 Variable faults

The variable fault blocks are more complicated to implement than the parameter fault blocks. These blocks need the information from a central block in which the fault signal is defined. To do so an inner-outer structure has been set up to communicate the fault signals. In this section, first the global block will be discussed followed by the local fault blocks.

Global variable faults control

For each variable fault (Real, Integer and Boolean), a single channel is reserved in a variable with n channels (with n the number of faults of each type). This variable is defined in a central `FaultTrigger` block. Each fault can be coupled to fault sources using modelica code in this global block. This can be done by hand or an automated script which is proposed in Section C.5.3. The partial model can be seen in Code C.5. This model is defined as "inner" in the annotations, so that the local fault injection blocks can communicate with this block.

Code C.5: Partial model for variable fault input framework

```
partial model Partial_FaultTrigger
  "partial model defining  fault classes"
  parameter Integer realFaultSize
    "Number of real fault channels";
  parameter Integer integerFaultSize
    "Number of integer fault channels";
  parameter Integer booleanFaultSize
    "Number of boolean fault channels";

  Real    realFault[realFaultSize]
            "Real Fault trigger";
  Integer integerFault[integerFaultSize]
            "Integer Fault trigger";
  Boolean booleanFault[booleanFaultSize]
            "Boolean Fault trigger";

 annotation (
 defaultComponentPrefixes="inner")
end Partial_FaultTrigger;
```

Variable fault modeling classes

The variable fault models get their signals from the global fault control model. In Code C.6 the code for a variable fault is given. In this model, the variable `fault` is the actual fault value. Each fault uses its own fault channel in the variables `realFault`, `integerFault` and `booleanFault`. To

select which channel is to be used from these variables, the parameter `faultNumber` is defined. This parameter is generally set by an automated system (see Section C.5.3).

To be able to directly operate a model with variable faults in the model for testing purposes, a parameter with a default fault value is defined in `fault_local`. Using the switch (`externalRealFault.externalFaultOn`), the local fault can be changed to the value defined in the global fault block. Using this, it is guaranteed that each block has a valid output without setting up a global fault block.

Code C.6: Real variable fault for textual modeling

```
block InternalRealFault
 "Generate variable Fault of type Real"
 extends ...Icons.RealFault;
 outer FaultTrigger faultTrigger;
 parameter Real fault_local = 1
  "Default fault value if no external
    triggering is used";
 parameter ...Types.Variable_Fault_Real
     externalRealFault =
      ...Types.Variable_Fault_Real()
  "External Fault Triggering parameters";
 Modelica.Blocks.Interfaces.RealOutput
   fault "Final fault value";

protected
...Types.Fault_SelectRealFault
        faultNumber;
equation
 faultNumber =
   externalRealFault.faultIndex;
 fault =
  if externalRealFault.externalFaultOn
  then
  faultTrigger.realFault[faultNumber]
  else fault_local;
end InternalRealFault;
```

The faults for graphical modeling are made by extending Code C.6 in a model with two outputs (Code C.7): One real output for the fault signal and one optional integer output for the mode signal.

Code C.7: Real variable fault for graphical modeling

```
block VariableRealFault
   "Generate variable signal of type Real"
extends ...Internal.InternalRealFault;
parameter Boolean useModelModeSelection
   "toggles external mode selection";
Modelica.Blocks.Interfaces.RealOutput y;
Modelica.Blocks.Interfaces.IntegerOutput
    mode = externalRealFault.faultMode
       if useModelModeSelection
    "Connector of Integer output signal";
equation
```

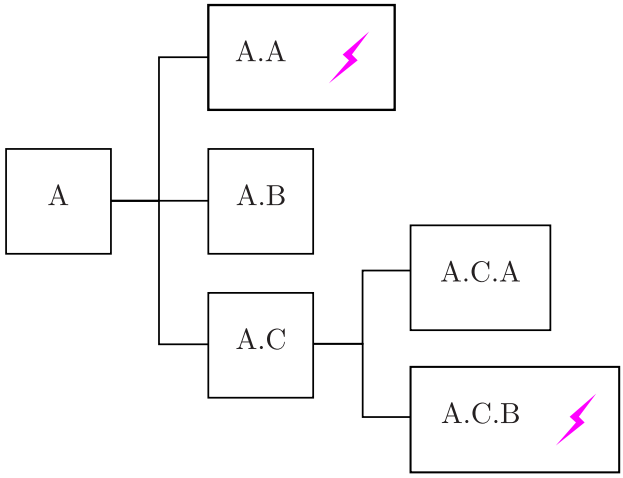

Figure C.2: Model tree with faulty models on several levels. Blocks with a lightning symbol (A.A & A.C.B) are extensions of the standardized fault classes.

```
  y = fault;
end VariableRealFault;
```

C.5.3 Automated fault handling

To keep overview of the faults in a model and help the user with fault channel selection for each fault, an automated fault handling algorithm is developed. This algorithm can detect the parameter and variable faults in the selected model. Also all faults in the instances used in this model can be detected. Setting and internal handling of these faults is different for parameter and variable faults. A library is automatically generated which contains a wrapper model that extends the original model. Also a central block to manage the faults is instantiated in this wrapper model. In this block, the configuration of the parameter and variable faults is handled.

Automated fault finding

Using the Dymola `ModelManagement` toolbox, it is possible to investigate a model with its sub-models. Using these features, it is possible to generate a model tree from a model with all instances. A schematical example of such a model tree can be found in Figure C.2. Using the type definitions from Section C.4, all faults in a model can be found and classified. Also the "path" to the model can be found. The complete path of the fault instance `bearing_stuck` in the model `Actuator` will be represented as `Actuator.bearing_stuck`. In the following sections, the generated fault tree and fault classification will be used in the implementation of the library features.

Global parameter setting

All the parameter faults can be found and identified using the described method. It is possible to directly change these values by using an instance modifier generated by the fault-search algorithm by hand.

However, in case of large models with many faults or many different cases to analyze, this can quickly become unclear and tedious. To aid the user, a structure is automatically generated using the scripts supplied in the library which includes all faults together with their default values.

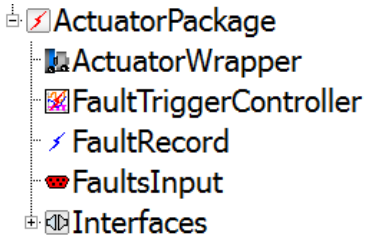

Figure C.3: Automatically generated Fault library

This structure is used as a parameter in the global `faultTriggering` model. These values are automatically linked to the instance modifiers in the wrapper model. By creating different fault structures, fault cases can be defined. Each fault structure stands for a clearly defined simulation case.

Global variable setting

To aid the user with setting the variable faults, a hierarchical `faultbus` is generated from the fault structure (see Figure C.1). It is possible to directly connect the fault source signals to the hierarchical bus. The hierarchical bus system itself is connected to the `realFault`, `integerFault` and `booleanFault` variables (see Section C.5.2). The corresponding fault index is automatically set in the model using component modifiers. Using this approach, mistakes with mixing up the channels are not possible, as this is automated. Also the use of an automatically generated bus makes connecting the fault sources easy.

In Figure C.3, a generated library is shown with its default components.

C.6 Examples

To test the library functionality a simple actuator model is built consisting of a motor with PID control, a simple driveline and a load. The total model has 6 faults: 2 parameter faults, and 4 variable faults. Using the fault processing algorithms presented in Section C.5.3, a package is generated. The model wrapper adds the `faultTrigger` block in which all faults can be set. In this block all fault inputs are defined. The variable faults are set in the block of type `FaultTriggerController` (instance `faultTrigger`). Using the parameter record in this block, it is possible to set all parameter faults. An overview of this functionality is shown in Figure C.1.

The result of a simulation with progressive faults is shown in Figure C.4. The dynamic effects of a breaking component can be seen by the changing response of motor speed and torque. By changing or duplicating the faultTrigger block, it is possible to create multiple fault scenarios for a single model. The original model stays unchanged and can be used for all analysis, healthy as well as broken.

C.7 Conclusion and discussion

In this section, a method to standardize the implementation of faulty components in Modelica is specified. It is possible to implement parameter, as well as varying fault signals. The code for the proposed faulty components is included to aid the standardisation of fault implementation in Modelica.

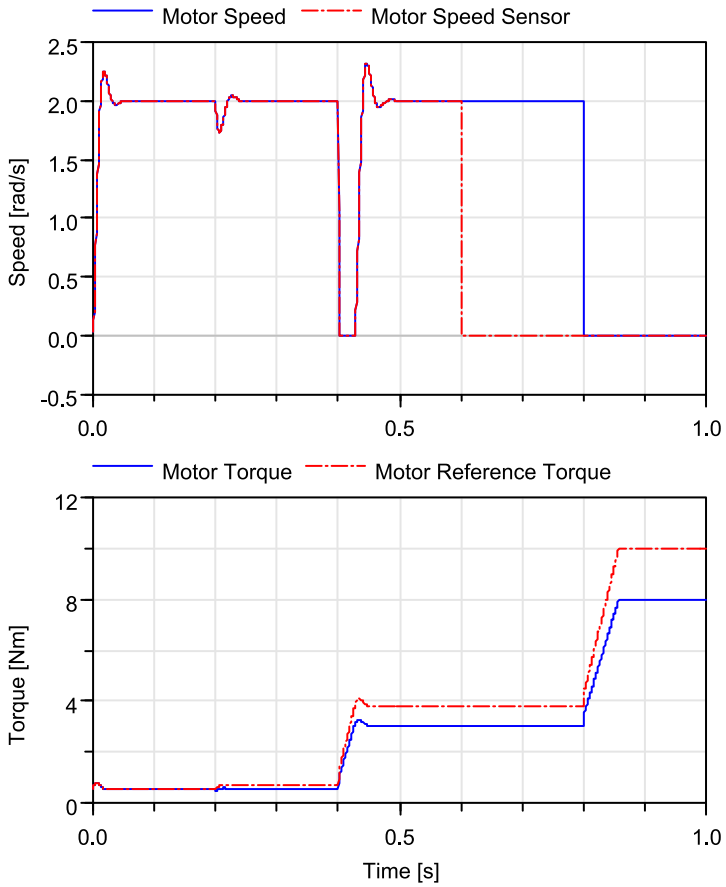

Figure C.4: Results of a simulation with progressive faults. At t=0.2s the motor constant drops, at t=0.4s, an increased friction in the driveline is triggered, at t=0.6s, the speed sensor of the motor breaks and finally at t=0.8s the driveline bearing gets stuck.

Moreover a library has been created which supports the user to set these faults by automatic generation of a wrapper library. This wrapper includes all parameter faults in a parameter structure and a bus system to connect the variable faults. This functionality is enabled by the implementation of a search algorithm to search the model for the standardized fault classes.

An example model has been built and the methods to implement the faults in the model have been proved valuable. At the moment the proposed Fault Library is used in the Actuator EMA library (Giangrande et al., 2014; Hill et al., 2014; F. L. J. Van der Linden et al., 2014). The standardization of these faults has led to an easy implementation process. The model designer can focus on implementing the faults in the model without paying attention to the interfaces and the compatibility between the models.

Acknowledgement

The research leading to these results has received funding from the European Union's Seventh Framework Program (FP7-284916) for ACTUATION 2015 under grant agreement no. 284915.

C.8 Modelica Code for Faults

The code for the implementation of the fault classes is given in this section. Using strictly this code, it is possible for automated fault systems to search for all faults in a model.

C.8.1 Real faults

Code C.8: Real parameter fault

```
type Parameter_Fault_Real =
        Real "Value of the Real Fault";
```

Code C.9: Real variable fault

```
record Variable_Fault_Real
   "External Fault Triggering parameters"
  Boolean externalFaultOn=false
   "External fault controlling
                 (true = global)";
  Integer faultIndex = 1
   "External fault index";
  Integer faultMode = 1
   "Optional fault mode for model
                 reconfiguration";
end Variable_Fault_Real;
```

C.8.2 Integer faults

Code C.10: Integer parameter fault

```
type Parameter_Fault_Integer =
    Integer "Value of the Integer Fault";
```

Code C.11: Integer variable fault

```
record Variable_Fault_Integer
   "External Fault Triggering parameters"
  Boolean externalFaultOn=false
   "External fault controlling
                 (true = global)";
  Integer faultIndex = 1
   "External fault index";
  Integer faultMode = 1
   "Optional fault mode for model
                 reconfiguration";
end Variable_Fault_Integer;
```

C.8.3 Boolean faults

Code C.12: Boolean parameter fault

```
type Parameter_Fault_Boolean =
    Boolean "Value of the Boolean Fault";
```

Code C.13: Boolean variable fault

```
record Variable_Fault_Boolean
   "External Fault Triggering parameters"
  Boolean externalFaultOn=false
   "External fault controlling
                (true = global)";
  Integer faultIndex = 1
   "External fault index";
  Integer faultMode = 1
   "Optional fault mode for model
                reconfiguration";
end Variable_Fault_Boolean;
```

D Calculation of $\overline{d_{tau}}$ and $\overline{d_F}$

D.1 Gear data calculation

In this Section the derivation of the distances needed for the calculation of $\overline{d_F}$, $\overline{d_{tau,A}}$ and $\overline{d_{tau,B}}$ is presented.

Using the geometry of the gear contact presented in Figure D.1, it is possible to calculate the distances needed for $\overline{d_F}$, $\overline{d_{tau,A}}$ and $\overline{d_{tau,B}}$.

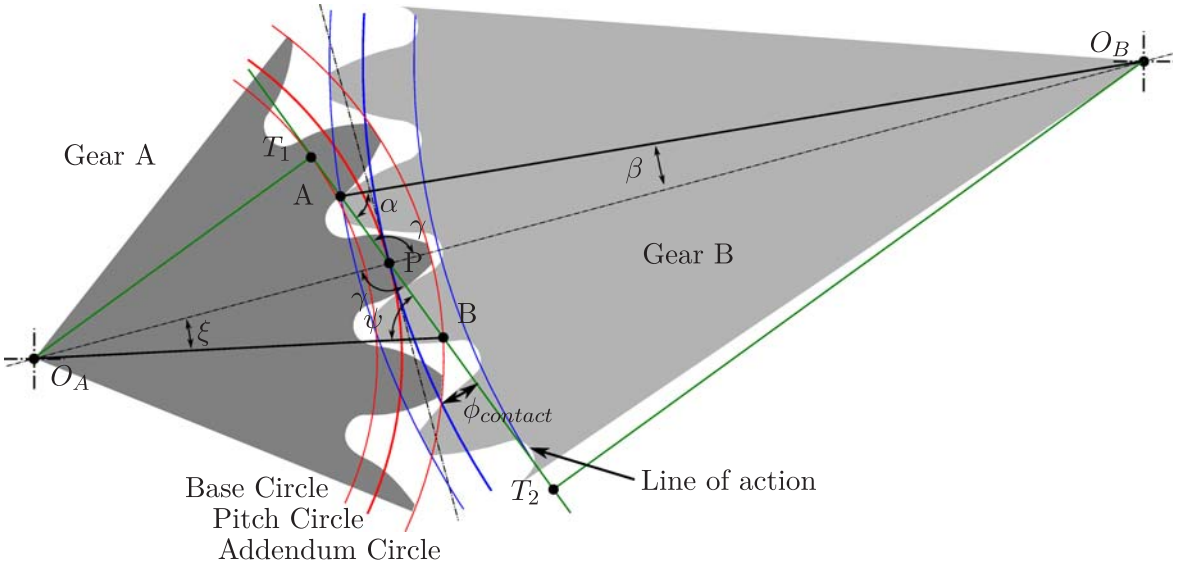

Figure D.1: Schematic overview of two involute gears in contact.

D.1.1 Calculation of $\overline{T_1P}$ and $\overline{PT_2}$.

The distances $\overline{T_1P}$ and $\overline{PT_2}$ are calculated by:

$$\overline{T_1P} = \overline{O_AP}\sin(\phi_{contact}) \tag{D.1}$$

$$\overline{PT_2} = \overline{PO_B}\sin(\phi_{contact}) \tag{D.2}$$

D.1.2 Calculation of $\overline{AP}$

Calculating the distance $\overline{AP}$ is starts by considering that γ and $\phi_{contact}$ form an 180° angle.

$$\gamma = \pi - \phi_{contact} \tag{D.3}$$

The law of sines yields:

$$\frac{\sin\gamma}{\overline{AO_B}} = \frac{\sin\alpha}{\overline{PO_B}} \tag{D.4}$$

This leads to:

$$\alpha = \arcsin\left(\frac{\overline{PO_B}}{\overline{AO_B}}\sin\gamma\right) \tag{D.5}$$

Now the angle β can be calculated:

$$\beta = \pi - \alpha - \gamma \tag{D.6}$$

Again using the law of sines gives $\overline{AP}$:

$$\overline{AP} = \frac{\sin\beta}{\sin\gamma}\overline{AO_B} \tag{D.7}$$

The Matlab symbolic toolbox is used to reformulate this equation and obtain $\overline{AP}$:

$$\overline{AP} = \overline{AO_B}\sqrt{1 - \frac{\overline{PO_B}^2\left(\cos\phi_{contact}\right)^2}{\overline{AO_B}^2}} - \overline{PO_B}\sin\phi_{contact} \tag{D.8}$$

D.1.3 Calculation of $\overline{PB}$

In the same way as $\overline{AP}$, $\overline{PB}$ can be calculated using the law of sines:

$$\psi = \arcsin\left(\frac{\overline{O_AP}}{\overline{O_AB}}\sin\gamma\right) \tag{D.9}$$

Again the angle ξ can be calculated:

$$\xi = \pi - \psi - \gamma \tag{D.10}$$

Using the law of sines, $\overline{PB}$ can be obtained:

$$\overline{PB} = \frac{\sin\xi}{\sin\gamma}\overline{O_AB} \tag{D.11}$$

Simplification is again done using the Matlab symbolic toolbox:

$$\overline{PB} = \overline{O_AB}\sqrt{1 - \frac{\overline{O_AP}^2\left(\cos\phi_{contact}\right)^2}{\overline{O_AB}^2}} - \overline{O_AP}\sin\phi_{contact} \tag{D.12}$$

D.2 Example gear calculation

In this Section an example gear connection is done. The gearing configuration is the gear transmission used in Chapter 3 which has a transmission ratio of 1:3. The properties of the transmission are given in the table below:

Property	value	unit
modulus	1	
pressure angle	20	
no. Teeth gear A	20	
no. Teeth gear B	60	
pitch circle gear A	20	mm
pitch circle gear B	60	mm
addendum circle gear A	22	mm
addendum circle gear B	62	mm

Using this properties the following, $\overline{d_{\tau,A}}$ and $\overline{d_F}$ can be calculated:

Property	value	unit
$\overline{d_{\tau,A}}$	-0.001	m
$\overline{d_F}$	0.044	-

References

Ahmed, F. S., Laghrouche, S., & El Bagdouri, M. (2012). Overview of the modelling techniques of actuator non-linearities in the engine air path. *Proceedings of the Institution of Mechanical Engineers, Part D: Journal of Automobile Engineering*, *227*(3), 443–454. DOI: 10.1177/0954407012453905

Åkerblom, M. (2001). *Gear Noise and Vibration : A Literature Survey.* Available at http://www.diva-portal.org/smash/record.jsf?pid=diva2:139878&dswid=-9504

Anderson, N. E., & Loewenthal, S. H. (1980). *Spur-gear-system efficiency at part and full load* (Vol. 79; Tech. Rep. No. 46). NASA.

Anderson, N. E., & Loewenthal, S. H. (1984). *Efficiency of nonstandard and high contact ratio involute spur gears.* National Aeronautics and Space Administration.

ASM. (1999). *Metals handbook* (J. R. Davis, Ed.). ASM International.

Buckingham, E. (1949). *Analytical mechanics of gears.* McGraw-Hill, London.

Burrows, M., & Sutton, G. (2013). Interacting gears synchronize propulsive leg movements in a jumping insect. *Science (New York, N.Y.)*, *341*(6151), 1254–6. DOI: 10.1126/science.1240284

Choy, F., Polyshchuk, V., Zakrajsek, J., Handschuh, R., & Townsend, D. (1996). Analysis of the effects of surface pitting and wear on the vibration of a gear transmission system. *Tribology International*, *29*(1), 77–83. DOI: 10.1016/0301-679X(95)00037-5

CONCEPT (Romax Technology). (2015). Available at http://www.romaxtech.com/

Cui, X., Ma, J., & Zeng, S. (2011). The fault modeling methodology of actuator system based on Modelica. *The Proceedings of 2011 9th International Conference on Reliability, Maintainability and Safety*, 997–1002. DOI: 10.1109/ICRMS.2011.5979411

Dao, D. D. V., Pham, P. H., Amaya, S., & Sugiyama, S. (2008). Micro Ratcheting Transmission Systems Based on Electrostatic Actuator. In *2008 international symposium on micro-nanomechatronics and human science* (pp. 17–20). IEEE. DOI: 10.1109/MHS.2008.4752415

D'Errico, J. (2005). *Surface Fitting using gridfit.* Available at http://www.mathworks.de/matlabcentral/fileexchange/8998-surface-fitting-using-gridfit

DIN 3990 Teil 4. (1987). *Tragfähigkeitsberechnung von Stirnrädern; Berechnung der Freßtragfähigkeit* (Vol. 4). Beuth.de.

Ebrahimi, S., & Eberhard, P. (2006). Rigid-elastic modeling of meshing gear wheels in multibody systems. *Multibody System Dynamics*, *16*(1), 55–71. DOI: 10.1007/s11044-006-9021-7

Fakhfakh, T., Chaari, F., & Haddar, M. (2004). Numerical and experimental analysis of a gear system with teeth defects. *The International Journal of Advanced Manufacturing Technology*, *25*(5-6), 542–550. DOI: 10.1007/s00170-003-1830-8

Fischer, K., Besnard, F., & Bertling, L. (2012). Reliability-Centered Maintenance for Wind Turbines Based on Statistical Analysis and Practical Experience. *IEEE Transactions on Energy Conversion*, *27*(1), 184–195. DOI: 10.1109/TEC.2011.2176129

Freeth, T., Bitsakis, Y., Moussas, X., Seiradakis, J. H., Tselikas, A., Mangou, H., ... Edmunds, M. G. (2006). Decoding the ancient Greek astronomical calculator known as the Antikythera Mechanism. *Nature*, *444*(7119), 587–91. DOI: 10.1038/nature05357

FVA-Workbench (FVA GmbH). (2015). Available at http://www.fva-service.de/software/

Gao, J., Ji, Y., Bals, J., & Kennel, R. (2012). Fault Detection of Power Electronic Circuit using Wavelet Analysis in Modelica. In *Proceedings of the 9th international Modelica conference* (pp. 513–522). Munich, Germany. DOI: 10.3384/ecp12076513

Gao, M., Hu, N., Qin, G., & Xia, L. (2008). Modeling and fault simulation of propellant filling system based on Modelica/Dymola. *2008 2nd International Symposium on Systems and Control in Aerospace and Astronautics*, 1–5. DOI: 10.1109/ISSCAA.2008.4776271

Garcia, E., de Santos, P., & de Wit, C. (2002). Velocity dependence in the cyclic friction arising with gears. *The International Journal of Robotics Research*, *21*(9), 761–771. DOI: 10.1177/027836490202100987 7

Giangrande, P., Hill, C. I., Gerada, C., & Bozhko, S. V. (2014). Multi-level library of electrical machines for aerospace applications. In *Proceedings of the 10th international Modelica conference* (pp. 737–746). DOI: 10.3384/ECP14096737

Giese, T., Schlabe, D., Slate, R., Crespo, M., Tichy, F., & Baumann, C. (2010). *Extended design office concept definition* (Tech. Rep.). Cleansky WP2.1.1 deliverable.

Gwinner, P., Otto, M., & Stahl, K. (2014). Lightweight Torque-Vectoring Transmission for the Electric Vehicle VISIO.M. In *Cofat 2014.* Available at http://mediatum.ub.tum.de/doc/1226683/1226683.pdf

Harris, S. L. (1958). Dynamic loads on the teeth of spur gears. *Proceedings of the Institution of Mechanical Engineers*, *172*(1958), 87–112. DOI: 10.1243/PIME_PROC_1958_172_017_02

He, S., Gunda, R., & Singh, R. (2007a). Effect of sliding friction on the dynamics of spur gear pair with realistic time-varying stiffness. *Journal of Sound and Vibration*, *301*(3-5), 927–949. DOI: 10.1016/j.jsv.2006.10.043

He, S., Gunda, R., & Singh, R. (2007b). Inclusion of Sliding Friction in Contact Dynamics Model for Helical Gears. *Journal of Mechanical Design*, *129*(1), 48. DOI: 10.1115/1.2359474

Heider, M. K. (2012). *Schwingungsverhalten von Zahnradgetrieben- Beurteilung und Optimierung des Schwingungsverhaltens von Stirnrad- und Planetengetrieben* (Doctoral dissertation). Technischen Universität München.

Henriksson, M. (2009). *On noise generation and dynamic transmission error of gears* (Doctoral dissertation). KTH.

Hepermann, P. (2013). *Untersuchungen zur Fresstragfähigkeit von Groß- , Schräg- und Hochverzahnungen* (Doctoral dissertation). Ruhr-Universität Bochum.

Hewitt, E., & Hewitt, R. E. (1979). The Gibbs-Wilbraham phenomenon: An episode in fourier analysis. *Archive for History of Exact Sciences*, *21*(2), 129–160. DOI: 10.1007/BF00330404

Hill, C., Giangrande, P., Gerada, C., & Bozhko, S. (2014). Implementation of a Multi-Level Power Electronic Inverter Library in Modelica. In *Proceedings of the 10th international Modelica conference* (pp. 523–532). DOI: 10.3384/ecp14096523

Houser, D. R., & Blankenship, G. W. (1989). *Methods for Measuring Gear Transmission Error Under Load and at Operating Speeds* (Tech. Rep.). DOI: 10.4271/891869

Howieson, D. (2003). Vibration Monitoring: Envelope Signal Processing. *SKF Reliability Systems*, 1–14. Available at http://www.aptitudexchange.com

Inalpolat, M., & Dynamics, S. (2015). A Computational Model to Investigate the Influence of Spacing Errors on Spur Gear Pair Dynamics Murat Inalpolat Structural Dynamics and Acoustic Systems Laboratory. In *Proceedings of the 33rd imac, a conference and exposition on structural dynamics.*

ISO 6336-1. (2007). *Calculation of load capacity of spur and helical gears* (Vol. 2006). ISO, Geneva, Switzerland.

Jia, S., & Howard, I. (2006). Comparison of localised spalling and crack damage from dynamic modelling of spur gear vibrations. *Mechanical Systems and Signal Processing*, *20*(2), 332–349. DOI: DOI:10.1016/j.ymssp.2005.02.009

Joos, H.-D. (2002). A multiobjective optimisation-based software environment for control systems design. In *Proceedings. IEEE international symposium on computer aided control system design* (pp. 7–14). IEEE. DOI: 10.1109/CACSD.2002.1036921

Junghanns, A., Mauss, J., & Tatar, M. (2008). TestWeaver - A Tool for Simulation-based Test of Mechatronic Designs. In *Proceedings of the 6th international Modelica conference* (pp. 341–348). Available at http://citeseerx.ist.psu.edu/viewdoc/summary?doi=10.1.1.182.5268

Kahraman, A., & Singh, R. (1990). Non-Linear Dynamic Analysis of Geared Systems. *Journal of Sound and Vibration*, *142*(1), 49–75. DOI: 10.1016/0022-460X(90)90582-K

Kahraman, A., & Singh, R. (1991). Interactions between time-varying mesh stiffness and clearance non-linearities in a geared system. *Journal of Sound and Vibration*, *146*(1), 135–156. DOI: 10.1016/0022-460X(91)90527-Q

Kar, C., & Mohanty, A. R. (2008). Vibration and current transient monitoring for gearbox fault detection using multiresolution Fourier transform. *Journal of Sound and Vibration*, *311*(1-2), 109–132. DOI: 10.1016/j.jsv.2007.08.023

Kelly, S. G. (2000). *Fundamentals of mechanical vibrations.* McGraw-Hill. Available at http://books.google.co.uk/books?id=yVjvAAAAMAAJ

Kiekbusch, T., Sappok, D., Sauer, B., & Howard, I. (2011). Calculation of the Combined Torsional Mesh Stiffness of Spur Gears with Two- and Three-Dimensional Parametrical FE Models. *Strojniški vestnik - Journal of Mechanical Engineering*, *57*(11), 810–818. DOI: 10.5545/sv-jme.2010.248

Kissling, U., & Raabe, M. (2006). Calculating Tooth Form Transmission Error. *gearsolutions.com*, *September*, 39–66. Available at http://gearsolutions.com/article/detail/5442/title/calculating-tooth-form-transmission-error

KISSsoft (KISSsoft AG). (2015). Available at http://www.kisssoft.ch

Klocke, F., Brumm, M., & Hellmann, M. (2014). Improvement of the design method for helical gears by considering manufacturing related bias errors. In *International gear conference 2014 volume i* (p. 219-229).

Kohler, H., & Regan, R. (1985). The Derivation of Gear Transmission Error from Pitch Error Records. *Proceedings of the Institution of Mechanical Engineers, Part C: Journal of Mechanical Engineering Science*, *199*(3), 195–201. DOI: 10.1243/PIME_PROC_1985_199_114_02

Kohn, B., Heider, M., Otto, M., & Stahl, K. (2014). Meeting NVH Requirements by Low Noise Mesh Design for a Wide Load Range. In *Fisita 2014 world automotive congress.*

Lenz, T. (2014). *Modelling and Simulation of Component Faults in an X-by-Wire Electric Vehicle* (Master Thesis). Fachhochschule Köln.

Lunde, K. (2000). Object-oriented modeling in model-based diagnosis. *Proceedings of Modelica Workshop, Lund, Sweden*, 111–118. Available at https://www.modelica.org/events/workshop2000/index_html/proceedings/Lunde.pdf

Marrant, B. (2012). Validation of MBS multi-megawatt gearbox models on a 13.2 MW Test Rig. *SIMPACK Newsletter Issue (May-June)*(July), 2–5. Available at http://www.simpack.com/fileadmin/simpack/doc/papers/Wind_Drivetrain_Conf_2012/Validation-MBS-multi-megawatt-gearbox-mod-on-13.2-MW-test-rig_Marrant_ZF.pdf

Metropolis, N., & Ulam, S. (1949). The Monte Carlo Method. *Journal of the American Statistical Association*, *44*(247), 335–341. DOI: 10.1080/01621459.1949.10483310

Mohammed, O. D., Rantatalo, M., & Aidanpää, J.-O. (2015). Dynamic modelling of a one-stage spur gear system and vibration-based tooth crack detection analysis. *Mechanical Systems and Signal Processing*, *54-55*(54-55), 293–305. DOI: 10.1016/j.ymssp.2014.09.001

Niemann, G., & Winter, H. (1989). *Maschinenelemente: Band 2: Getriebe allgemein, Zahnradgetriebe - Grundlagen, Stirnradgetriebe (German Edition)*. Springer.

Otter, M., Elmqvist, H., & Mattsson, S. E. (1999). Hybrid modeling in Modelica based on the synchronous data flow principle. In *Computer aided control system design, 1999. proceedings of the 1999 IEEE international symposium on* (pp. 151–157). DOI: 10.1109/CACSD.1999.808640

Ottewill, J. R., Neild, S. a., & Wilson, R. E. (2009). Intermittent gear rattle due to interactions between forcing and manufacturing errors. *Journal of Sound and Vibration*, *321*(3-5), 913–935. DOI: 10.1016/j.jsv.2008.09.050

Oyague, F. (2009). *Gearbox Modeling and Load Simulation of a Baseline 750-kW Wind Turbine Using State-of-the-Art Simulation Codes* (Tech. Rep. No. NREL/TP-500-41160). Colorado: National Renewable Energy Laboratory.

Parey, A., & Tandon, N. (2003). Spur Gear Dynamic Models Including Defects: A Review. *The Shock and Vibration Digest*, *35*, 465–478. DOI: DOI:10.1177/05831024030356002

Pelchen, C., Schweiger, C., & Otter, M. (2002). Modeling and simulating the efficiency of gearboxes and of planetary gearboxes. In *2nd international Modelica conference* (Vol. 3, pp. 257–266). DOI: 10.1.1.16.9542

Rigaud, E., & Barday, D. (1999). Modelling and Analysis of Static Transmission Error. Effect of Wheel Body Deformation and Interactions between Adjacent Loaded Teeth. In (pp. 1961–1972). Available at https://hal.archives-ouvertes.fr/hal-00121847

Russo, R., Brancati, R., & Rocca, E. (2009). Experimental investigations about the influence of oil lubricant between teeth on the gear rattle phenomenon. *Journal of Sound and Vibration*, *321*(3-5), 647–661. DOI: DOI:10.1016/j.jsv.2008.10.008

Schallert, C. (2011). Inclusion of Reliability and Safety Analysis Methods in Modelica. In *Inclusion of reliability and safety analysis methods in modelica* (pp. 616–627). DOI: 10.3384/ecp11063616

Shi, X., & Polycarpou, A. a. (2005). Measurement and Modeling of Normal Contact Stiffness and Contact Damping at the Meso Scale. *Journal of Vibration and Acoustics*, *127*(1), 52–60. DOI: 10.1115/1.1857920

Shibahata, Y. (1995). *Torque distributing mechanism in differential.* US Patent 5387161. Available at http://www.google.com/patents/US5387161

Stahl, K., Otto, M., & Zimmer, M. (2013). Striving for High Load Capacity and Low Noise Excitation in Gear Design. In *Agma fall technical meeting* (pp. 1–14).

Stridsberg, L. (2005). Low Weight, Highly Reliable Anti-Jamming Device for Electromechanical Actuators. In *Sae technical papers.* DOI: 10.4271/2005-01-3396

Sweeney, P. J., & Randall, R. (1996). Gear Transmission Error Measurement Using Phase Demodulation. In *Proceedings of the institution of mechanical engineers, part c: Journal of mechanical engineering science* (Vol. 210, pp. 201–213). DOI: 10.1243/PIME_PROC_1996_210_190_02

Tangasawi, O., Theodossiades, S., Rahnejat, H., & Kelly, P. (2008). Non-linear vibro-impact phenomenon belying transmission idle rattle. *Proceedings of the Institution of Mechanical Engineers, Part C: Journal of Mechanical Engineering Science*, *222*(10), 1909–1923. DOI: 10.1243/09544062JMES922

Todeschi, M., & Baxerres, L. (2014). Airbus - Health Monitoring for the Flight Control EMAs 2014

status and perspectives. In *Recent advances in aerospace actuation systems and components* (pp. 73–83). Toulouse.

User: Marsyas. (2005). *NAMA Machine d'Anticythère. Copyright: CC-BY-2.5.* Retrieved 2001-06-20, from `http://commons.wikimedia.org/wiki/File:NAMA_Machine_d'Anticythère_1.jpg`

Van der Linden, F. L. (2012). Modelling of Elastic Gearboxes Using a Generalized Gear Contact Model. In *Proceedings of the 9th international Modelica conference* (pp. 303–310). Munich: Linkoping University Electronic Press. DOI: `10.3384/ecp12076303`

Van der Linden, F. L. J. (2014a). Gear test rig for health monitoring and quasi static- and dynamic testing; design, construction and first results. In *Proceedings of the international gear conference 2014* (pp. 976–985). Lyon: Woodhead Publishing. Available at `http://elib.dlr.de/90564/`

Van der Linden, F. L. J. (2014b). General fault triggering architecture to trigger model faults in Modelica using a standardized blockset. In *Proceedings of the 10th Modelica conference* (pp. 427–436). DOI: `10.3384/ecp14096427`

Van der Linden, F. L. J. (2015). Modeling of geared positioning systems: An object-oriented gear contact model with validation. *Proceedings of the Institution of Mechanical Engineers, Part C: Journal of Mechanical Engineering Science.* DOI: `10.1177/0954406215592056`

Van der Linden, F. L. J., Dreyer, N., & Dorkel, A. (2016). EMA Health Monitoring: An overview. In *Recent advances in aerospace actuation systems and components* (pp. 21–26). Toulouse, France. Available at `http://elib.dlr.de/104367/`

Van der Linden, F. L. J., Schlegel, C., Christmann, M., Regula, G., Hill, C., Giangrande, P., … Egaña, I. (2014). Implementation of a Modelica Library for Simulation of Electromechanical Actuators for Aircraft and Helicopters. In *Proceedings of the 10th international Modelica conference* (pp. 757–766). DOI: `10.3384/ecp14096757`

Van der Linden, F. L. J., & Tobolár, J. (2015). Modelling of Torque-Vectoring Drives for Electric Vehicles: a Case Study. In *Proceedings of the 11th Modelica conference* (pp. 151–158). Versailles. DOI: `10.3384/ecp15118151`

Van der Linden, F. L. J., & Vazques de Souza Silva, P. (2009). Modelling and Simulating the Efficiency and Elasticity of Gearboxes. In *Proceedings of the 7th international Modelica conference, como, italy* (pp. 270–277). DOI: `10.3384/ecp09430052`

Velex, P., & Cahouet, V. (2000). Experimental and Numerical Investigations on the Influence of Tooth Friction in Spur and Helical Gear Dynamics. *Journal of Mechanical Design*, *122*(4), 515. DOI: `10.1115/1.1320821`

Yan, H.-S., & Chen, C.-W. (2006). A Systematic Approach for the Structural Synthesis of Differential-Type South Pointing Chariots. *JSME International Journal Series C*, *49*(3), 920–929. DOI: `10.1299/jsmec.49.920`

Yang, Z., Shang, J.-z., & Luo, Z.-r. (2013). Effect analysis of friction and damping on anti-backlash gear based on dynamics model with time-varying mesh stiffness. *Journal of Central South University*, *20*(12), 3461–3470. DOI: `10.1007/s11771-013-1870-7`

Zimmer, D. (2012). A Planar Mechanical Library for Teaching Modelica. In *Proceedings of the 9th international Modelica conference* (pp. 681–690). Munich: Linköping University Electronic Press. DOI: `10.3384/ecp12076681`

Zimmer, D., & Otter, M. (2010). Real-time models for wheels and tyres in an object-oriented modelling framework. *Vehicle System Dynamics*, *48*(2), 189–216. DOI: `10.1080/00423110802687596`